

**EXTENSION OF ULTRA PRECISION MACHINING TO
TITANIUM ALLOYS**

EXTENSION OF ULTRA PRECISION MACHINING TO TITANIUM ALLOYS

By

Rahmath Zareena ABDUL GANI, M.ENG (Mechanical Engineering)

National University of Singapore, Singapore

A Thesis

Submitted to the School of Graduate Studies

in Partial Fulfillment of the Requirements

for the Degree

Doctor of Philosophy

McMaster University

©Copyright by Rahmath Zareena ABDUL GANI, December, 2010

DOCTOR OF PHILOSOPHY (2010)
(Mechanical Engineering)

McMaster University
Hamilton, Ontario, Canada

TITLE: Extension of ultra precision machining to titanium
alloys

AUTHOR: Rahmath Zareena ABDUL GANI

M.ENG – Research (National University of Singapore,
Singapore)

B.E (Madurai Kamaraj University, India)

SUPERVISOR: Dr. Stephen C Veldhuis

Department of Mechanical Engineering

McMaster University

NUMBER OF PAGES: XX, 193

Abstract

High-end optical grade applications would benefit greatly from the unique mechanical and chemical properties of titanium alloys. However, the standard process of manufacturing optical components has not been explored in depth for titanium alloys.

Thus the focus of this work was to extend ultra precision machining technology to produce optical grade surfaces on titanium components. An optical surface is characterized by surface roughness less than 10 nm R_{rms} which are typically produced with single crystal diamond tools having a cutting edge radius on the order of 50-100 nm. A cutting speed of 60m/min, feed rate of 1.5 $\mu\text{m}/\text{rev}$ and depth of cut of 2 μm , was identified to achieve the surface finish target, but the practical limitation of this process was still with tool life and the rapid degradation of surface finish over time.

This was attributed to the adhesion of titanium material on the tool that resulted in material pull out and side-flow during machining. Results obtained from the characterization of the tool and workpiece led to the identification of graphitization as the initial wear mechanism. As the cutting edge rounds-off due

to graphitization, the rate of adhesion of the workpiece material onto the tool increased. For this reason solutions were explored that would reduce the graphitization process and delay the onset of intense adhesion.

Thus a coating technology involving Perfluoro Polyether (PFPE) was chosen. Tribometer analysis under a load of 500N and temperature of 450°C between the uncoated and PFPE coated diamond tools and titanium pins showed a remarkable reduction in COF from 0.275 to 0.05. A significant enhancement in tool life and surface quality was also achieved in single point diamond turning (SPDT) of titanium alloys using PFPE coated diamond tools. Tool life was based on an assessment of the cutting length achieved before the surface roughness exceeded the targeted value of 10 nm R_{rms} and it improved from 1.25 km to 5.1 km with PFPE coated tools.

With all my love, to my beloved parents:

Mrs. Fathima Gani and Late Mr. M. Abdul Gani

&

With all due respect to my teachers who taught me from

Kindergarten to Doctorate

Acknowledgements

This thesis was made possible with the guidance of the Infinite Intelligence.

I would like to express my sincere gratitude and heartfelt thanks to my advisor, Dr. Stephen Veldhuis, for his constructive guidance, motivation, constant support, encouragement, and above all his patience throughout this research. I am deeply indebted to him for his valuable suggestions and critical reviews that added great value to this work. Also the support from the McMaster Manufacturing Research Institute (MMRI) to this work was remarkable.

No words would be sufficient to thank Dr. Eu-Gene Ng for all his time, support and enthusiastic guidance in both technical and emotional aspects. I would like to thank Dr. Joey Kish for his technical insight and guidance on my Ph.D. committee. I would also like to thank Dr. Philip Koshy and Dr. David Conochie for serving as committee members as well and Dr. Mukesh Jain and Dr. Ravi Selvaganapathy for the knowledge they shared through their courses. Special thanks also to Dr. Sumanth Shankar for his help and technical discussions.

Sincere thanks to Mr. Maneesh Khanna for his constant support and technical guidance. This work would not have been possible if not for the technical expertise of Mr. Chris Butcher and Dr. Glynis De Silvera at CCEM. Special thanks to my colleague, Mr. Andrew Biksa for sharing his tribometer expertise, Dr. Szymnaski (University of Guelph), Ms. Mary Jane (Surface Science Western) and Dr. Steve Kornic (Dept. of Chemistry) for all of their technical assistance. I like to thank my colleagues Ms. Aml El-Fizy and Mr. Mohammed Tauhiduzzaman for their support and cooperation.

I would like to express my appreciation to Mr. J.P.Talon, Mr. Jim McLaren, and Mr. Ron Loedwyks for helping me in the machine shop. I would also like to thank Mr. Terry Wagg, Mr. Steve Remilli and Mr. Doug Culley for all of their technical assistance. Special thanks to Ms. Janet Murphy whose assistance and kindness made my days in MMRI more memorable. Many thanks to our department staff: Ms. Florence Rosato, Ms. Vania Loyzer, Ms. Melissa Vasil and Ms. Lily Sazz-Fayter for their assistance and help.

I would also like to thank NSERC (PGS D – scholarship) and OCE as well as B-Con Engineering® for their financial support which made this project possible. I would sincerely thank Dr. Mustafizur Rahman, my M.Eng thesis supervisor and

Dr. N.Y. Nee (NUS, Singapore) and Dr. Amir Khajepour (University of Waterloo) for their continuous support and valuable references to NSERC.

Special thanks to my wonderful sisters, Farida, Jahan and Fouzia and all my family and friends for their love and support. Above all, I would like to thank my lovely son, Roshan for his sacrifices and patience and also my husband, Rajesh for his encouragement and support while this thesis was being made.

Table of Contents

ABSTRACT	III
ACKNOWLEDGEMENTS.....	VI
TABLE OF CONTENTS	IX
LIST OF FIGURES	XV
LIST OF TABLES	XX
CHAPTER 1 : INTRODUCTION	1
1.1. Background and Motivation.....	1
1.2. Research Objective	2
1.3. Thesis Outline	6
CHAPTER 2 : LITERATURE REVIEW & RESEARCH APPROACH.....	8
2.1. Titanium and its alloys.....	8
2.2. Machinability of titanium alloys.....	11
2.3. Precision engineering	18

2.4. Ultra precision Machining	21
2.5. Single point diamond turning (SPDT)	22
2.5.1. Significance of cutting edge radius	25
2.5.2. Cutting Edge Radius and Tool life in SPDT	29
2.5.2.1. Challenges in measuring the cutting edge radius.....	30
2.5.3. Cutting Scale and Machining Properties	32
2.5.3.1. Influence of workpiece material microstructure on size-effect	33
2.5.4. Influence of Size-effect on tool wear in SPDT	35
2.6. Tool wear mechanisms in SPDT.....	36
2.6.1. Chemical wear in diamond tools	39
2.6.1.1. Graphitization	44
2.6.2. Workpiece Modifications.....	52
2.6.3. Process Modifications.....	56
2.6.4. Cutting Tool Modifications	63
2.7. Friction in metal cutting	65
2.7.1. Coefficient of Friction in cutting	68
2.8. Friction and tool wear	72
2.9. Perfluoro Polyether-PFPE	74
2.10. Tribometer	81

2.11. Ultra-precision machining of titanium alloys	82
2.12. Summary	84
2.13. Research Approach.....	86
2.13.1. Workpiece modification:	86
2.13.2. Process modification	87
2.13.3. Cutting Tool modification	87
CHAPTER 3 : EXPERIMENTAL PROCEDURE AND SET-UP	89
3.1. Test procedure	89
3.2. Machine tool.....	90
3.3. Workpiece material	93
3.4. Cutting tool.....	93
3.5. Cutting parameters.....	95
3.5.1. Cutting environment.....	96
3.6. Design of experiments.....	97
3.7. Machine set-up.....	98
3.8. Coating technique	99
3.9. Tribometer.....	99
3.10. Cutting force measurement	102

3.10.1. Data collection and processing.....	102
3.11. Surface roughness measurement	103
3.12. Tool life criterion	104
3.12.1. Scanning Electron Microscopy (SEM)	105
3.12.2. Laser Raman Spectroscopy	105
3.12.3. X-ray Photoelectron Spectroscopy	106
3.12.4. TEM – Transmission Electron Microscopy.....	107
3.13. Nano indentation.....	107
CHAPTER 4 : RESULTS AND DISCUSSIONS.....	109
4.1. Phase-I: Selection of cutting parameters	109
4.1.1. Surface quality requirement.....	111
4.1.2. Tool life criterion.....	113
4.1.2.1. Measuring the cutting edge radius.....	113
4.2. Phase-II: SPDT of Titanium alloys	118
4.2.1. Surface Roughness.....	118
4.2.2. Cutting force analysis.....	122
4.2.3. Tool wear mechanisms	124

4.2.4. Adhesion wear and cutting edge radius	128
4.2.5. Cutting edge - wear mechanism.....	130
4.3. Phase-III: Wear mechanisms and surface modifications	136
4.4. Characteristic requirements of coating material	136
4.4.1. Characteristics of PFPE coating	139
4.5. Phase-IV: Evaluation of PFPE coating.....	141
4.6. Phase -V: Machining with PFPE coated diamond tool	146
4.6.1. Surface Roughness.....	146
4.6.2. Cutting force Analysis	152
4.6.3. Tool wear mechanisms	155
4.6.4. Chip analysis.....	160
4.6.4.1. TEM analysis of chips	163
4.7. Material microstructure analysis	164
CHAPTER 5 : CONCLUSIONS & SCIENTIFIC CONTRIBUTIONS.....	167
5.1. Conclusions.....	167
5.2. Scientific contributions.....	168
5.3. Recommendations and future works.....	171

REFERENCES	172
APPENDIX -1.....	185
APPENDIX -2.....	186
APPENDIX -3.....	187
APPENDIX -4.....	188
APPENDIX -5.....	189
APPENDIX -6.....	192
APPENDIX -7.....	193

List of Figures

Figure 2-1: Distribution of thermal load when machining titanium and steel [4]	14
Figure 2-2: Properties of titanium alloys resulting in accelerated tool wear	17
Figure 2-3: Primary aspects associated with advancing cutting technology. [13]	19
Figure 2-4: Structure dimension and surface roughness comparison (based on [13])	20
Figure 2-5: Classification of mechanical machining	21
Figure 2-6: (a) Controlled radius and (b) uncontrolled radius SPDT tools (K-Y Diamond)	24
Figure 2-7: Tool geometry of a diamond tool.	25
Figure 2-8: Schematic showing (a) conventional and (b) ultra precision cutting	26
Figure 2-9: Cutting models (a) Sharp edge and (b) Round edge [20]	28
Figure 2-10: Schematic showing effect of edge radius in (a) conventional cutting and (b) SPDT	29
Figure 2-11: Material removal in (a) macro scale machining and (b) nano scale machining	34
Figure 2-12: Wear mechanism as a function of temperature [31]	37
Figure 2-13: Electronic configuration of Ti, Al and Fe.	39
Figure 2-14: Diamond to graphite transformation – Graphitization	45
Figure 2-15: Schematic of SPDT of a transition metal & wear components in atomic scale [46]	47
Figure 2-16: Tool wear in machining Ti-6Al-4V with and without LN ₂ [70]	60
Figure 2-17: (a) Tool-chip contact in cutting (b) Merchant's circle	65

Figure 2-18: Coefficient of Friction and Area of contact in friction	67
Figure 2-19: (a) Load and Force at the asperities contact point (b) Principle of soft coatings	68
Figure 2-20: Friction angle in (a) Negative and (b) Positive rake tools	69
Figure 2-21: (a) Deformation zones and (b) COF in cutting	70
Figure 2-22: Stress distribution on the rake face	71
Figure 2-23: COF as a function of unpaired d-electron in transition metals [84]	73
Figure 2-24: PFPE Molecule [90]	76
Figure 3-1: Precitech Freeform 700G Ultra precision machining system	91
Figure 3-2: Schematic of (a) initial and (b) modified machine axes and spindle set-up	91
Figure 3-3: Machine set-up for SPDT.	92
Figure 3-4: Design of diamond insert and the tool holder (K&Y – used with permission)	95
Figure 3-5: Zygo NewView 5000 White light interferometer	104
Figure 4-1: Surface roughness (R_{rms}) Vs cutting speed (V), feed (f), and depth of cut (DOC)	110
Figure 4-2: Trace of diamond cutting edge in Mitutoyo Formtracer.	114
Figure 4-3: Cutting edge radius – Zygo white light interferometer image	115
Figure 4-4: (a) Silflo replica of the diamond tool (b) sliced	116
Figure 4-5: SEM images of edge profile measurement	117
Figure 4-6: Roughness profile of CP-Ti surface machined (R_{rms} : 11.25 nm)	118
Figure 4-7: Tool life - Cutting length Vs Surface Roughness in (a) CP-Ti, (b) Ti-6Al-4V	120

Figure 4-8: Comparison of (a) Zygo and (b) SEM – FOV showing CP-Ti machined surface	121
Figure 4-9: SEM image of Ti-6-4 machined surface	121
Figure 4-10: Force ratio as a function of thrust and cutting forces in CP-Ti	123
Figure 4-11: SEM images of the diamond tool (a) new tool, (b, c) adhesion of material on flank face (c, d) rake face after machining (CP-Ti)	125
Figure 4-12: SEM images of cutting edge at (a) run-in and (b) end of cutting cycle (Ti-6Al-4V)	126
Figure 4-13: SEM image of tool used for cutting aluminum (after 5.42km)	127
Figure 4-14: EDS spectrum of the adhered material (CP-Ti)	128
Figure 4-15: XRD image of CP-Ti workpiece	132
Figure 4-16: XRD image of CP-Ti chips	132
Figure 4-17: Raman spectrum of a worn diamond tool	133
Figure 4-18: XPS spectrum of worn diamond tool with graphite	135
Figure 4-19: SEM images of CP-Ti pins (a & b), Diamond tools (c & d) without and with PFPE coating	141
Figure 4-20: SEM images of Ti-6Al-4V pins (a & b), Diamond tools (c & d) without and with PFPE coating	142
Figure 4-21: Co-efficient of Friction Vs Temperature plot of CP-Ti without and with PFPE coated tool	143
Figure 4-22: Co-efficient of Friction Vs Temperature plot of Ti-6Al-4V without and with PFPE coated tool	145

Figure 4-23: Roughness profile of CP-Ti surface machined with PFPE coated tool (R_{rms} : 7.718 nm)	146
Figure 4-24: Comparison of surfaces generated in CP-Ti with PFPE coated and uncoated tools	147
Figure 4-25: Comparison of surfaces generated in Ti-6Al-4V with PFPE coated and uncoated tools	148
Figure 4-26: Cutting Length Vs Surface Roughness of CP-Ti without and with PFPE coating	149
Figure 4-27: Cutting Length Vs Surface Roughness of Ti-6Al-4V without and with PFPE coating	149
Figure 4-28: SEM image of PFPE coated diamond tool	150
Figure 4-29: CP-Ti machined surface: (a) No coat and (b) PFPE	151
Figure 4-30: Ti-6Al-4V machined surface: (a) No coat and (b) PFPE	152
Figure 4-31: Cutting length Vs Force ratio in CP-Ti	153
Figure 4-32: Cutting length Vs Force ratio in Ti-6-4	153
Figure 4-33: Tool cutting edge at the run-in (a,c) and intermittent cutting distance (b,d) without and with PFPE	156
Figure 4-34: Raman spectrum of PFPE coated single-crystal diamond tool	157
Figure 4-35: XPS spectrum of PFPE coated diamond tool	158
Figure 4-36: Schematic of a diamond tool with an imperfect cutting edge without and with PFPE coating (magnitude of imperfections enlarged to highlight effect)	160
Figure 4-37: SEM images of CP-Ti chips with torn edges	161

Figure 4-38: SEM images of CP-Ti chips obtained with PFPE coated tool	162
Figure 4-39: TEM – EELS of chips	164
Figure 4-40: Optical image of the cross-section of the machined surface (CP-Ti)	165
Figure 4-41: Nano Indentation on machined surface obtained without and with PFPE coated tool	166

List of Tables

Table 2-1: Characteristics of Ti compared to Fe, Ni and Al (based on [2])	10
Table 2-2: Cutting edge radius Vs uncut chip thickness	26
Table 2-3: Data for elements with known diamond turning properties [11]	41
Table 2-4: Literature review on tool wear of single point diamond tools	49
Table 2-5: Properties of PFPE	76
Table 2-6: Literature available on ultra precision machining of titanium alloys	82
Table 3-1: Chemical composition of workpiece and pin materials	93
Table 3-2: Tool geometry	94
Table 3-3: Cutting parameters	96

Chapter 1 : **INTRODUCTION**

1.1.BACKGROUND AND MOTIVATION

Precise flat, spherical and aspherical surfaces as well as geometries with high-precision can be ultra precision machined in large volumes with high repeatability in metals such as copper and aluminum by Single Point Diamond Turning (SPDT). Such surfaces and geometries cannot be easily achieved using traditional precision metal removal operations such as grinding or polishing. At the time of its development SPDT represented a breakthrough in the field of optical manufacturing and was applied to the field of ultraviolet and soft X-ray optical mirrors. Two axes SPDT has been widely used to produce parabolic beam-focusing optics, spherical mirrors for laser cavities, aspherical focusing lenses, reflective beam expanders, aerospace components, reflective telescopes and seeker-sensor optics and components for space and cryogenic applications. Free-form turning has been used for machining faceted beam integrators (reflective and transmissive), optical arrays, long working distance parabolas, free-form phase correction optics and cylindrical optics.

These applications would benefit greatly from the use of titanium alloys. This is due to the fact that titanium alloys have a unique combination of properties including high strength-to-weight ratio and high strength at elevated temperatures. But these same properties also make titanium and its alloys difficult to machine traditionally and generally considered non diamond turnable due to excessive tool wear which limits the functional size of the components that can be produced with the desired surface quality. Thus, the progress in titanium ultra precision machining has not kept pace with the advances in ultra precision machining of other alloys.

The success with SPDT titanium alloys will largely depend on overcoming the principal problems associated with excess tool wear. A detailed analysis of tool wear mechanisms and wear reduction technologies associated with the SPDT of Ti alloys has not been performed to date and thus is the primary focus of this thesis work.

1.2.RESEARCH OBJECTIVE

Machining is a major industrial activity despite recent developments in near-net shape forming techniques. The overall objective of machining research

in general is to study the interactions between the cutting tool and the workpiece in order to optimize tooling and cutting conditions and hence minimize operational cost as well as maximize product quality and productivity. [1] Improved machinability of certain difficult to cut alloys can also open up new applications for materials with unique properties which can in turn promote the creation of new products.

Machining productivity can be significantly improved by employing the right combination of cutting tools and cutting conditions that will promote higher tool life as well as higher surface quality and tolerances of the machined components. This is particularly essential for the economic machining of difficult-to-machine materials such as titanium alloys.

The primary objective of this study was to make titanium a viable option for applications that require surface finishes in the range of 7 nm to 10 nm R_{rms} that are typically associated with optical applications. This could only be achieved through the identification of tool wear mechanisms that impair the ability of the SPDT process to achieve the desired optical grade surface quality. The goal was to derive methodologies to overcome the current machining challenges without

compromising the desired properties of these alloys that make them attractive for their respective applications. A further objective was to keep these methods and techniques cost effective so that industrial applications could benefit with the technology transfer without incurring prohibitively high costs.

An extensive study was carried out to investigate the challenges involved in SPDT of commercial pure titanium (CP-Ti) and Ti-6Al-4V alloys. A comprehensive experimental study and characterisation of the tool, workpiece and chips, as well as the literature review led to the identification of graphitization as the most probable wear mechanism that initiates tool wear in SPDT of titanium and leads to a more rapid rate of tool wear and surface finish degradation. Thus the critical need for a protective barrier to inhibit graphitization was postulated. However, to achieve the small scale of material removal associated with SPDT the edge sharpness of the tool has to be retained as it is the most critical component of SPDT. For this reason conventional coating techniques, which are generally used as protective barriers for cutting tools are not applicable for SPDT. Such coatings would result in a rounded cutting edge due to the coating thickness building up the edge and thus increasing the radius of the cutting edge. Thus an ultra thin protective coating that would not significantly alter the cutting edge radius of the

tool was required. Also, the coating should be able to withstand the localized high cutting temperature and normal stress experienced in the contact zone. It also must enhance the lubricity between the tool and workpiece to reduce the coefficient of friction (COF) and the adhesion of the workpiece material onto the tool. Ideally the coating technique needs to be simple and cost effective so that it can be carried out in-house with minimal equipment.

An ultrathin polymer coating in the form of a Perfluoro Polyether (PFPE) was identified as a potential material. PFPE's ability to reduce the COF between the diamond tool and titanium workpiece was first evaluated using a heavy load and high temperature tribometer. Based on the favourable results of this testing the PFPE coating was applied to the single crystal diamond tool and tested in SPDT machining studies.

Cutting tests performed with PFPE coated tools showed a reduction in the COF and material adhesion. Also when compared to uncoated tools, significant improvements in tool life and surface quality were achieved.

1.3.THESIS OUTLINE

Following this introductory chapter, Chapter 2 presents the comprehensive background information on the relevant and critical topics within the scope of this research including:

- General background on the machinability of titanium alloys
- SPDT operation, cutting scale and machining properties
- Tool life and tool wear mechanisms in SPDT
- Impact of friction on tool wear &
- Research approach

Chapter 3 describes the experimental procedure and the set-up used in this study. Information on various characterisation techniques such as scanning electron microscopy (SEM), energy dispersive spectrum (EDS), Raman spectroscopy, X-ray photoelectron spectroscopy (XPS), transmission electron microscope (TEM) and nano-indentation used in this study was also included.

Chapter 4 explains the four phases of the experimental work carried out:

- Phase I: Selection of cutting parameters
- Phase II: SPDT of titanium alloys with regular single crystal diamond tools

- Phase III: Wear mechanisms and modifications
- Phase IV: Evaluation of PFPE coating
- Phase V: SPDT of titanium alloys with PFPE coated tools

The results obtained from detailed force, surface roughness, chip analysis and hardness studies are shown as well in this chapter.

Chapter 5 summarizes the findings and the scientific contributions of this study and also includes recommendations for future work on SPDT.

Chapter 2 : LITERATURE REVIEW & RESEARCH APPROACH

2.1.TITANIUM AND ITS ALLOYS

Individual industrial branches drive the specific demands for new innovations using different engineering materials. In particular in the automotive and the aerospace sectors, the use of light weight and energy saving materials play a vital role not only for structural components, housings and drive system components, but also for components that demand high accuracy and optical grade surface quality. The high strength to weight ratio of titanium and its ability to maintain this strength at elevated temperatures, along with its exceptional corrosion resistance make it an attractive choice for high-grade optical applications. Thus an improvement in machinability for the SPDT process would be a substantial asset to this industry.

Pure titanium undergoes an allotropic transformation at 882° C, changing from a low temperature α -phase hexagonal close-packed (hcp) structure, to a high temperature β -phase body centered cubic (bcc) structure. The HCP structure of titanium has fewer slip or shear planes. The bcc structure has a greater

number of slip planes than the hcp structure, which enables it to deform more easily. This phase transformation temperature can be altered with the addition of impurities. For example addition of α stabilizers such as Al, O, N, Ga and C would increase the transition temperature and that of β stabilizers such as Mo, V, Ta, Cu, Cr, Fe, Mn, Ni, Co and H would reduce the transformation temperature.

Titanium alloys can generally be classified into four main groups, according to their metallurgical characteristics: α - alloys, near α - alloys, α - β alloys and β -alloys. α -alloys such as CP-Ti are used chiefly for their excellent corrosion resistance and cryogenic applications. Near α -alloys behave more like α -alloys and are capable of operating at temperatures greater than α -alloys. α - β alloys contain both α and β stabilizers and Ti-6Al-4V is its most common alloy. The α - β alloys can be heat-treated to high strength levels and hence are used chiefly for applications at elevated temperatures between 350 and 400°C. They are stronger than the alpha or the beta alloys. β -alloys contain significant quantities of β -stabilizers and are characterized by high hardness, improved forgeability and cold formability, as well as high density. Ti-6Al-4V comprises about 45% to 60% of all titanium used, followed by CP-Ti for its excellent corrosion resistance and low strength. It is for these reasons; CP-Ti and Ti-6Al-4V were chosen for this study.

The properties of pure Ti as compared to that of Fe, Ni and Al are given in the following Table 2-1[2].

Table 2-1: Characteristics of Ti compared to Fe, Ni and Al (based on [2])

PROPERTY	Ti	Fe	Ni	Al
Melting temperature (°C)	1670	1538	1455	660
Allotropic Transformation (°C)	$\alpha \xrightarrow{882} \beta$	$\alpha \xrightarrow{912} \gamma$	-	-
Crystal structure	hcp → bcc	bcc → fcc	fcc	fcc
Room Temperature E (GPa)	115	215	200	72
Yield Stress Level (MPa)	910	260	90	414
Density (g/cm ³)	4.5	7.8	8.9	2.7
Comparative Corrosion Resistance	Very high	Low	Medium	High
Comparative reactivity with oxygen	Very high	Low	Low	High
Comparative price of metal	Very high	Low	High	Medium
Thermal Conductivity (W/m ^{°K})	7.3	42	52	144

Commercially pure titanium (CP-Ti) is a low density element - 4.5g/cc, which is approximately 60% of the density of steel-7.8g/cc and about 60% higher

than that of aluminum- 2.7g/cc. The yield strength (910 MPa) of titanium is greater than most steel alloys (260MPa- 1040 steel alloy).

The major application of titanium alloys to date has been in the aerospace industry, mostly as a structural element. Components made of titanium alloys are stronger than aluminum alloys and lighter than conventional steel. Optical components used in aerospace applications are generally made of aluminum or copper alloys since they are easily diamond turnable. But titanium alloys would be a better alternative for optical applications that require high strength, light weight and high corrosion resistance if the appropriate surface finish could be achieved. In short the high cost and difficulty in producing the desired surface finish needs to be resolved in order to make titanium an attractive and economic industrial solution for these optical applications.

2.2.MACHINABILITY OF TITANIUM ALLOYS

Extensive work has been carried out to study the machinability of titanium and its alloys using conventional machining techniques. Titanium is generally considered to have poor machinability due to its low thermal conductivity resulting in high temperatures being generated during machining. This coupled

with its high chemical reactivity leads to rapid tool wear which limits the range of parts that can be competitively manufactured. The machinability of a material may be assessed by tool life, metal removal rate, surface finish and resultant cutting forces [3].

As discussed earlier, the principle issue with machining titanium alloys is the high cutting temperature. In general, cutting speed, feed rates, material compatibility, and uncut chip thickness increases the cutting temperature. Cutting speed is frequently the largest contributor to high temperatures. Unlike conventional cutting which uses large uncut chip thickness the cutting temperature in SPDT is highly localized. In order to limit the temperature generated at the cutting zone, the cutting speed needs to be restricted. However this reduces the material removal rate for the process which in turn affects the economics of the process, thus a balance must be achieved. To minimize the tool wear, current machining practice limits the cutting speed to less than 60 m/min [77]. Feed rates should be relatively higher for such low cutting speeds to maintain a reasonable level of productivity for the process.

Challenges associated with the machining of titanium alloys are summarized below:

1. Titanium and its alloys are poor thermal conductors with a thermal conductivity of 7.3 W/mK compared to 15-42 W/mK for steel. As a result, the heat generated when machining titanium cannot dissipate quickly; rather, much of the heat is concentrated on the cutting edge and tool face resulting in highly localized temperatures [4]. Thus the machining of titanium alloys is considered a thermally dominant process [5]. When cutting with diamond tools, of the generated heat, about 80% is retained in the diamond tool and only 20% gets transferred to the chips as shown in Figure 2-1 resulting in an accelerated rate of tool wear [4,6] whereas almost 60% of the heat gets transferred to the chips with steel.

In practice diamond turnable materials are those where the tool wear rate is low enough that reasonable areas with an optical grade surface can be economically produced. Also due to the nature of the dimensional accuracy and surface finish, multiple tools cannot be used to create a part. So the functional size of a part is limited by the amount of surface that can be generated by a single tool.

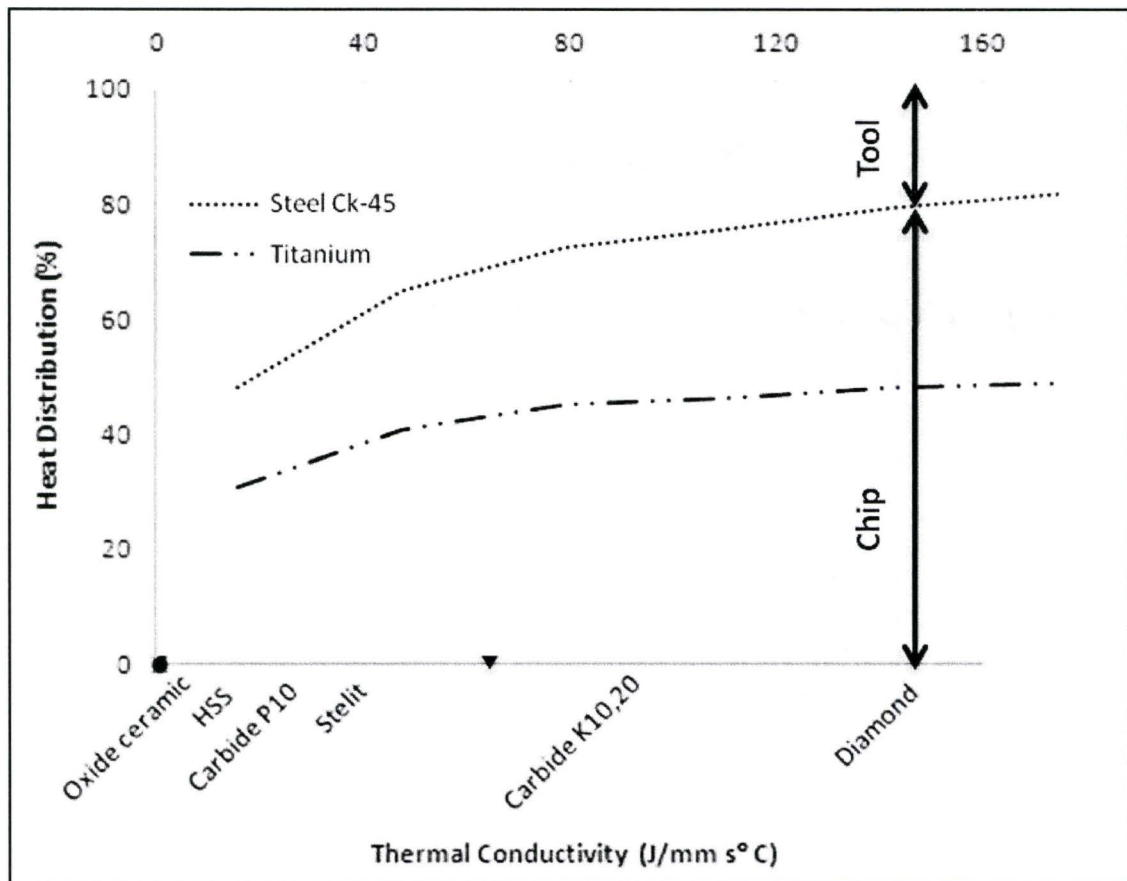


Figure 2-1: Distribution of thermal load when machining titanium and steel [4]

2. Tool wear in machining titanium is also accelerated due to its high shear strength and localized temperatures which could exceed 1000°C in aggressive cutting conditions. Titanium also has a strong alloying tendency and high chemical reactivity with cutting tools at this high temperature. This results in severe wear via adhesive (i.e. galling due to removal of built-up-edge:BUE)

and diffusive wear mechanisms. This will affect the surface quality and the workpiece tolerances [7, 8].

3. The tool-chip contact length with titanium is typically shorter than with other metals such as steel (up to 2/3 less than steel). This implies that the high cutting temperatures and the high stresses are concentrated near the cutting edge which leads to potentially catastrophic failure of the cutting tool.

4. Titanium alloys maintain their high strength at elevated temperature which further impairs their machinability [9]. In general the lower the shear strength of the material at elevated temperatures the greater their machinability. Energy consumed in a typical cutting operation is largely converted into heat. Most problems, encountered during machining are due to heat generation, mainly during the deformation process at the shear plane and friction at the tool-chip interface [1].

5. During traditional machining, titanium alloys exhibit thermal plastic instability which leads to unique characteristics of chip formation. The shear strains in

the chip are not uniform but they are localized in a narrow band that forms serrated chips. [10].

6. Serrated chips create fluctuations in the cutting force. This situation is further promoted when α - β alloys like Ti-6Al-4V are machined. The vibrational force together with the high temperature exerts a micro-fatigue loading on the cutting tool, which is believed to be partially responsible for severe flank wear.
7. According to Paul et al. [11] the number of unpaired d-electrons in titanium is responsible for the increased surface energy, which promotes adhesion and a higher coefficient of friction. These d-electrons also enhance the chemical reactivity. This concept is further explained in section 2.6.1 in this chapter.

The above mentioned characteristics of titanium alloys leads to accelerated tool wear. Various aspects of titanium alloys that would accelerate the tool wear rate in SPDT are compiled in the following Figure 2-2.

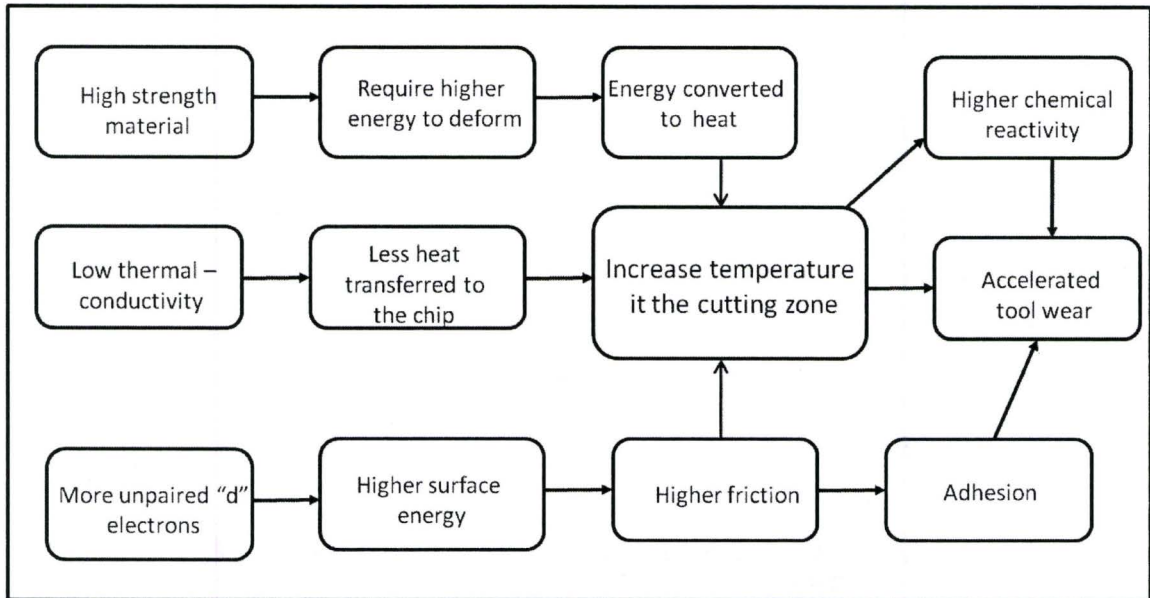


Figure 2-2: Properties of titanium alloys resulting in accelerated tool wear

Therefore, success in machining titanium alloys depends largely on overcoming the issues of localized high temperatures and stresses, as well as chemical reactivity. Machining of titanium alloys requires tools with high hardness, wear durability, retained hot hardness, good thermal resistance and a high coefficient of thermal conductivity. A single crystal diamond tool meets many of these requirements compared to any other cutting tool material such as high speed steel or tungsten carbide [4]. Moreover, a nanometric cutting edge radius that is required for producing optical grade surface quality could only be achieved in single crystal diamond tools.

2.3.PRECISION ENGINEERING

Precision engineering is often defined as manufacturing to tolerances smaller than 1 μm , whereas microengineering is where the physical dimensions of the component are on the order of 1 μm . Nanotechnology is a term coined by Professor Norio Taniguchi as early as 1974; for the work carried out on components and features with sizes in the range of 0.1 nm (1Å) to 100 nm [12]. Ultra precision machining refers to machining techniques such as SPDT, which manufacture to tolerances smaller than 1 μm and producing surface finishes at the nanometric scale. Given the wide range of applications for optics some of the overall part dimensions can vary from a few millimeters to a few meters.

Thus minimizing component size, enhancing surface quality, decreasing weight, adding tighter tolerances and reducing costs are the key drivers this industry is experiencing (Figure 2-3).

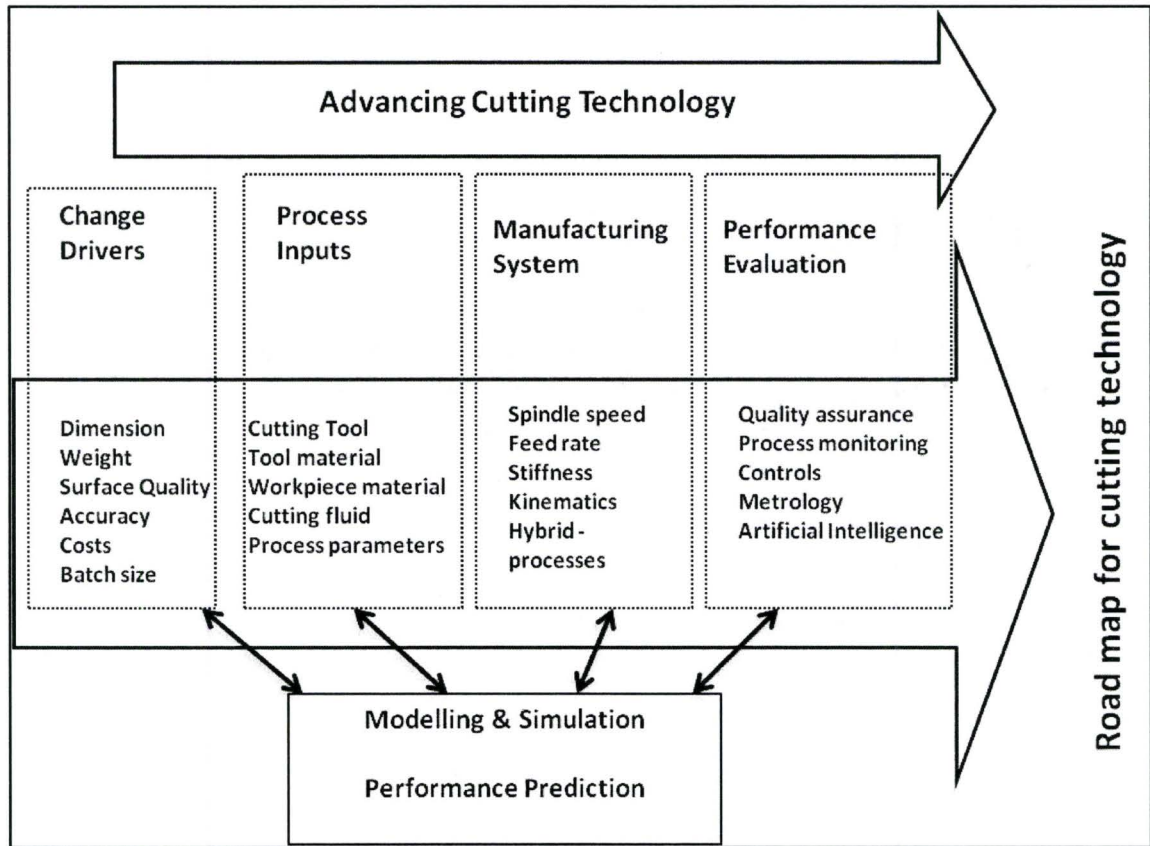


Figure 2-3: Primary aspects associated with advancing cutting technology. [13]

Laser machining, electrical discharge machining (EDM), grinding, silicon etching and lithography (LIGA) are some of the processes that meet such demands. Figure 2-4 shows the capability of ultra precision machining relative to other machining processes. It can be seen that surface roughness as small as 5 nm can be attained for features down to 5µm or less.

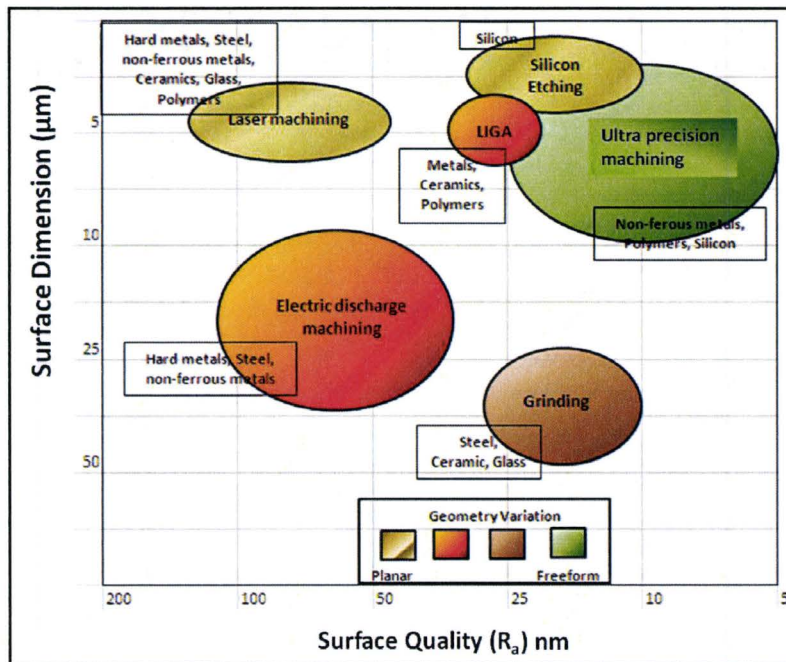


Figure 2-4: Structure dimension and surface roughness comparison (based on [13])

Machining could be classified into macro, meso, micro and nano scale machining based on the accuracy and scale of the machining as shown in Figure 2-5. It could be seen that ultraprecision machining technique could be employed in both micro and nano scale cutting for ultraprecise accuracy. The other advantage of ultra precision machining is that component sizes are not restricted to micro or nano sizes and surfaces are not constrained to 2 dimensions. Technologies such as fast tool servos can be used to generate complex 3 dimensional surfaces.

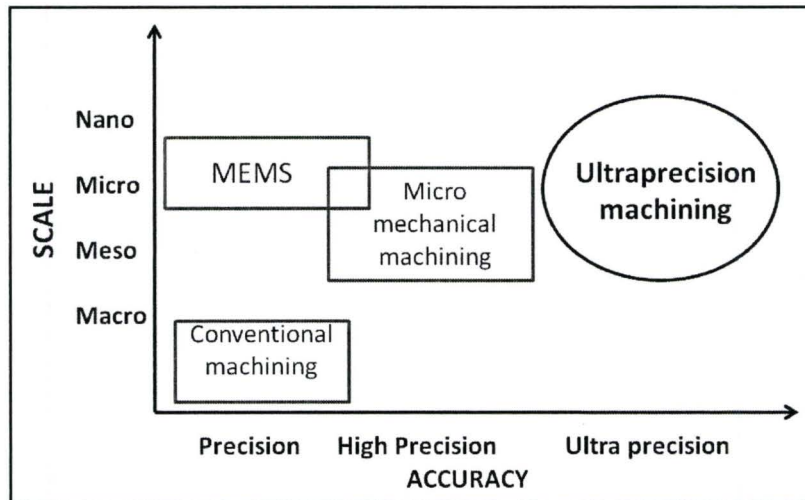


Figure 2-5: Classification of mechanical machining

2.4. ULTRA PRECISION MACHINING

Ultra precision machining can be defined as a cutting technique which enables the production of optical and mechanical components with micrometer and sub-micrometer form accuracy and surface roughness within a few nanometers [14]. Ultra precision machining facilitates direct machining of complex parts such as optical components with minimal post processing techniques such as polishing or lapping.

Ultra precision machining processes include, SPDT; multi-point fixed abrasive process, e.g. diamond grinding; free abrasive - erosion process, e.g.

chemical polishing; chemical – corrosion processes, e.g. electro lithography; biological processes, e.g. chemolithographic bacteria processing and energy beam processes, e.g. electrical discharge machining (EDM). Among these processes, SPDT has dramatically improved over the past 2 decades to allow it to enter the nanotechnology regime [12] and the term ultra precision cutting has become synonymous with SPDT.

2.5.SINGLE POINT DIAMOND TURNING (SPDT)

SPDT produces a nanometer level surface finish, which is made possible in part by the extremely small material removal rate achieved with micrometer level uncut chip thickness on a highly rigid, precise and environmentally controlled ultra precision machine tool. Single crystal diamond tools [14] have high hot hardness and toughness and are the only material available that retain the nanometric edge sharpness which is necessary for realizing the small scale of cutting.

The quality of the diamond tool is important. The diamond must have minimal point defects [15]. Conventional polycrystalline diamonds with edge

accuracy from 4 μm to 6 μm are not appropriate for this application. The cutting tools need to have a cutting edge radius down to 150 nm or better, which can only be achieved by honing natural or synthetic single-crystal diamonds. The orientation of the diamond must also be carefully controlled in order to align the maximum direction of the cutting loads with the orientation that provides the highest strength. Diamond tools with {110} crystallographic orientation at the rake face yield longer tool life and greater wear resistance compared to those with {100} and {111} orientation at the rake face. But the surface finish was found to be not affected by the crystallographic orientation. In addition to the sharpness of the cutting edge, the waviness of the tool also plays an important role in machining complex surfaces. Figure 2-6 shows the trace of a controlled radius tool with overall waviness of 50nm and uncontrolled radius tool with waviness of 420 nm.

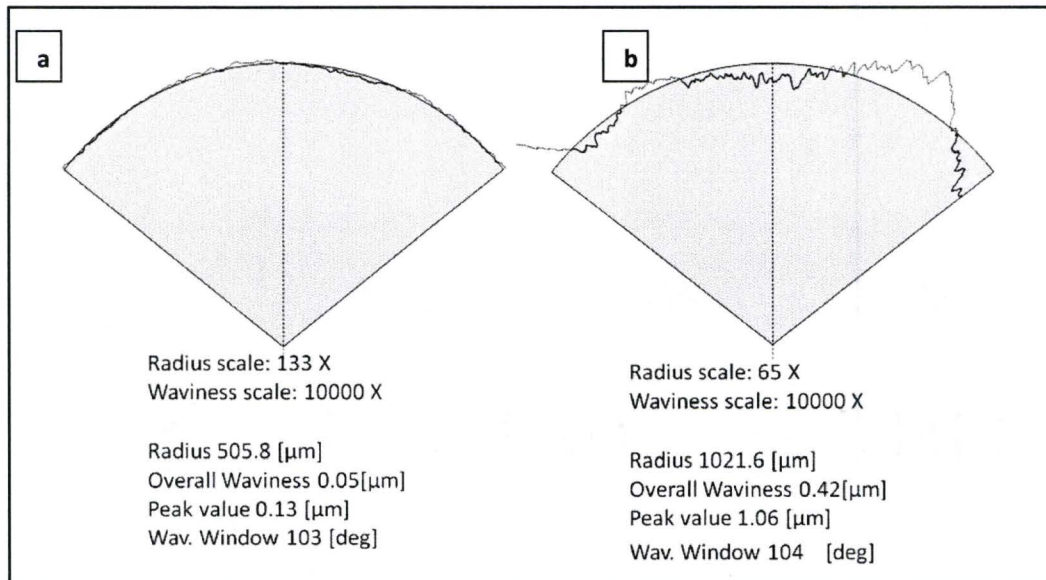


Figure 2-6: (a) Controlled radius and (b) uncontrolled radius SPDT tools (K-Y Diamond)

Waviness is the amount of deviation from a true circle, measured from peak to valley and should be smooth and shallow. Controlled waviness tools are required for machining complex contour surfaces where a deviation in tool nose radius will result in surface form errors on the component with a curved surface as the cutting contact point moves along the nose radius of the tool.

2.5.1. SIGNIFICANCE OF CUTTING EDGE RADIUS

The arc or the radius at which the flank face and the rake face of the tool meet is called the cutting edge, as shown in Figure 2-7. The sharpness of this arc is called the cutting edge radius which is generally in the range of 50 to 150 nm for SPDT applications. The nose radii of the tools, used in this study are between 0.3 and 1.5 mm. The nose radius is generally chosen to be large to provide the cutting edge with strength and improve the surface finish generated by multiple passes of the tool.

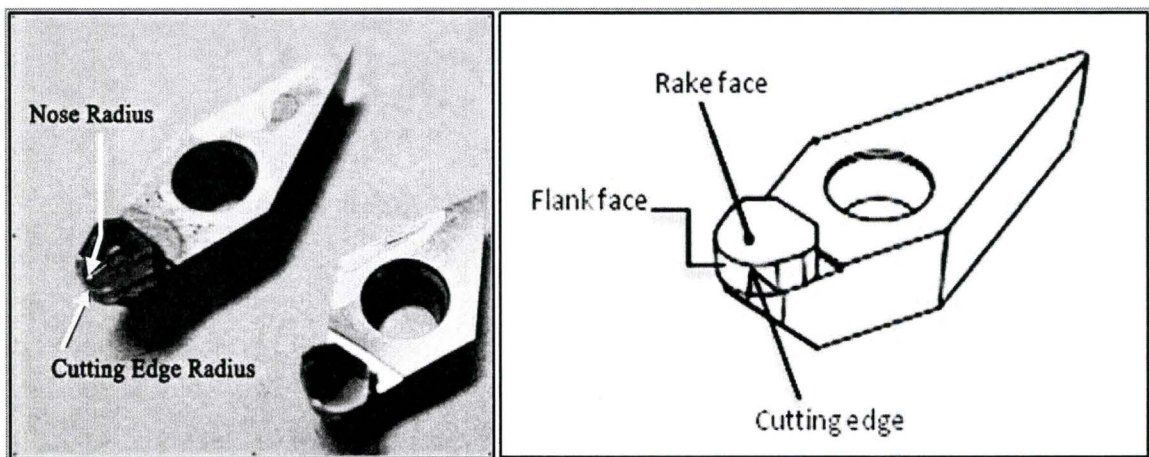


Figure 2-7: Tool geometry of a diamond tool.

For conventional machining the uncut chip thickness is generally orders of magnitude larger than the cutting edge radius. This effectively makes the cutting

edge sharp. In contrast ultra precision machining has an uncut chip thickness and cutting edge radius at comparable values which leads to a different cutting mechanism [16] as outlined below in Figure 2-8.

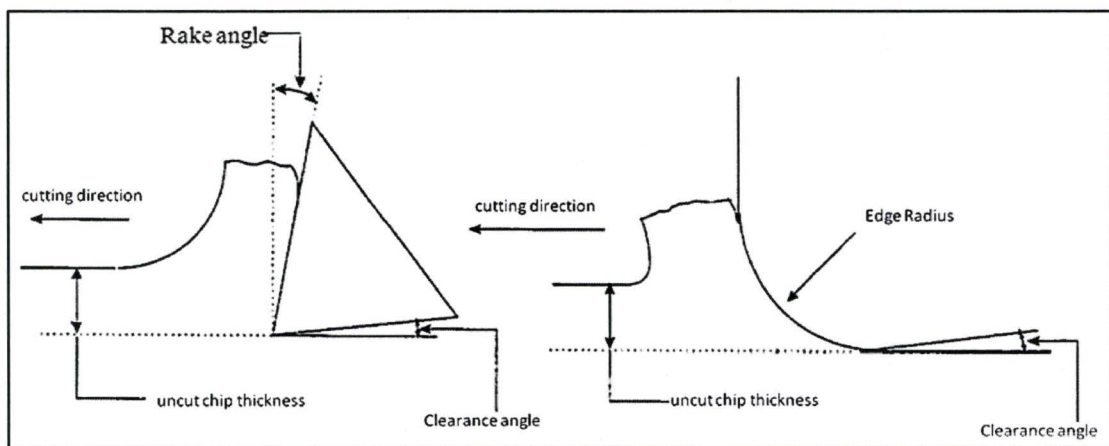


Figure 2-8: Schematic showing (a) conventional and (b) ultra precision cutting

Chae, J et al. [17] classified the scale of machining based on the uncut chip thickness of the cutting operation. The difference in the scale of cutting and the significance of the cutting edge radius is shown in the Table 2-2 below.

Table 2-2: Cutting edge radius Vs uncut chip thickness

Mechanical machining	Macro scale cutting	Microscale cutting	Nano scale cutting (Ultra precision machining)
Cutting edge radius	> 10 μm	8-10 μm	0.05 - 0.15 μm
Uncut chip thickness	> 500 μm	20-100 μm	0.5 - 1.5 μm

It has been shown that the surface roughness, strain hardening, residual stress and the dislocation density of the machined surface were largely affected by the sharpness of the cutting edge [18]. The sharpness of the cutting edge and the mechanical properties of the workpiece material determine the critical minimum uncut chip thickness, below which a ploughing mechanism occurs rather than a shearing mechanism. Ploughing is a less efficient process that is more energy intensive than shearing and affects the quality of the surface machined. In this case material is pushed outside of the cutting zone instead of being sheared off resulting in a rough surface. The critical minimum thickness of cut would affect the chip formation as well in SPDT [19].

Jeong et al. [20] introduced an orthogonal round edge cutting model for ultra precision machining, which considers the cutting edge radius and elastic recovery to quantify ploughing along the rounded edge and sliding on the clearance face. The authors compared their results with that of Merchant's conventional cutting model. In Merchant's model shear occurs along a shear plane and friction occurs along the rake face of the tool with the assumption that the cutting edge of the tool is perfectly sharp as shown in Figure 2-9(a) [20]. In the so-called round-edge cutting model as shown in Figure 2-9(b), the uncut chip

thickness is of the same order as the edge radius of the single-crystal diamond tool. The two cutting models are contrasted below.

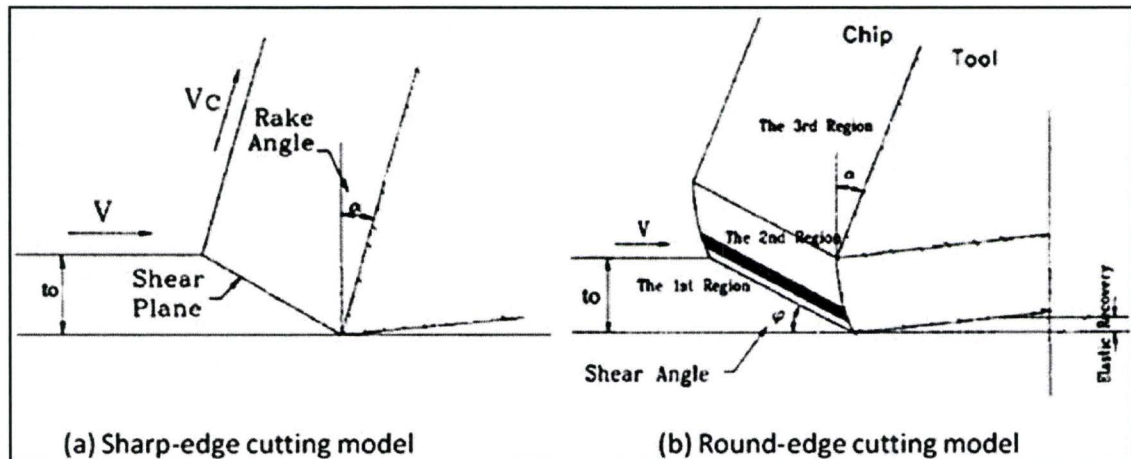


Figure 2-9: Cutting models (a) Sharp edge and (b) Round edge [20]

Jeong et al. concluded that, since the effective negative rake angle of the rounded edge of the tool and friction due to the elastic recovery of the workpiece at the clearance face takes place under $1\mu\text{m}$ depth of cut, micro-cutting takes place in this range. According to Simoneau et al. [21] micro cutting takes place at a point where the uncut chip thickness is less than the average grain size of the smallest grain type. It can be concluded that this rounded edge model is more appropriate for modeling an ultra precision cutting process compared to Merchant's sharp edge model.

2.5.2. CUTTING EDGE RADIUS AND TOOL LIFE IN SPDT

When modeling conventional machining the cutting edge is always considered being sharp to simplify the analysis. This is generally a reasonable assumption. Also, the chip flows on the rake face where crater and galling wear forms. The interaction between the tool and the workpiece takes place at the flank face. Wear on the flank face of the tool affects the surface roughness which is generally in the range of a few micrometers. The ISO standard for tool life typically states that a tool is no longer usable once the flank wear reaches 300 microns.

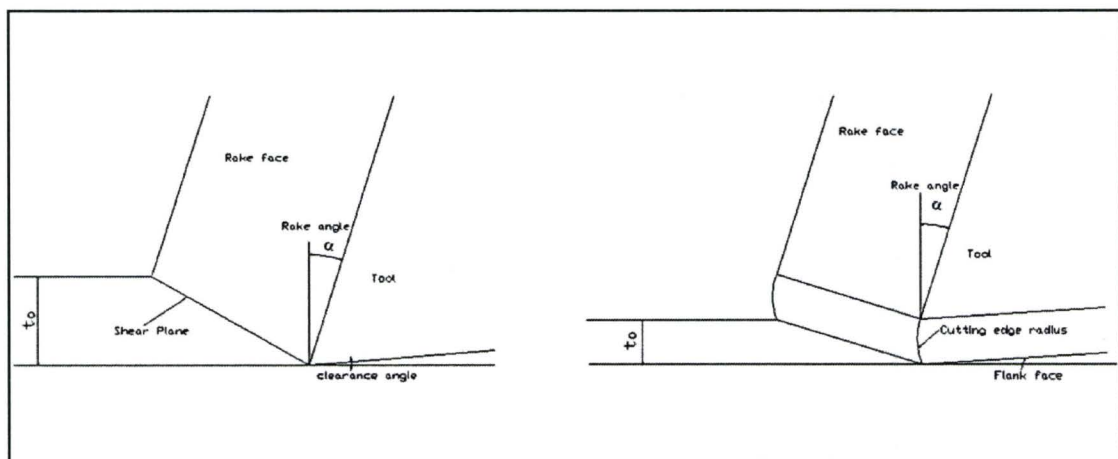


Figure 2-10: Schematic showing effect of edge radius in (a) conventional cutting and (b) SPDT

But from Figure 2-10b it is evident that unlike conventional machining (Figure 2-10a), in SPDT the wear at the cutting edge is more significant than flank wear. The uncut chip thickness in SPDT is on the range of 0.5 to 1.5 μm . Thus tool-chip, as well as tool-workpiece interactions takes place predominantly in the cutting edge region versus the flank or the rake face of the tool. Thus, the tool wear in SPDT is typically localized to the cutting edge region rather than in the rake or flank face, as in conventional machining. As such there are no international standards for measuring tool life in SPDT. Measuring the cutting edge wear instead of the standard flank wear would be more appropriate, however this requires a precise way of measuring the sharpness itself which given the dimensions involved is very difficult.

2.5.2.1. Challenges in measuring the cutting edge radius

Single crystal diamond tool manufacturers generally certify that the tool has no visible cracks or defects near the cutting edge at x800 magnification. Unlike the standard specifications such as the nose radius, rake angle and clearance angle, the cutting edge radius is not typically provided, as performing a non-destructive measurement of the edge radius is not trivial.

The work of Asai et al. [22] has shown that the cutting edge radius could be accurately estimated using a SEM. The SEM used in his application contained a pair of secondary electron detectors. Also, a confocal laser-scanning microscope was used to determine the cutting edge radius [23]. However, charging effects present with uncoated tools and the potential of non-uniform conducting coating thickness, which is required for the SEM to function, limit the accuracy of these results. Other profiling instruments such as a white light interferometric microscope and step height profilometer, which can vertically resolve atomic scale features, are limited by their spatial resolutions [24]. The main facilities currently used for measuring the cutting edge radius are the SEM and the atomic force microscope (AFM).

Li et al. [25] proposed a non-destructive nano-precision measurement method for tool edge radius measurement. They copied the profile of the tool cutting edge by indenting the edge on the surface of selected materials with the copied profile then measured using an AFM. However spring back effects of the indented material may lead to significant errors and thus, requires extensive study. Gao et al. [26] developed a special instrument with an AFM assembly consisting of an AFM scanner and an AFM cantilever, the later making use of

three PZT actuators, an optical probe assembly and a micro-tool assembly to measure the cutting edge radius. The time for mounting and aligning the AFM cantilever and the tool was approximately 20 minutes and that for measuring the 3D cutting edge profile of the tool was approximately 3.5 min. This could be useful as a dedicated apparatus for single-crystal diamond tool manufacturers and suppliers to precisely measure the edge radius and also the edge roundness of the ultra precision tools. The author's attempts to measure the cutting edge radius are further explained in Chapter 4.

Due to the challenges associated with the precise measurement of cutting edge radius, an alternate way of measuring tool life in SPDT was considered. In this case the cutting length that can sustain a certain surface finish quality was reported. In this way the final effect was measured, as opposed to the underlying cause which is the tool wear.

2.5.3.CUTTING SCALE AND MACHINING PROPERTIES

As seen in the above section 2.5.2, due to the reduced scale of cutting the need for an ISO standard for tool life measurement in SPDT was identified.

Similarly direct scaling of macro-knowledge related to machining was not successful to the micro and nano-domain and is mainly attributed to size-effect in many instances. Size-effect is the increase in specific cutting energy with the decrease in the deformation size. The microstructure of the workpiece material, cutting tool material and the cutting parameters all affect the material removal process. Furthermore the size-effect plays a significant role in ultra precision machining given that the uncut chip thickness are typically 0.5 to 1.5 μm which is on the same order as the grain size for the titanium alloys being considered.

2.5.3.1. Influence of workpiece material microstructure on size-effect

In SPDT, the minimum chip thickness depends on the cutting edge sharpness and the physical and mechanical properties of the material being cut. In micro and nano scale machining, the nature of the workpiece must be considered in order to fabricate parts with high accuracy, since the uncut chip thickness could be less than the grain size in the workpiece material. The assumption of homogeneity in workpiece material properties is no longer valid. Since the micro-grain structure size is often of the same magnitude as the edge radius, the grain structure will have a large effect on the overall cutting properties. This is a distinct difference between micro / nano and conventional

macro mechanical cutting [17]. Simoneau et al., after examining the chip formation process defined microscale cutting, as the point where the uncut chip thickness is less than the average grain size of the workpiece material [21]. Based on the dimensions involved in SPDT this is the regime that this process is operating under.

All metals contain defects such as grain boundaries, missing and impurity atoms. As a result, when the size of the material removed decreases, the probability of encountering a stress-reducing defect within the small region in front of the cutting zone decreases as well (Figure 2-11).

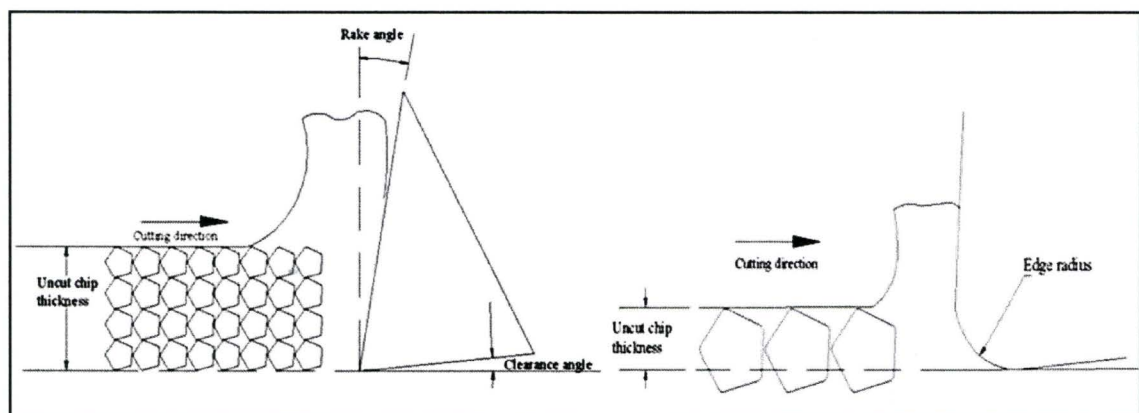


Figure 2-11: Material removal in (a) macro scale machining and (b) nano scale machining

When metallic single crystals were plastically deformed, it was found that slip does not occur uniformly on every atomic plane but only on active slip planes, which are relatively far apart. Polycrystalline metals also strain block-wise and crystal imperfections are responsible for this inhomogeneous behaviour. When the volume of material deformed at any given time is relatively large, there is a uniform density of imperfections and for all practical purposes, strain and strain hardening may be considered to be uniform. However, as the volume deformed approaches the size of an imperfection or defect, the material behaves inhomogeneously resulting in a higher specific cutting energy.

2.5.4. INFLUENCE OF SIZE-EFFECT ON TOOL WEAR IN

SPDT

As discussed above, the size-effect can be used to explain the substantial increase in the specific cutting energy (u). If the specific cutting energy increases substantially, the energy at the shear plane and the friction at the tool face also increases. Given the size of the chip and extremely small contact length between the chip and the tool a localized high cutting temperature will result closer to the cutting edge (ref. Figure 2-9b) in an extremely small area on the order of 10^{-5}

mm² [27]. This localized high cutting temperature and high normal stress contributes to the accelerated tool wear in SPDT of difficult to machine materials.

2.6.TOOL WEAR MECHANISMS IN SPDT

Currently SPDT is successfully used for copper alloys, aluminum alloys, silver, gold, electroless nickel and PMMA (Polymethyl-methacrylate) plastics. However, extension of this technology to advanced materials like titanium has not been well investigated. This is attributed to the excessive wear rate of the diamond tool in this application. The wear of diamond tools in ultra precision machining has been the subject of many studies and is still not well understood. Several different mechanisms such as mechanical, thermal, chemical and possible electrical effects can contribute to diamond wear with multiple mechanisms at work under some circumstances. However, the predominant wear mechanism will depend on the material properties and cutting parameters [28].

Evans et al. [29] has discussed the wear mechanisms in three categories (a) adhesion and formation of a built-up edge, (b) abrasion, micro chipping, fracture and fatigue and (c) tribo-thermal and tribo-chemical wear. The dominant wear mechanism reported in commercial aluminum alloys, is abrasion and

chipping caused by impurities on the grain boundaries. Adhesion between clean surfaces may also be a significant tool wear mechanism [30]. It can be observed from Figure 2-12, that the wear mechanism that operates in the widest range of cutting temperatures is the adhesion mechanism.

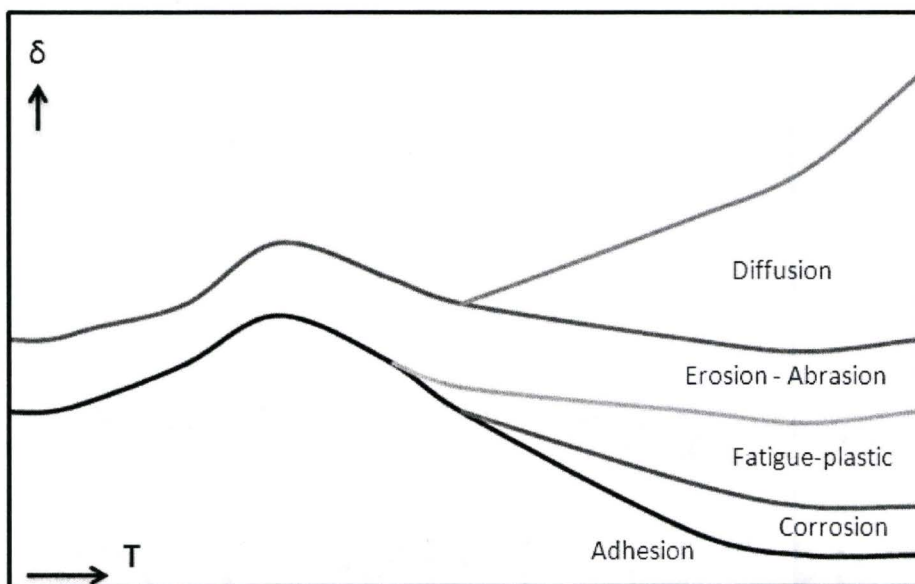


Figure 2-12: Wear mechanism as a function of temperature [31]

The tool wear (δ) takes place by the adhesion of microscopic fragments of the workpiece material on the tool surface [31]. These built-up fragments are mechanically unstable and thus could get pulled off the cutting edge as the cutting action continues. When this happens, there is a possibility that tool material will also be pulled out of the cutting edge of the tool [32] leading to

catastrophic failure. In SPDT, when a diamond tool is new and sharp, conditions on the rake face are much more severe than that on the flank face. Temperature and normal stress are very high and the rake face constitutes a heavily loaded slider [33].

In SPDT of titanium alloys, as the cutting distance increases, the cutting edge recedes and the flank wear becomes dominant. The resulting flank wear results in a loss of the clearance angle, which gives rise to increased friction. The flank face is normally a loaded slider with maximum temperature at the edge which increases with flank wear [33]. The wear rate rises abruptly when the temperature at the cutting edge of the tool reaches the thermal deterioration point of diamond.

The thermal deterioration under these circumstances involves the diamond-graphite transformation at high temperature, high stress [34] and the chemical reaction between carbon, oxygen and the workpiece material, which can often serve as a catalyst for graphitization. Subsequently the deteriorated layer at the trailing edge drops off due to the rubbing force between the tool and the workpiece, forming step structures on the wear land. This kind of wear is

catastrophic and will lead to the total destruction of the tool. The flank wear land also causes unacceptable form error in the finished workpiece surface and can induce unwanted surface micro-fractures.

2.6.1. CHEMICAL WEAR IN DIAMOND TOOLS

In applications involving the machining of steel [29, 35, 36] chemical aspects combined with mechanical interaction between carbides and the tool edge causes wear. Chemical wear can be distinguished by examining the surface of the worn tool [37]. The chemical wear theory proposed by Ed Paul et al. [11] identifies that materials with unpaired d-electrons generate high rates of tool wear during SPDT. Figure 2-13 shows the electronic configuration of Ti with 2 unpaired d-electrons, Al with no unpaired d-electrons and Fe with 4 unpaired d-electrons.

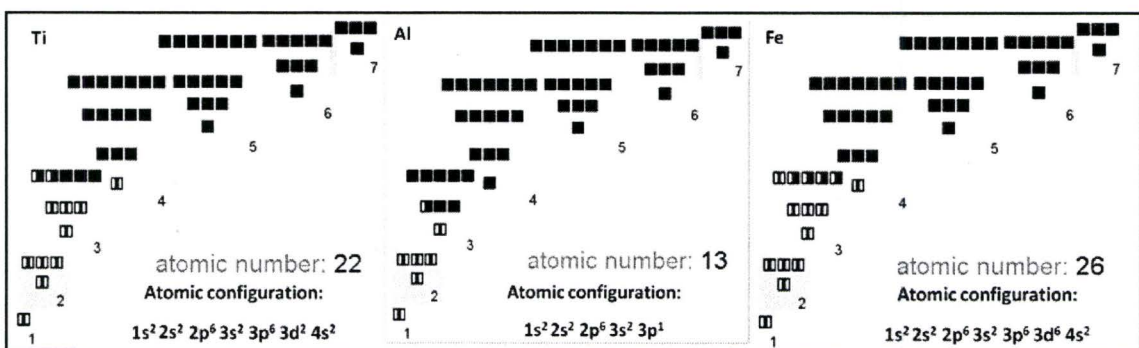


Figure 2-13: Electronic configuration of Ti, Al and Fe.

Thus the theory is that the unpaired d-electrons in the workpiece react with diamond in order to complete its valance shell. The carbon atoms from the diamond lattice are pulled to pair with the unpaired d-electrons of the workpiece material. This is how the unpaired d-electrons facilitates carbon-carbon bond breaking in diamonds followed by metal-carbon complex formation, leading to chemical wear of diamond tools.

It was postulated that metals with a greater number of unpaired d-electrons may cause an increase in carbon atom removal leading to an increase in wear. Table 2-3 provides data on various materials, including the number of unpaired d-electrons. The table also notes if the material is machinable with diamond.

The authors also confirm the theory that wear tends to be directly proportional to the number of unpaired d-electrons. There is a substantial correlation between the number of unpaired d-electrons, melting point and crystal structure. In particular, elements with no unpaired d-electrons tend to have a lower melting point and many unpaired d-electrons lead to a higher melting point. It was found that materials with a low melting point are diamond

turnable and those with a higher melting point are generally not. It was also noted that the hardness in transition metals also correlates with the number of unpaired d-electrons.

Table 2-3: Data for elements with known diamond turning properties [11]

Element		Melting point °C	Crystal structure	Microhardness		No.of unpaired d-shell electrons	Diamond Turnable?
				Brinell	kg/mm ²		
In	Indium	157	t	0.022	10	0	Y
Sn	Tin	232	f		9	0	Y
Pb	Lead	373	f		5	0	Y
Zn	Zinc	420	h		51	0	Y
Pu	Pluotonium	640	m			0	Y
Mg	Magnesium	649	h	30	48	0	Y
Al	Aluminum	660	f		25	0	Y
Ge	Germanium	937	d		721	0	Y
Ag	Silver	962	f		96	0	Y
Au	Gold	1064	f		96	0	Y
Cu	Copper	1083	f		76	0	Y
U	Uranium	1132	o	245		1	N
Mn	Managanese	1244	b		384	5	N
Be	Beryllium	1277	h	60		0	Y
Si	Silicon	1410	d		1211	0	Y
Ni	Nickel	1453	f		189	2	N
Co	Cobalt	1495	h	100	247	3	N
Fe	Iron	1535	b	50		4	N
Ti	Titanium	1660	h	75	142	2	N
Cr	Chromium	1857	b	63	250	5	N
V	Vanadium	1890	b		248	3	N
Mo	Molybdenum	2617	b		192	5	N
Ta	Tantalum	2996	b	70		3	N
W	Tungsten	3410	b		348	4	N

f -fcc, b -bcc, h-hcp, d-diamond, m-monoclinic, o-orthorhombic, t-tetragonal

Chemical wear of diamond tools has been observed experimentally for many alloys. The results [38, 39] agree with the unpaired d-electron theory. For most alloys, the behavior reflects the parent material. Thus, in terms of chemical wear, aluminum alloys are generally diamond turnable, as are copper based alloys such as brass and beryllium copper. Ferrous steels, with unpaired d-electrons are not generally diamond turnable. That steels shows less tool wear than iron, despite being harder, is attributable to the presence of carbon atoms in the alloy. These atoms complex some of the unpaired d-electrons in the iron and reduce their availability to complex with the carbon atoms in diamond.

Another example is Ni which has two unpaired d-electrons and is generally considered to be not diamond turnable; however electroless nickel is diamond turnable. Electroless nickel is actually a nickel phosphorous alloy in which the unpaired d-electrons from the nickel atoms become paired with the p-electrons from the phosphorous atoms. Since the resulting alloy has fewer free unpaired d-electrons, it forms fewer complexes with the carbon atoms in the diamond tool and the chemical wear is substantially reduced. Designer alloys, containing metal atoms whose d-electrons are taken by alloying atoms, such as phosphorus or

boron, might have metallic properties yet still can be considered as diamond turnable.

The theory implies that the number of unpaired d-electrons in materials being diamond turned is significant as well. The rate of tool wear in SPDT is directly proportional to the number of unpaired d-electrons in the workpiece material. Paul et al, also reported this observation experimentally as the wear of cerium, titanium, and iron increased respectively with one, two and four unpaired d-electrons each. Thus, for metals with only one unpaired d-electron (such as Ce and Pt) the implication is that, although there should be some chemical wear, the wear rate may be low enough to make machining cost effective if a high-precision surface is needed for a particular application. The experimental result shows that Mo, with five unpaired d-electrons, is much more strongly attached to the carbon atoms in diamond tools than Ti, Zr, V, or Co, with fewer unpaired d-electrons. Materials with many unpaired d-electrons are predicted not to be diamond turnable.

Chemical wear of diamond tools in SPDT occurs when the carbon atoms are pulled from the tightly bonded diamond lattice. Once an atom leaves the

diamond, it may graphitize or diffuse into the chip, or react with oxygen to form CO or CO₂. If the carbon is diffused into the chip it may form a carbide with the workpiece material. Each of these processes is preceded by carbon-carbon bond-breaking.

2.6.1.1. Graphitization

Bundy et al. [40] has postulated that the atoms that evaporated from the diamond surface recondense into disordered graphitic aggregates. This two-stage mechanism is unlikely for a perfect crystal because of the very large vaporization energy of $E=57.6$ eV/atom, but is very probable for a crystal with surface defects and stacking faults with an estimated energy barrier of about 0.3eV/atom. Another model for the diamond-graphite phase transition was offered by [41] Kern and Hafner. Their molecular dynamics simulations showed that at high temperatures the top layers at the surface of diamonds could be lifted from the crystals. Once the interlayer bonds are disrupted, the upper layer flattens rapidly to form a graphitic crystal structure. Further reaction proceeds along the direction perpendicular to the surface leading to graphitic nanocrystallites embedded into the diamond. This scenario is the most likely model for the mechanism of transformation as shown in Figure 2-14 [42].

A direct transition from sp^3 bonding to sp^2 bonding is observed instead of a two stage transition where carbon atoms sublime and condense into a graphitic structure, as proposed by Davies and Evans [43]. De Vita et al. [44] have reported that when the graphitization process occurs graphitic micro-crystals could form at the diamond surface by a direct transformation in spite of the dissimilarities between the structural and electronic properties of diamond and graphite.

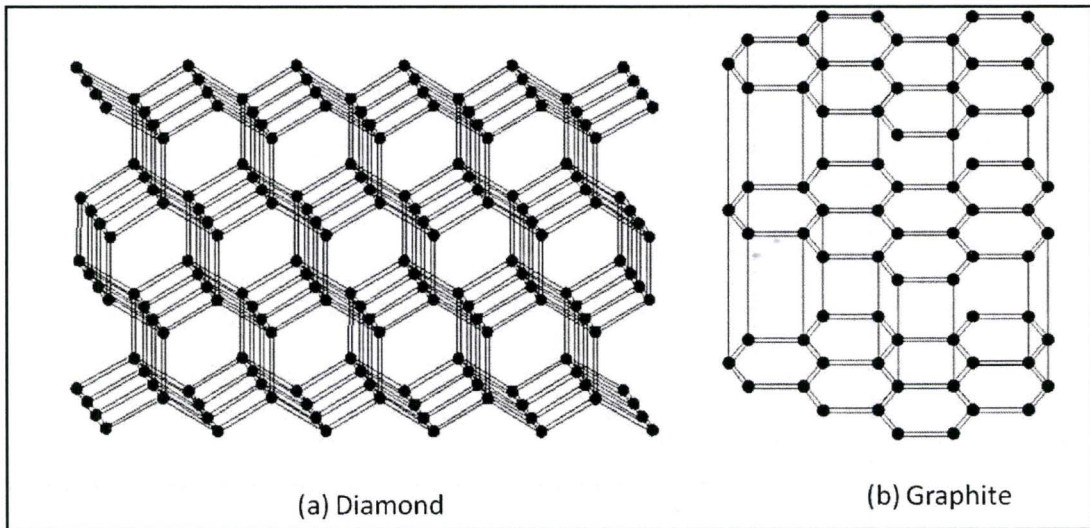


Figure 2-14: Diamond to graphite transformation – Graphitization

The chemical wear rate of the diamond tool depends upon the probability of a carbon atom leaving the diamond matrix. Some studies [14, 45] assert that graphitization of diamond must precede diffusion, because carbon atoms are held so much more tightly by the diamond lattice than by graphite structures.

Graphite formation i.e. graphitization is the most commonly cited result of diamond wear. The presence of oxygen would facilitate oxygen-metal-carbon complex formation thus accelerating the wear rate as opposed to oxygen deficient environments, which tend to suppress such chemical activity. The activation energy for the diffusion mechanism is smaller than for graphitization. Furthermore the activation energy for graphitization increases at a greater rate than diffusion with an increase of temperature. Thus, the diffusion mechanism becomes less dominant at higher temperatures and the graphitization mechanism dominates [45]. It should be noted that the amount of graphite formed is significant in terms of cutting edge wear but not enough to enhance the lubricity at the cutting zone. Also, the graphitized carbon reacts with the chips to form TiC.

For machining of transition metals of the groups IVa-VIa such as Ti and Ni, carbide formation occurs at the tool-workpiece interface [46]. In the contact zone between the tool and workpiece a complex interaction of sliding surfaces takes place including abrasive, chemical and adhesive wear components. Figure 2-15 shows the process of machining a transition metal alloy with a single crystal diamond tool. In this case, the chemical reaction leads to the transformation of

diamond to graphite (i.e. graphitization), which is the stable form of carbon under the conditions experienced in the cutting zone.

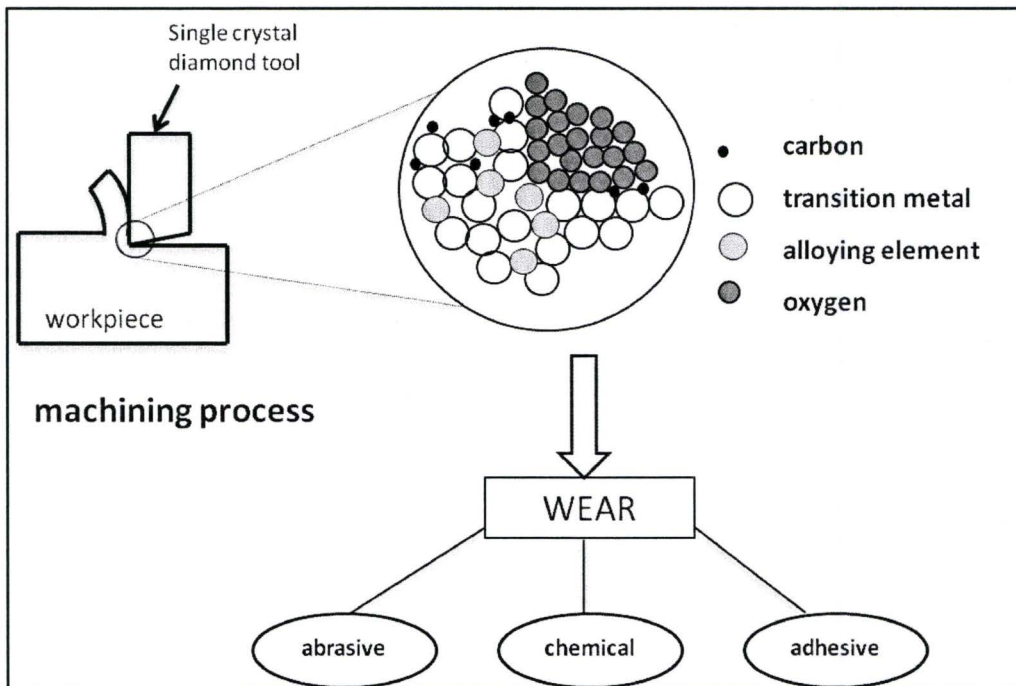


Figure 2-15: Schematic of SPDT of a transition metal & wear components in atomic scale [46]

Narulkar et al. [42] used Molecular Dynamics (MD) simulations to provide evidence for the diamond-graphite transformation i.e. graphitization and suggested that could be the principal mechanism of tool wear of single-point diamond turning of ferrous materials. Jiang Qian et al. confirmed that contact pressure is another important parameter in the diamond to graphite transformation. Thornton and Wilks [47] observed high rates of tool wear owing

to graphitization of the diamond and they found that under certain conditions, such as high load, graphitization may proceed at a considerable rate even if there is no appreciable temperature rise.

It was postulated that under appropriate conditions of pressure and temperature diamond at room temperature, which is in a metastable state of sp^3 bonding will transform into graphite - sp^2 bonding. It was observed that graphite ultimately breaks down because of the shear stress acting along the cutting edge and subsequently enters the workpiece where it diffuses or forms carbide over a longer time scale [48]. Ti also, acts as a catalyst for the graphitization process [48, 49] and synthesises TiC with Ti and graphite under high temperature and pressure [46, 50].

But in the case of SPDT of brittle materials such as Si, cleavage fracturing occurs, forming micro craters in front of the cutting edge [51]. The micro craters make the cutting process intermittent and cause micro impacts. These micro impacts will take place at a very high frequency, leading to tool edge chipping. [52-54]. The wear mechanisms of a single point diamond tool in machining different materials, as reported by some researchers, are compiled in Table 2-4.

Table 2-4: Literature review on tool wear of single point diamond tools

Ref. No.	Workpiece material	Wear mechanism	Explanation
[55]	Ferrous metals	Thermo-chemical reaction. Two different mechanisms depending on the ambient temperature.	Temperature > 1000 K - dissociation of carbon atoms from diamond surface by the interaction with iron atoms and removal of the carbon from the tool-workpiece interface. <i>Wear rate controlled by the removal rate of carbon.</i> Temperature < 900 K - the mechanism involves the removal of carbon atoms due to oxidation accompanied with deoxidization of iron oxide.
[56]	Steel Moulds	Chemical wear with unpaired d-electrons	Workpiece modifications of steel and steel alloys by nitriding, where all iron atoms are bonded with nitrogen atoms. Chemical tool wear can be prevented by thermo-chemical modification of the surface zone of the workpiece in a way that the chemical reaction between the carbon atoms of the diamond lattice and the iron atoms in the w/p cannot take place.
[57]	Nickel and electroless Nickel	Chemical reactivity	Ni-P wear 1000 times less than pure Ni wear. Phosphorous reduces the chemical reactivity of the 3d electron levels responsible for strong interaction between w/p and diamond.

Ref. No.	Workpiece material	Wear mechanism	Explanation
[58]	Amorphous polymers	Tribo-chemical tool wear	Chain scission that results in highly reactive radicals that are the main active particles that initiates chemical transformations.
[59]	Nano-scale ductile cutting of silicon	Crystallographic orientation	Diamond tools with {110} crystallographic orientation at the rake face yield longer tool life and greater wear resistance compared to those with {100} and {111} orientation at the rake face. But the surface finish was not affected by the crystallographic orientation.
[11]	Transition metals, iron, single crystal silicon	Chemical wear	Metals with unpaired d-electrons shown excessive tool wear by forming carbon-metal complexes. <i>Inert atmosphere and cryogenic cutting may reduce the wear rate</i>
[28]	Single crystal silicon	Micro chipping and wear depending on undeformed chip thickness	High uncut chip thickness in brittle mode machining lead to edge micro chipping. Lower uncut chip thickness in ductile mode machining, gradual wear caused by thermal deterioration and chemical reaction. Thermal wear - diamond-graphite transformation at high temp, chemical wear - between carbon, silicon and oxygen.

Ref. No.	Workpiece material	Wear mechanism	Explanation
[37]	Electroless-nickel plated die material	Under investigation	Electroless nickel - chemically inert - high wear resistance
[46]	Ni and Titanium based coatings	Ni-P and Ti-N, NiTi	Presence of P in Ni and N in Ti leads to complex hybridization with parent metal's valence orbital so that the thermally activated reaction of the workpiece material with carbon atoms of diamond can be suppressed. A transition metal can be made diamond turnable by adding a suitable element forming covalent bonds thus reducing chemical wear and other forms of wear.
[60]	TiN _x , TiAlN _x , CrN _x coatings		Varying levels of nitrogen content were deposited by magnetron sputtering. The best diamond-turning results were achieved with TiN _x . Dissolving nitrogen into α-titanium leads to lattice widening and reduced grain size thus improving the tool life.

Tool wear in SPDT will cause the loss of original edge profile and sharpness and so degrade the machined form accuracy [61].

The following section discusses various methodologies to reduce tool wear in SPDT. The modifications are classified into 3 categories: (a) workpiece modifications (b) process modifications and (c) cutting tool modifications.

2.6.2.WORKPIECE MODIFICATIONS

To overcome the non-homogeneity in workpiece material, Weule et al. [62] suggested precision machining with a uniform workpiece material. In their research they quenched and tempered SAE 1045 steel with temperatures ranging from 180 to 600°C in order to obtain a homogenized workpiece. Thus, heat treatment of the workpiece could be considered to provide uniform micro-structural properties [17]. Care should be taken that the treatment should not affect the desired mechanical properties of the material for its intended applications.

In the workpiece modification approach, a modification of the chemical composition of the workpiece within a thin zone beneath the surface to be diamond machined was tested [56] for ultra precision diamond cutting of steel molds. In principle, this could be achieved by inserting group IV to VIII elements in the subsurface zone by a thermo-chemical process.

Brinskmeier et al. developed a nitriding process for the thermo-chemical modification of steel and steel alloys. The study observed that after the nitriding process, the surface zone of the workpiece material consisted of a layered structure. The nitriding was carried out on a heat treatable steel alloy. The compound layer was composed of two phases where the iron atoms were bonded to nitrogen atoms. The nitrogen content was approximately 8 wt% at the surface of the workpiece and 6 wt% at a depth of 12 μm . Single point diamond turning of the thermo-chemically modified steel exhibited a more homogenous texture and resulted in the reduction of tool wear by three orders of magnitude. The results demonstrated that SPDT is possible if the surface zone of the workpiece is thermo-chemically modified in a way such that chemical reactions between the carbon atoms of the diamond lattice and the atoms of the workpiece are minimized.

In contrast to pure Ni, as outlined earlier NiP_x coating material can be diamond machined with negligible tool wear. Kohlscheen et al. [46], studied the technique of coating steel with an electroless deposited NiP_x ($x \sim 0.25$). It has been suggested that the chemical behavior of the nickel atoms is changed by the presence of the phosphorus atoms due to interaction between the valence orbital of the two elements [57]. This might minimize the chemical wear component when SPDT NiP_x coatings because the interaction of nickel with carbon atoms from the diamond tool would be suppressed [46].

In addition to NiP_x , the transition metal/non-metal combination of Ti-N was also shown to be diamond machinable [60]. Kohlscheen et al. [46] also investigated the electronic valence configuration that is responsible for such chemical reactions to understand the effect of reactivity and its impact on diamond tooling interactions. The investigation of the valence states between 0 and 20eV binding energy of the electrons was done by X-ray photoelectron spectroscopy (XPS). The measurements were compared to calculate binding states of the molecular cluster using Gaussian software. In order to describe the bonding in the highly sub-stoichiometric fine crystalline TiN_x coating, a hexagonal

cluster consisting of 1 N and 13 Ti (Ti_{13}N , corresponding to 7 at.% nitrogen) was calculated with the Gaussian software package – DMol [46].

The results validated the assumptions that filling the Ni-3d valence band is a simplified model. It suggests that a chemical deactivation of the nickel valence states was enabled by sufficient covalent bonding, so that a reaction with the carbon atoms of diamond is suppressed. A XPS valence band spectrum of Ti and $\text{TiN}_{0.1}$ was compared to the electron states of a Ti_{13} and Ti_{13}N cluster. For pure Ti the XPS measurement yields the Ti-3d band at approximately 1eV and the spectrum of the $\text{TiN}_{0.1}$ coating shows a significantly decreased Ti-3d band. The thermal contact test of TiN_x surfaces with diamond was reported and the EDS analysis of the surfaces revealed strong roughening of diamond with the almost pure Ti coating, whereas smooth surfaces were visible with coatings containing N ($\text{TiN}_{0.1}$) and EDS analysis showed no visible traces of Ti on the diamond surfaces. Fine crystalline structure, ductility, anti-adhesive and chemically inert properties of the TiN_x coating has been found to be favourable for SPDT [46].

Based on the above discussions, it could be concluded that sufficient covalent bonding between Ti and N valence orbital deactivated the Ti valence

electrons, so that the chemical reactivity of Ti atoms with the C atoms of diamond could be minimized.

2.6.3.PROCESS MODIFICATIONS

Ferrous alloys cannot be directly diamond turned due to excessive tool wear. It has been reported that ultrasonic vibration assisted cutting solves this issue [36]. Ultrasonic vibration of 40 kHz when applied to the single crystal diamond tool in the cutting direction has produced a surface roughness of 30 nm R_{\max} in steel. Brehl et al. [63] have noted that vibration assisted machining in SPDT has extended the tool life for all types of tools cutting ferrous and hard metals and brittle materials like Si and glass and also metal matrix composites with reduced surface roughness and improved form accuracy. It has been postulated that diamond tool life was extended by vibration assisted machining because the intermittent tool-work contact time may minimize the probability that thermochemical wear mechanisms are operating [64-69].

For conventional machining significant research has been done to modify the nature of coolant application. In machining operations coolant is used to both lubricate and reduce the temperature at the cutting zone. Given the

geometries, forces and temperatures involved it is very difficult to get coolant into the contact zone. The effectiveness of the coolant is greatly determined by its ability to meaningfully be engaged in the cutting zone. Thus, significant process development work has gone into exploring different coolant liquids and application methods.

In conventional machining, high pressure coolant has been effectively applied to reduce cutting temperature. This has resulted in an improvement in the machinability of Ti and other advanced materials. However, the cooling capacity of high pressure coolant has not always met the industry needs of ultra precision machining due to the high mechanical and thermal shock loads that the fluids impart on the workpiece and tool. These loads will vary over time due to the complex dynamics of fluid flow and result in significant dimensional accuracy issues for the part.

Liquid nitrogen (LN_2) coolant has stronger cooling effects than high pressure cooling and the temperature dependent tool wear reduced significantly in tests conducted when traditionally machining steels and Ti alloys [70].

Evans [29] and Li [25] independently proposed reducing the energy input into the system. Li has used LN₂ as a coolant and reported a substantial reduction in tool wear. Evan's proposal was to chill the tool or workpiece independently. Evans [29] from his cryogenic tests on SPDT of 440 stainless steel concluded that the tool life was significantly improved at cryogenic temperatures and both diffusion and catalyzed graphitization rates were decreased at these lower temperatures.

As discussed earlier, Ti and its alloys are poor thermal conductors. As a result, the heat generated when machining Ti cannot dissipate quickly; rather, most of the heat is concentrated on the cutting edge and tool face. Also the chemical reactivity of Ti increases aggressively with an increase in the cutting temperature. Thus, most cryogenic machining studies on Ti and its alloys have documented improved machinability when freezing the workpiece or cooling the tool using a cryogenic coolant. In the past, common cryogenic machining cooling approaches have included: (1) pre-cooling the workpiece, (2) indirect cooling, (3) general flood cooling and (4) an enclosed bath. Hong et al. [71] proposed a new approach for cryogenic machining of Ti-6Al-4V by introducing specially designed micro-nozzles to supply LN₂ to the tool rake and to the tool flank to reach and

effectively cool the localized “hot-zones” in the cutting area with a minimized LN₂ consumption. This new economical cryogenic machining approach that used LN₂ jets focused on the cutting region significantly improved the tool life in macro machining [72].

Paul et al. [73] observed the role of cryogenic cooling in machining AISI 1060 steel using carbide inserts and concluded that cryogenic cooling by LN₂ jets provided reduced tool wear, improved tool life and surface finish as compared to traditional dry and wet machining processes. The beneficial effects of cryogenic cooling might be attributed to effective cooling and retention of tool hardness. LN₂ is highly effective when it is released to the chip-tool interface via a primary nozzle. This effectiveness could be further enhanced by positioning the chip breaker-nozzle so it can lift the chip, allowing LN₂ to reach the tool-work interface and to potentially form a fluid cushion [74].

Wang and Rajurkar [70] experimented macro-machining of Ti-6Al-4V with and without LN₂ using H13A cemented carbide tools. LN₂ coolant circulating through a sealed cap located on the top of the cutting insert to reduce the cutting temperature. Turning Ti-6Al-4V with the H13A insert with LN₂ produced

better surface quality ($R_a = 1.9\mu\text{m}$ for 108mm cutting distance) than that without LN_2 ($R_a = 15\mu\text{m}$ for 40mm cutting distance) and the tool life increased significantly (Figure 2-16). By changing the convection conditions surrounding the tool the temperature in the tool and workpiece was largely decreased which in turn has increased the tool life.

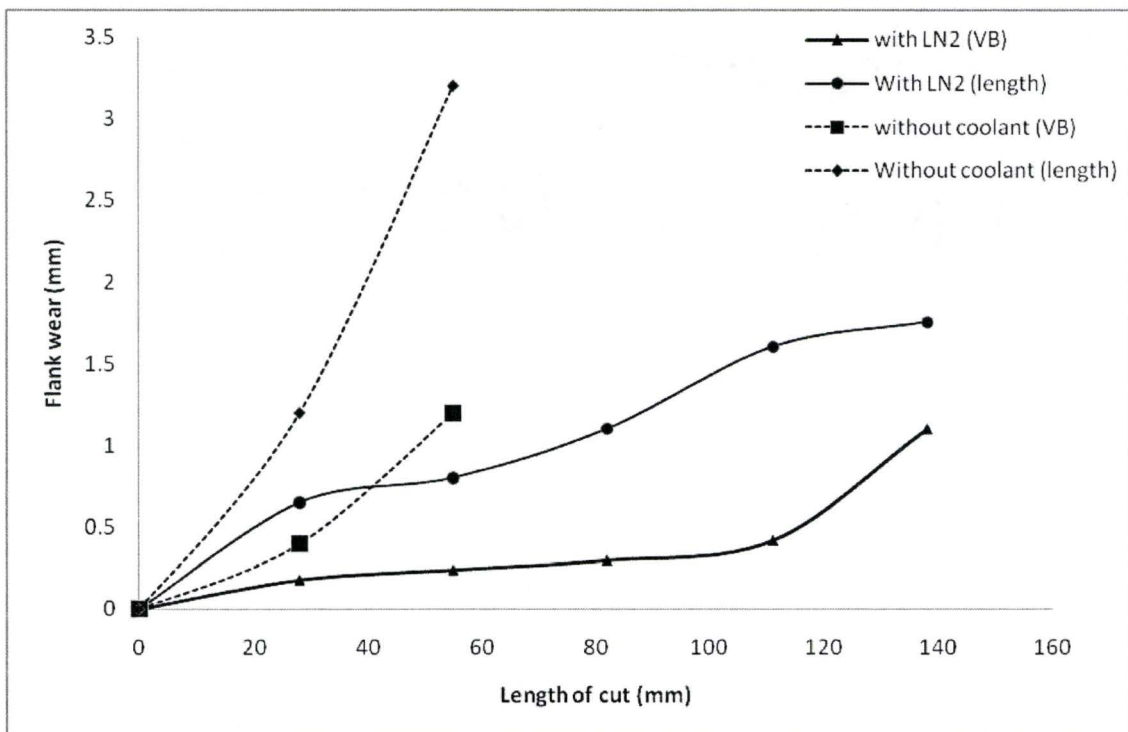


Figure 2-16: Tool wear in machining Ti-6Al-4V with and without LN_2 [70]

Venugopal et al. [75] tried TiB_2 -coated carbide tools in a turning operation with a Ti-5Al-5Mo-2Sn-V alloy with and without cryogenic cooling and concluded that TiB_2 -coated carbide tools are ineffective in machining titanium alloys, even

with cryogenic cooling. The reason given was the removal of the coating while cutting. However cryogenic cooling was found to improve the retention of the tool cutting edge radius sharpness, yielding reduced cutting forces. The extent of tool wear under cryogenic cooling was observed to be less compared to dry machining at the macro scale.

The main limitation with all of these coolant applications and cryogenic techniques in SPDT is the impact it has on the delicate temperature profile of the workpiece and the tool. Small changes in workpiece, tool or machine structure temperature on the order of 1-2°C can impact the dimensional accuracy of the final machined surface. Many of the higher heat removing methods are also difficult to control at this level making them less applicable to SPDT applications.

In ultra precision machining using slow feed rates, low surface speeds and small depths of cut, the highest temperatures are expected to be highly localized. In these circumstances, diffusion/dissolution may not be the dominant wear mechanism. Rather the significant mechanism is more likely to be the solid state catalytic graphitization as proposed by Hitchiner and Wilks [57]. The rate of chemical reactions increased exponentially with temperature.

Other techniques employed for reducing the cutting temperatures was MQL – minimum quantity lubricant. Due to the overwhelming environmental concerns caused by flood coolants and for clean-machining, MQL is being emphasized. MQL uses a small amount of oil or coolant directed at the tool cutting edge. Promising results were reported in milling and turning operations of various metals and alloys. Pressure welding of chips to the cutting edge is the main cause for tool failure in machining Ti alloys. There is evidence that with MQL this failure mode can be reduced drastically thus showing significant improvement in tool life and surface finish [1].

Currently MQL delivery methods are the standard cooling approach used for SPDT. A fine coolant mist is gently sprayed at the tool-chip and tool-workpiece interfaces under pressure, thereby reducing friction as well as the forces generated during machining. The fine mist also works well to remove chips from the cutting zone with minimal interference in cutting. The main disadvantage of using this system is that the mist generation could pose a health hazard if inhaled by the operators. This hazard can be mitigated by the careful choice of

environmentally friendly nontoxic lubricants such as canola oil and the use of an effective exhaust system placed close to the cutting zone.

2.6.4.CUTTING TOOL MODIFICATIONS

An alternative approach used to enhance machinability in traditional machining is the use of different cutting tool materials such as polycrystalline diamond (PCD), cubic boron nitride (CBN) and binderless CBN (BCBN) tools. Performance of pure or binderless CBN tools for ultra precision machining of steel was investigated by Neo et al.[76]. It was reported that the BCBN tool wear is significantly lower than CBN tools. This could be attributed to the high thermal conductivity of BCBN tools, which is three times higher than CBN tools and the fact that no binder material is used to hold the CBN particles together. BCBN tools also possess superior mechanical properties. In limited machining trials a near mirror finish of less than 30nm Ra was achieved in an application involving the direct machining of steel. Excess tool wear due to diffusion-dissolution of the binder material (cobalt) from the CBN tool and longer tool life of binderless CBN tools comparable to the performance of PCD tools during high-speed machining of Ti alloys was reported by Zareena et al. [77]. At present BCBN materials

themselves are still under development making it very difficult to get tools for testing.

Another cutting tool modification approach reported was to reduce tool workpiece contact with microscale or nanoscale textures. Femtosecond lasers were used to imprint a range of textures on the tool surfaces rake and-or flank face. The textures were reported to reduce the friction in cutting by decreasing the area of contact between tool-workpiece and tool-chip and by better retaining the cutting fluid in the contact zone. A reduction in cutting forces was also observed [78]. The textured tools also showed improved anti-adhesive properties while cutting Al [79].

Shigehiko et al. [80] developed a new shape-formed coated cemented carbide tool in-house, for precision machining of titanium alloys. They reported surface finish of 13nm Ra for Ti-6Al-4V (α - β) alloys and Ti-22V-4Al (β) alloys. No information is available on the sharpness of the cutting edge that can be realized by grinding and honing these coated tools. In most traditional machining applications a properly selected tool coating is found to be beneficial as they add

a friction reducing diffusion barrier to the surface of the tool which can be customized to meet the specific demands of the material being machined.

From experience in traditional machining it has been seen that cutting tools can be effectively modified with the objective of reducing friction due to its influences in tool wear. Thus, in order to define the characteristic requirements of a protective barrier to reduce friction, a good understanding of friction in metal cutting is required.

2.7. FRICTION IN METAL CUTTING

Friction in traditional cutting occurs in the chip-tool interface over the chip-tool contact area and the flank face (Figure 2-17). The chip-tool contact length depends on the chip thickness t_c .

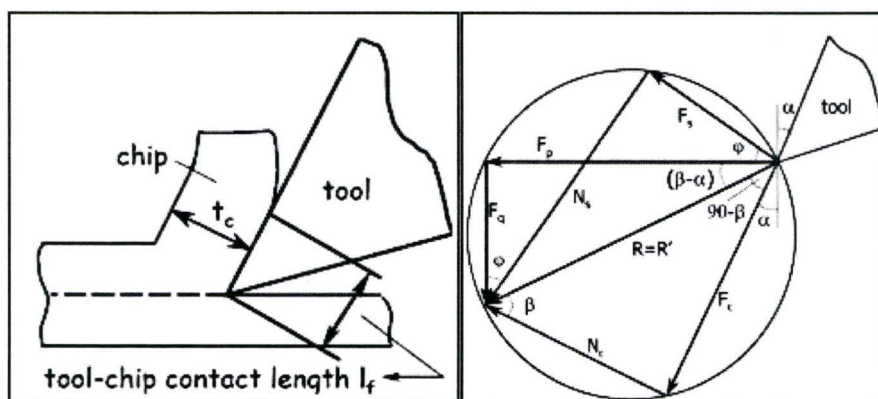


Figure 2-17: (a) Tool-chip contact in cutting (b) Merchant's circle

Coefficient of friction (COF)

$$\text{COF } (\mu) = \tan(\beta) = \left(\frac{F_c}{N_c} \right)$$

This assumes that F_c and N_c are distributed uniformly over the tool-chip contact area, and therefore represents an average value. In classical friction, the frictional force F is proportional to the normal load P applied. The coefficient of friction (COF) also referred to as μ is the ratio of F divided by P which is independent of the apparent area of contact (A). But the actual interaction between the sliding surfaces subjected to light loads, even if it is specially prepared to be flat and smooth, occurs over only a few asperities. Thus for most engineering applications, the real area of contact - A_R would be much smaller when compared to the apparent area of contact - A . For example, for 2 ground blocks of area 1 cm^2 under a normal load of say 10 N the apparent area of contact can be as low as $A_R = 0.01\%$ of A (Figure 2-18).

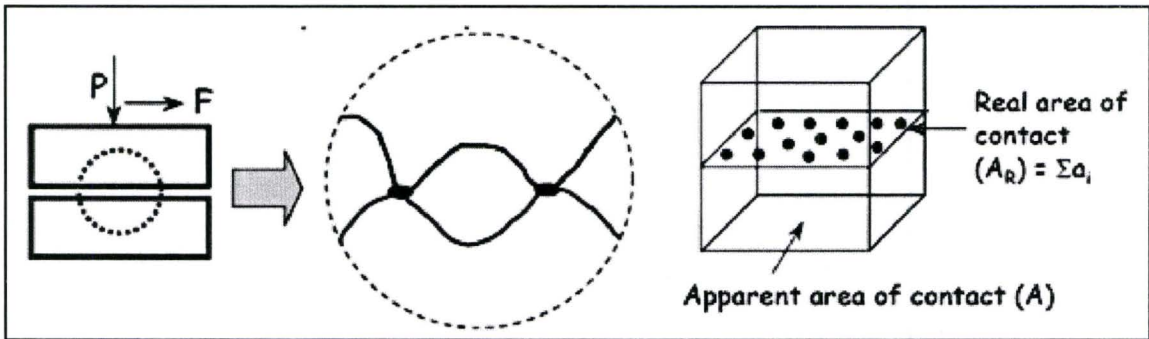


Figure 2-18: Coefficient of Friction and Area of contact in friction

When the normal load P is high, yielding occurs at the tips of the contacting asperities and then $A_R = P / \sigma_y$, where σ_y , the yield strength of the softer material, may be used as an estimate. The tangential load F required to shear the cold welded junction of area A_R is then given by $F = \tau A_R$, where τ is the shear strength of the weaker material.

Hence, COF (μ) = $F / P = \tau A / \sigma_y A_R = \tau / \sigma_y$.

Thus COF - μ is independent of the area of contact and is constant for a material pair according to the classic law of friction. In order to reduce friction, it is desirable to have a material of a low shear strength τ and a high normal strength σ_y or hardness. However τ and σ_y tend to scale proportionally. The principle associated with using a soft coating such as a polymer is therefore to use a third body material of low shear strength. When coupled with materials of

high hardness such as diamond tools, a combined properties of low shear strength and high hardness under load may be used to both lower friction and subsequent wear (Figure 2-19b). Thus polymer coatings when coupled with diamond could lower friction in metal cutting operations as well provided the loads and temperatures do not immediately damage the polymer coating.

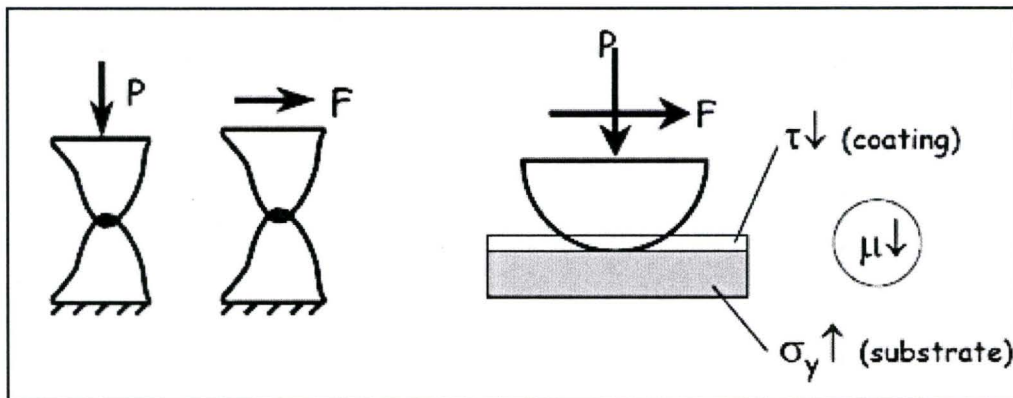


Figure 2-19: (a) Load and Force at the asperities contact point (b) Principle of soft coatings

2.7.1. COEFFICIENT OF FRICTION IN CUTTING

Previously, it was shown that COF is estimated as a constant for a material pair. However, in machining, COF varies considerably; for instance, it increases with an increase in rake angle and will change with temperature. The increase in friction angle β with an increase in rake angle can be interpreted geometrically by examining the friction angle in negative and positive rake tools.

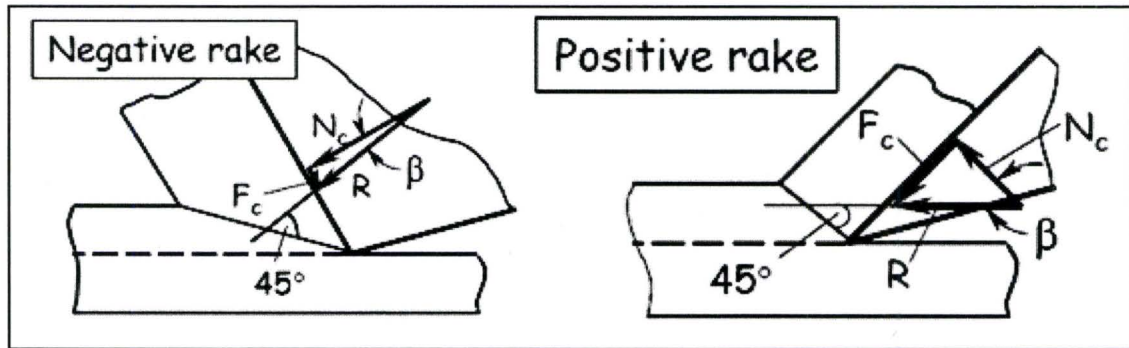


Figure 2-20: Friction angle in (a) Negative and (b) Positive rake tools

Based on the Merchant's circle (Figure 2-17b), where the cutting edge is considered sharp, the resultant force in cutting, R , creates an angle of $(\phi + \beta - \alpha)$ with the shear plane. The Lee and Shaffer model indicates that this angle is equal to 45° [33]. On increasing the rake angle from negative to positive (Figure 2-20), the shear plane angle increases, and the resultant force decreases and the friction angle β can be seen to increase.

In machining, classical friction laws do not hold over the entire tool-chip contact length, due to the very high values reported as high as 3.5 GPa [28] normal pressures acting on the tool rake face. Under such high pressures, the real area of contact A_R would approach the apparent area A (Figure 2-21b). Shearing is then not confined to surface asperities but takes place within the body of the

softer material, which in this case is the chip. Thus, the frictional force is no longer dependent on the normal force, but corresponds to the shear strength of the softer material and the shear area. The shear within the chip gives rise to the secondary shear deformation zone (SSDZ) and the primary shear deformation zone (PSDZ) refers to the shear plane as shown in Figure 2-21a.

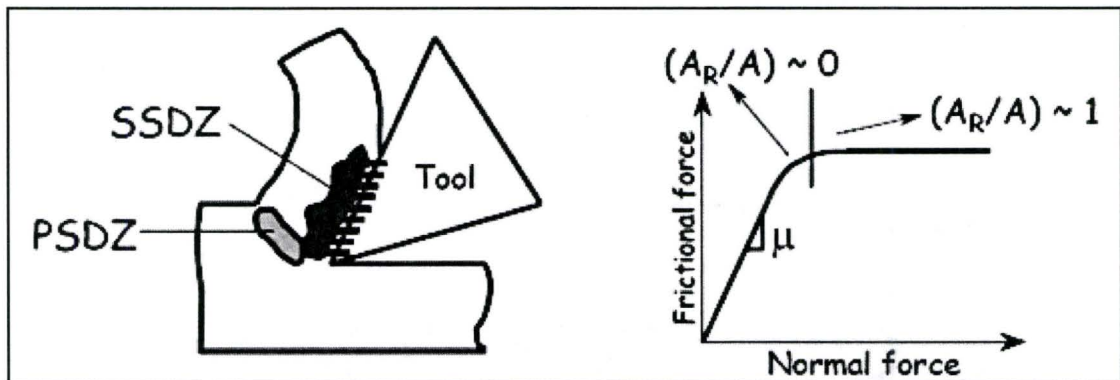


Figure 2-21: (a) Deformation zones and (b) COF in cutting

The tool tip is under the maximum normal stress. It decreases exponentially and becomes zero at the point where the chip loses contact with the tool. The shear stress is constant over roughly half the tool-chip contact length and this domain is known as the sticking zone (Figure 2-22). In this domain, classical light load friction concepts are not relevant due to the high normal stress applied to this region.

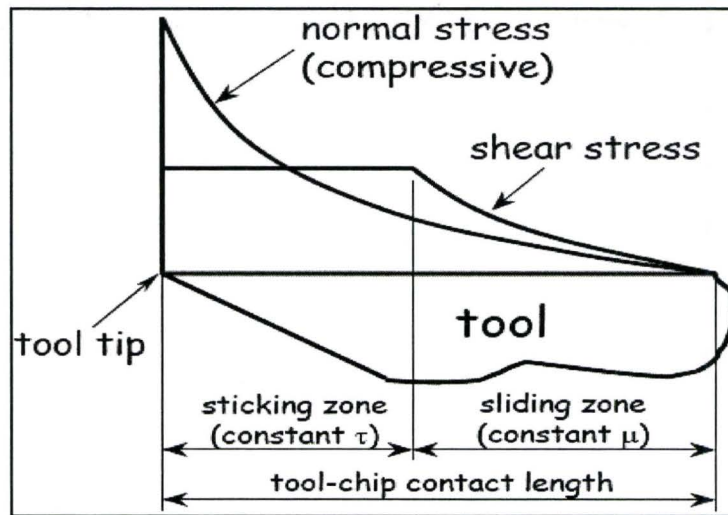


Figure 2-22: Stress distribution on the rake face

Classical friction laws hold well in the other half of the contact length, known as the sliding zone, where the normal stresses are not as high. The COF would be approximately constant in this length of sliding zone [81]. As can be seen, the chip flow on the cutting edge is not included in this model as it is considered to be extremely sharp. Round edge cutting model as explained earlier (Figure 2-9), considers the cutting edge radius and the friction components of this zone. Thus, it is obvious that the friction at the cutting edge is more critical than that along the tool rake or flank face in SPDT.

2.8. FRICTION AND TOOL WEAR

In general there is a positive correlation between adhesion, friction and wear [82]. Adhesion is a dominant mechanism in wear and often it is postulated that adhesion mechanisms underlies the majority of friction issues and often lead to subsequent wear. For metals, adhesive wear is proportional to the fourth power of the COF, whereas for non-metals it is more on the order of a second power relationship. The reason why metals tend to wear more is attributed to the fact that the surface energy to hardness ratio is higher. Adhesiveness arises from the attractive atomic forces that exist between the surface atoms of the interacting materials [82].

As discussed earlier, the d- valance bands are not completely filled in transition metals. The filling of the d-electron band is responsible for physical and chemical properties including the adhesive energy, shear modulus, chemical stability and magnetic properties of the metal. In general, the greater the number of unfilled electrons the metal posses, the more chemically active its surface would be, which in other words has more surface energy. As surface energy increases so does the probability for friction and wear. Thus the d- valance bond of the metal influences the COF [83]. It was experimentally shown that Ti has the

highest COF of 0.7 among the transition metals, when in-sliding contact with single-crystal diamond in vacuum (Figure 2-23), whereas the COF between diamond and Al alloys was found to be 0.13. This is attributed to the higher chemical reactivity and stronger interfacial adhesive bonding of Ti when in contact with diamond. These characteristics lead to high adhesive wear of the diamond tool in SPDT.

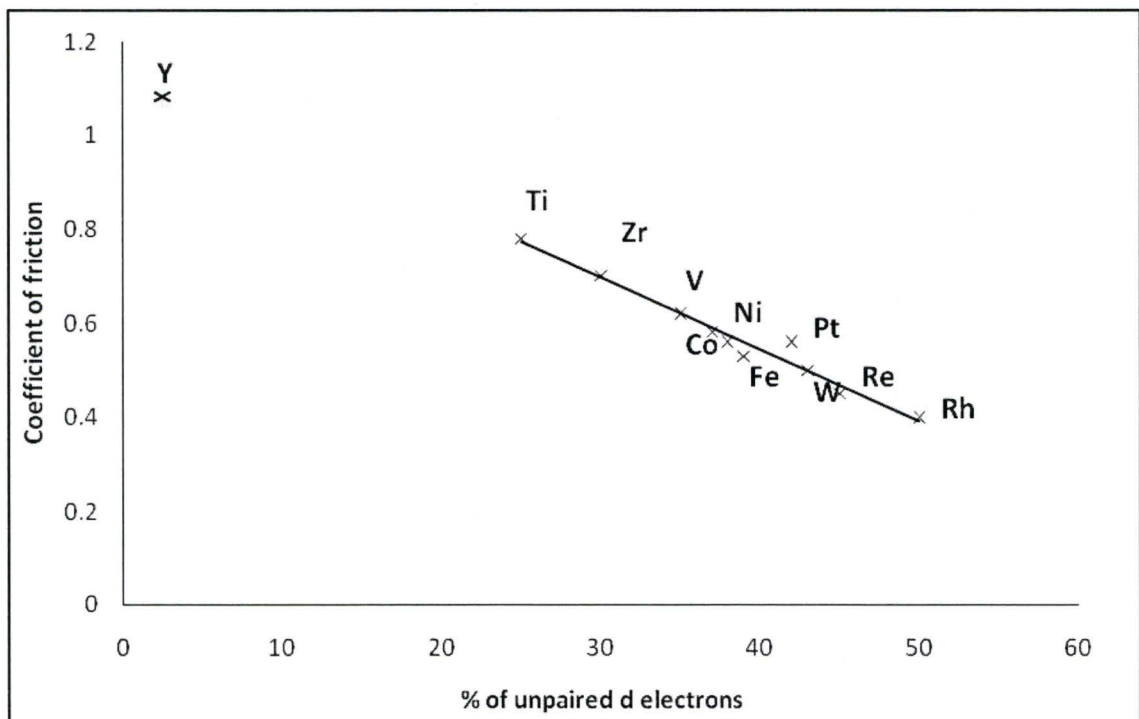


Figure 2-23: COF as a function of unpaired d-electron in transition metals [84]

Since, tool wear results from friction and thermal loads in the tool-chip contact zone, applying a hard lubricious coating could influence the frictional

behaviour between the tool and the chip by altering the surface energy between the sliding surfaces. When the friction is reduced by the coating, the chip will slide with less resistance over the tool. However, many conventional hard coatings are around 10 μm thick. If applied on single crystal diamond tools, this would affect the nanometric edge radius of the tool. Thus conventional hard coating techniques such as physical vapor deposition (PVD) and chemical vapor deposition (CVD) are not suitable for SPDT unless it can be polished and honed to a sharp edge. Due to the nature of the coating process, high residual stresses generated within the coating layer during deposition make it difficult to polish or hone the edge of the tool without chipping [33].

Coating material requirements for SPDT and the reasons for choosing PFPE for this particular application is detailed in section 4.3.

2.9. PERFLUORO POLYETHER-PFPE

Perfluoropolyethers (PFPEs) are often employed as lubricants in harsh environments, which include seizure prevention in the joints of astronaut's pressurized suits, bearings of spacecraft antenna arrays and also in magnetic recording disk drives, to improve tribological properties [85]. PFPE has also been

used to reduce the coefficient of friction of bare Si and surface active substances (SAS) coated Si surfaces [86]. An ultrathin PFPE lubricant film has also been shown to be effective in decreasing the wear of a carbon protective overcoat layer used in a hard disk system. [87]. PFPE was also found beneficial in injection moulding precision components, when applied on the cavities it was found to aid ejection or demolding, while maintaining the dimensional accuracy of the part [88]. PFPE coatings have also helped to improve the tribological properties: both in terms of friction and wear in micro-electro- mechanical-systems (MEMS) components, which was attributed to its lowered surface energy.

PFPEs are well suited for these applications because it provides hydrophobic properties to surfaces, as evidenced by the large contact angle it forms with fluids; chemical and thermal stability, which minimize degradation under use, high adhesion to substrate via organic-functional bonds; and good lubricity, which reduces the contact surface wear [89]. Careful thermal treatment of the coating can result in an improved density of the polymer film that can increase the wetting contact angle, which helps to retain a liquid lubricant and reduce wear.

The chemical structure of PFPE is $\text{HO-CH}_2\text{CF}_2\text{-(CF}_2\text{CF}_2\text{O)}_p\text{-(CF}_2\text{O)}_q\text{-CF}_2\text{CH}_2\text{O-OH}$ where the ratio p/q is $2/3$ (Figure 2-24) and its molecular weight is 4000 g/mol [90]. The PFPE film used in this study has the properties as listed in Table 2-5 [91, 92].

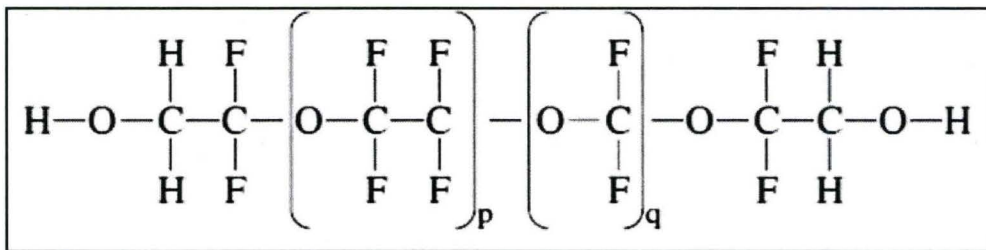


Figure 2-24: PFPE Molecule [90]

Table 2-5: Properties of PFPE

Properties	Units	PFPE
Functional group	—	Alcohol
Appearance	visual	Clear liquid
Color	APHA	Colorless
MW (NMR)	amu	4000
Difunctional content (NMR)	%	90
C2/C1 ratio (NMR)	—	1
Kinematic viscosity	cSt	100
Density @ 20°C	g/ml	1.82
Vapor pressure @ 20°C	Torr	1×10^{-8}
Vapor pressure @ 100°C	torr	1×10^{-4}
Refractive index @ 20°C	—	1.296
Surface Tension @ 20°C	dyne/cm	22
Polydispersity	Mw/Mn	1.15

PFPE coating is composed of two phases: a bounded layer that is chemically adhered to a substrate and a mobile layer that is allowed to disperse across the surface. These two components individually have poor lubrication properties but when placed on the surface together show significant improvement by working in synergy. The bound layer decreases diffusion of the mobile phase out of the contact region and thereby, prevents the loss of lubricity that often leads to rapid failure [92].

The wear durability of these coatings strongly depends on the retention and replenishment of the lubricant on the protective overcoat surface, which is controlled by the interaction between the lubricant molecules and the overcoat surface. When applied on cutting tools, PFPE molecules adhere to the surface by chemisorption forces with the lubricant penetrating into the micro-pores typically found at the surface layer of the cutting tools. In another application a diamond like coating surface, coated with PFPE has shown reduced friction and enhanced durability in a ball-on-disk tribo-tester since solid contact was avoided with these coating [93].

The main mechanism by which the use of PFPE helps in reducing friction and wear is explained as follows:

When two surfaces come in contact under load, the contact takes place at the tips of the asperities and the load is supported by the deformation of the contacting asperities. The proximity of the asperities results in adhesive contacts caused by interatomic attractions. Experimental data suggests that adhesion is primarily due to weak Van-der-Waals forces [33]. When the two surfaces (in contact) move relative to each other these bonds must shear and break to sustain motion. As a result a resistive force occurs, which has the potential to cause wear depending on how the sheared adhesive junction breaks [94].

PFPE coatings lower the surface energy, which is one of the most important properties required to minimize adhesive wear. PFPE has shown higher water contact angles and it was found to lower the COF between surfaces. The homogeneity of the PFPE coating structure is characterized by a fine fluorine dispersion that provides excellent barrier properties [95]. Other researchers have confirmed that the thickness of these fluorocarbon films is around 1 nm at most and that there are minimal irregularities in the film thickness [96]. PFPEs

are multi component systems containing fluorine-organic surface active substances – fluorine SAS and controlling agents in various organic solvents. The coating process involves the application of fluorine-SAS molecules on the frictional surface and a thin film forms with oriented fluorine-SAS molecules. This surface treatment lowers the surface energy and aids in retaining the lubricant in the contact region during cutting [97] and also protects the surface against adhesion [90]. Also, for a coating material to effectively adhere on the substrate surface, the surface energy of the coating must be low or lower than the surface energy of the substrate to be bonded. Surface energy derives from the unsatisfied bonding potential of molecules at a surface, and will try to reduce this free energy by interacting with molecules in an adjacent phase. Since fluorine is the most powerful electro-negative charge, the surface coated will not allow any oxidation or electrochemical process. Also fluorine in this bonded condition makes the surface chemically inert.

PFPE also reduces friction with its bonded adhesive and mobile fluidic layers. It was experimentally shown that the bonded PFPE layer alone is insufficient and the mobile layer is necessary for reducing the friction further and enhancing the durability of the surface in this application [93]. The mobile

molecules move easier and replenish the wear scars compared to the bonded molecules which adsorb strongly on the surfaces [89].

There is evidence for reduced tool wear with PFPE coated tools in metal cutting as well. Dosbaeva et al. [97], found a reduction in cutting torque and an improvement in tool life and surface finish when PFPE was applied to drill bits already coated with a diamond like coating (DLC) while drilling aluminum. They also provided evidence for the increase in wetting angle with PFPE that has improved the lubricity there by reducing the friction between the tool and workpiece. The surface energy of oils contained in the typical coolants used for machining is higher than the surface energy of the PFPE films used. As a result of the molecular interaction of the oil and the PFPE film, the oil is not sheared from the cutting zone during the initial stages of cutting. The tool and workpiece surfaces are separated by a layer of oil maintained by the PFPE film that acts as an anti-frictional layer and prevents severe seizure and wear during the initial stages of cutting [98]. Veldhuis et al. [99] also found that the application of PFPE reduced the coefficient of friction by 18% over an uncoated surface in an aggressive thread cutting operation. It has also reduced the tool/work adhesion and torque improving the overall wear behavior in a spiral tapping operation.

PFPE has also enhanced chip formation by improving the metal flow on the tool surface.

2.10. TRIBOMETER

Tribology is the term used to describe the performance of surfaces relative to lubrication, friction and wear. Tribometers are designed to accurately replicate friction conditions, calculate the coefficient of friction and study wear rates. A pin-on-disk tribometer is a widely used instrument for performing tribological studies for a wide range of typical applications. The tribometer at the MMRI is novel in that it is specifically designed to duplicate machining conditions involving high load and temperature. It measures the coefficient of friction under a heavy load as a function of applied torque and contact area. This type of tribometer has been used to study the tribological effects of various coatings used in metal cutting applications [86, 90, and 94,100-102]. This system was used to investigate the performance of the PFPE coating applied to diamond tooling under conditions relevant for this application. More details of this tribometer and the testing performed are explained in Chapter 3.

2.11. ULTRA-PRECISION MACHINING OF TITANIUM ALLOYS

Only a few studies have been reported to date on the precision machining of Ti alloys. A list of studies found and their outcomes are compiled in Table 2-6.

Table 2-6: Literature available on ultra precision machining of titanium alloys

Ref.	Tool	Ti Alloy machined	Surface Roughness	Remarks
[103]	Single crystal diamond tool	Ti-22V-4Al	Rz=97-200 nm Ra=16-30 nm	V=55 – 66m/min f = 50 μ m/rev DOC=1 μ m Nose Radius = 4 mm
[80]	TiCNO- formed coated cemented carbide	Ti-22V-4Al Ti-6Al-4V	Rz=80. 44nm Ra=13. 6 nm	V=31-65/min f = 2 μ m/rev DOC=5 μ m Nose Radius =0.4 mm
[104]	Diamond, carbide, cermet, coated carbide	Ti-22V-4Al Ti-6Al-4V	Rz=100-200 nm	Published in Japanese
[105]	Ultrasonic vibration assisted diamond tool	No info available	Ra=250 nm	f = 10 μ m/rev DOC=8 μ m Amplitude=14 μ m Frequency = 30kHz
[106]	Diamond tool (Truncated roof shaped)	CP-Ti Ti-6Al-4V	Rt(min)= 590 nm Rt (min) 416 nm	f = 5-20 μ m/rev DOC=5-15 m rpm=1000(?)

SPDT of Ti-22V-4Al alloys has been performed in the past. In general the undeformed chip thickness and depth-of-cut (DOC) values are large compared to values typically used for SPDT. The resulting surface roughness values reported

are also high for optical grade applications. These results do indicate that SPDT of these materials is possible with a diamond tool; unfortunately there is no reporting of length of cut achieved in this research.

For the one case that comes close to meeting optical grade requirements there is no detailed information on the tool other than they used a TiCNO coated tool. Critical information on cutting edge radius and tool preparation is also missing from this reference. Furthermore in their work they report surface roughnesses as R_a values, which in general are less stringent than the typically used R_{rms} values. The reported R_a value of 13.6 nm in terms of R_{rms} could be greater than 16 nm. The maximum cutting length reported was 2 km. Overall the surface roughness data reported in the past are not at optical grade levels with no work reporting SPDT of optical grade surfaces with surface roughness less than 10 nm R_{rms} .

2.12.SUMMARY

- Ti and its alloys are attractive materials in aerospace, automotive, biomedical and optical applications due to their unique combination of high strength-to-weight ratio that is maintained at elevated temperatures and their exceptional corrosion resistance.
- Ti alloys are considered as “difficult-to-machine” materials due to their high strength maintained at elevated temperature, low thermal conductivity and high chemical reactivity that accelerates the tool wear rate and limits cutting speeds.
- The demand for precision machined Ti components and Ti surfaces with optical quality is increasing.
- SPDT is the process widely employed to manufacture components with ultra precision and optical grade surface qualities.
- Materials that are generally diamond turned are Cu, Al and brass. Due to their chemical affinity towards diamond tools, Ti alloys are generally classified as non-diamond-turnable.
- General approaches taken to enhance machinability are classified as workpiece modification, process modification and cutting tool modification.

- A promising designer alloy to pair the unpaired d-electrons was reported successful in SPDT of ferrous alloys with electroless Ni and Ti-N, which are otherwise non-diamond turnable.
- Process modification with ultrasonic vibration assisted tooling has also been employed for SPDT of ferrous alloys and was found to enhance tool life. Other approaches such as high-pressure coolant supply and cryogenic cooling technique have produced promising results in the traditional machining of Ti alloys. But MQL has been reported as the standard method in SPDT.
- Other cutting tool materials such as PCD, CBN and binderless CBN and coated carbide tools had produced promising results in traditional machining of Ti alloys. Micro and nano scale texturing on diamond tools were reported to have reduced friction in machining and were found to enhance tool life.

2.13.RESEARCH APPROACH

Initially research was done to test the basic feasibility of SPDT of Ti. A set of machining conditions were then identified which met optical grade surface finish requirements. Once this was in place, tool life testing was performed which identified tool life as the main issue limiting the wide spread use of SPDT of Ti alloys. Then a detailed investigation was carried out to understand the tool wear mechanisms involved in SPDT of Ti alloys with a focus on reducing wear. Three different approaches were considered. They were workpiece modification, process modification and tool modification.

2.13.1.WORKPIECE MODIFICATION:

Workpiece modification involving the use of designer alloy that could deactivate the unpaired d-electrons, which have been identified to be correlated with tool wear, would require significant alloy development and was considered to be outside the scope of this research.

2.13.2.PROCESS MODIFICATION

Process modification involving the testing of a wide range of machining conditions was performed early in the research. Other techniques generally adapted to reduce the tool wear rate that correlates with higher cutting temperature such as cryogenic cooling techniques, were considered but not tested. Unfortunately these approaches are not practical when machining optical grade products due to the extremely tight dimensional tolerances imposed on the parts. Overall the impact that thermal variation will have on part-dimensions through the coefficient of thermal expansion of Ti and through variation in the tool and machine would be excessive for this application.

2.13.3.CUTTING TOOL MODIFICATION

Cutting tool modification was considered as the main approach taken in this thesis to address the tool life issues identified. Micro and nano scale texturing, which currently requires femtosecond lasers, was not tested due to difficulties in preparing sample tools and the expectation that small notches located near the end of the tool would excessively weaken the tool. Also a number of different tool materials such as PCD, CBN, binderless CBN and various coated carbide tools

were considered, but none of them could achieve the nanometric cutting edge radius that is required for SPDT. Cutting tools are generally coated with hard coatings to reduce friction during cutting. Conventional coatings which are typically 10 μm thick are not applicable for SPDT, as it would round the cutting edge and so alter the sharpness of the tool. Furthermore, these coatings and their associated processes have not been developed for diamond tooling. It is for these reasons non-traditional ultrathin coating technologies were explored. A unique polymer based coating was identified and its properties studied to see if it is applicable for this application. Following this, tribometer testing was performed followed by SPDT tests.

Chapter 3 : **EXPERIMENTAL PROCEDURE AND SET-UP**

In this chapter the workpiece material, cutting tool and machine tool details used for conducting the cutting tests are outlined. Also the process of selecting the initial set of the cutting parameters is presented and the final machining conditions used are outlined. Various equipment used for analyzing cutting force, tool wear, surface finish, chemical composition of the cutting tool and workpiece are also discussed.

3.1.TEST PROCEDURE

The experimental study was carried out in five phases. In phase-I, on designing and fabricating the fixtures to use the 5-axis milling machine for SPDT, the cutting speed, feed, depth of cut and tool geometry were selected to meet the required surface finish criterion. Then, in the next phase (phase-II); cutting was carried out with these parameters and tool wear mechanisms were studied. From the analysis, the need for a protective barrier for the cutting tool was postulated. In phase-III, requirements of such a barrier for SPDT were identified.

Search of a suitable coating material meeting those requirements was carried out and PFPE was identified as a suitable coating material. The performance of PFPE was evaluated with a tribometer in phase-IV. Cutting tests with the parameters selected in phase-II were then repeated with the PFPE coated tools in phase-V and then compared with the results obtained in phase-II in order to test the effectiveness of PFPE in reducing tool wear rates.

3.2.MACHINE TOOL

All the cutting tests were performed on a Precitech Freeform 700G ultra precision 5-axis machining system (Figure 3-1) with 1.4 nm position feedback accuracy, 1 nm programming resolution, maximum spindle speed of 5000 rpm and maximum feed rate of 1500 mm/min. The machine is equipped with a self-levelling dual chamber, is passively damped with a pneumatic vibration isolation system to minimize the vibration influences during machining operations, spray mist coolant system and a vacuum chuck for mounting the workpiece. The slideways are linear motor driven with hydrostatic oil bearings for high stiffness and damping characteristics. The system also has a thermal enclosure and is temperature controlled to within 1°C.



Figure 3-1: Precitech Freeform 700G Ultra precision machining system

The as-is set-up of the machine axes and the spindle were for 5-axes contour milling as shown in Figure 3-2 (a).

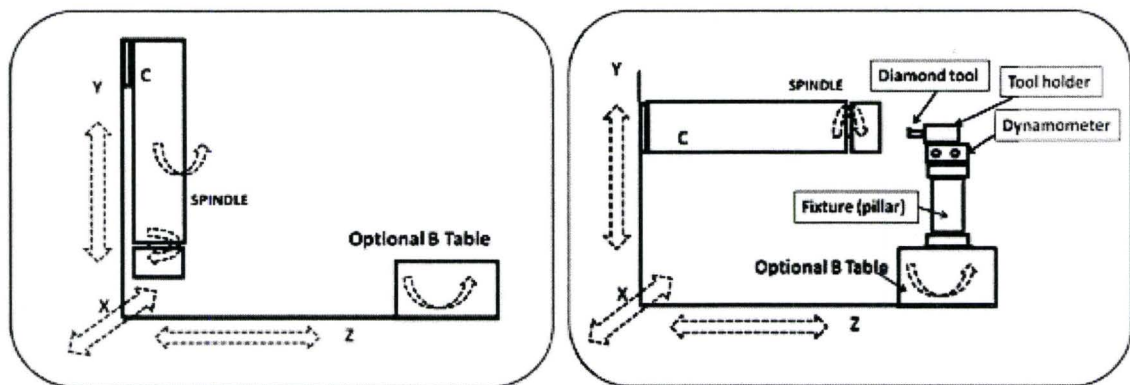


Figure 3-2: Schematic of (a) initial and (b) modified machine axes and spindle set-up

In order to utilize this machine for SPDT i.e. for facing, the C-axis was rotated 90° to hold the workpiece and additional fixtures were designed and fabricated to match the pre-existing tapped holes in the rotating “B” table and the dynamometer. The fixture was then mounted on the “B” table with the dynamometer on the top. The machine was configured for SPDT using a standard tool-holder fixture, supplied by Precitech which was mounted on a Kistler Dynamometer (Figure 3-2b). The modified set-up of the tool holder, tool, dynamometer, fixture, workpiece and coolant spray nozzle is shown in Figure 3-3.

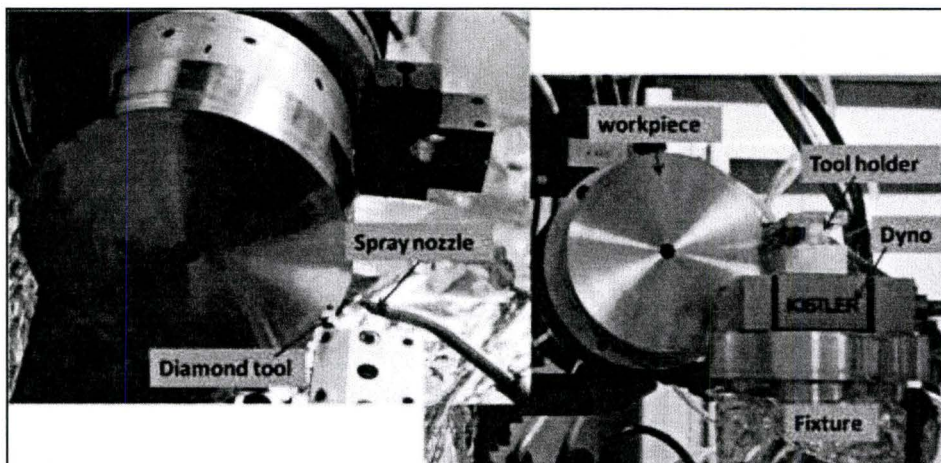


Figure 3-3: Machine set-up for SPDT.

3.3. WORKPIECE MATERIAL

Forged Commercial Pure – Grade II Titanium (CP-Ti) and Ti-6Al-4V alloy discs annealed at 700°C for 2 hours and air cooled, supplied by Industrial Metals Inc., NY were used as workpiece materials in this study. The discs were turned to 100 mm diameter to match the vacuum chuck of the same size and the discs were about 25 mm thick. The chemical composition of both the materials is listed in Table 3-1. Titanium pins used in the tribometer tests were machined from titanium rods with the same chemical composition and were supplied by Industrial Metals Inc as well.

Table 3-1: Chemical composition of workpiece and pin materials

W/p Material	Fe	O	N	C	Al	V	Ti
CP-Ti Grade-II	0.09	0.165	0.009	0.0165	-	-	Balance
Ti-6Al-4V	0.18	0.18	<0.01	0.01	6.54	4.01	Balance

3.4. CUTTING TOOL

Single crystal diamond tools used in this study were supplied by K&Y Diamond. K&Y specialises in manufacturing diamond tools for ultra precision

machining. Instead of solid shanks, cutting tool inserts were used for fast replacement and enhanced accessibility. Table 3-2 shows the cutting tool geometries tested during the cutting parameter selection stage and the ones selected for the experimental work. The reasons for selecting this particular set of geometry are explained in the next chapter.

Table 3-2: Tool geometry

Parameters	Tool mtrl	Rake angle (°)	Clearance angle (°)	Clearance type	Nose radius (mm)	Sweep angle (°)	Tool type
Tested	Natural, Synthetic	0	5, 7.5	Conical, Cylindrical	0.3, 0.5, 1.5	90, 140	Shank, Insert
Optimized	Natural	0	7.5	Cylindrical	0.5	90	Insert

Natural diamond tools are known to produce better results than synthetic tools and thus only natural diamond tools were used in this research. Diamond was vacuum brazed onto a tungsten carbide insert, which was then mounted in a specially designed tool holder as shown in Figure 3-4.

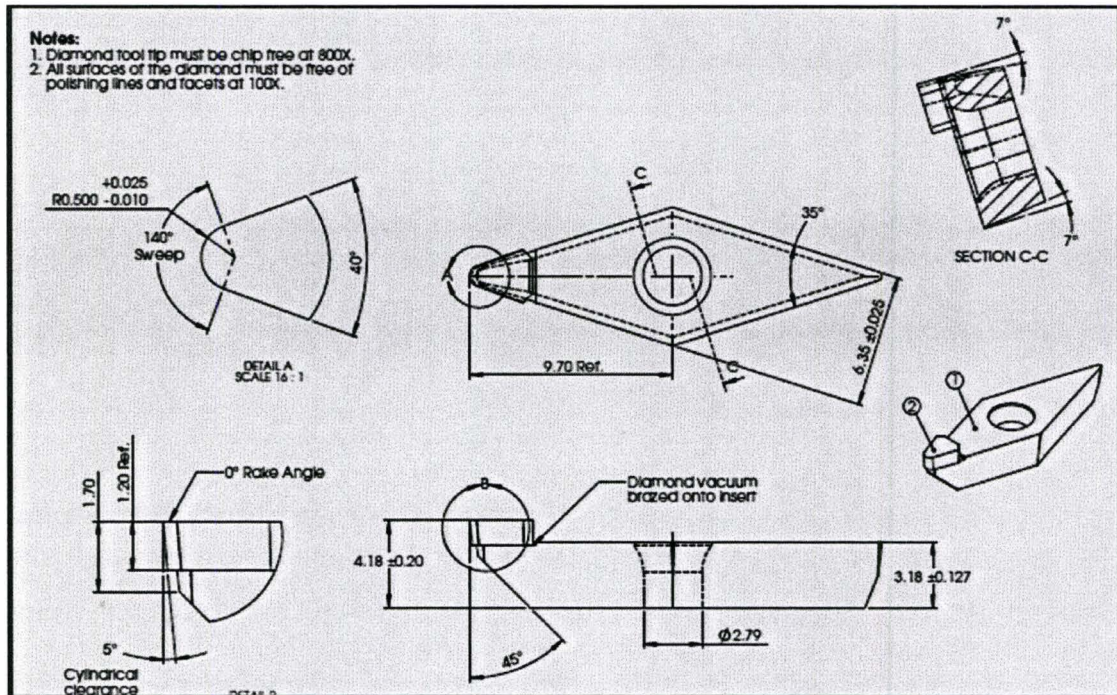


Figure 3-4: Design of diamond insert and the tool holder (K&Y – used with permission)

3.5. CUTTING PARAMETERS

Since Ti is not currently ultra precision machined using SPDT for the targeted surface quality, a series of cutting tests was initially performed in order to identify the best conditions to use for all future testing. The criteria for selection were the set of conditions that produced the targeted surface roughness i.e. $R_{rms} \leq 10$ nm. The subsurface region was also investigated to ensure that no subsurface cracks were forming under these cutting conditions

since titanium components are generally utilized for parts of high reliability [107]. The range of cutting parameters tested for both CP-Ti and Ti-6Al-4V and the conditions that met the above criteria are listed in Table 3-3. All the cutting tests reported in this work were repeated at least three times.

Table 3-3: Cutting parameters

Parameter	Cutting Speed (m/min)	Feed ($\mu\text{m}/\text{rev}$)	Depth of cut (μm)
Test range	50 ~ 70 m/min	0.5 ~ 1.66	1 ~ 10
Selected	60	1.5	2

3.5.1. CUTTING ENVIRONMENT

Minimum quantity lubricant (MQL) method is commonly used in ultra precision machining and was also found to provide favourable performance in the conventional milling of titanium [108] (ref. 2.6.3). A fine spray mist of canola oil dispensed in a compressed air stream was used as coolant and lubricant for all of the testing performed. The flow was directed at the cutting edge in such a way as to redirect the chip away from the finished surface of the workpiece. This is commonly done to avoid damaging the surface of the machined part.

Temperature reduction at the cutting zone with MQL system is achieved mainly by the cooling effect of the compressed air and partially by evaporation of the oil mist.

3.6. DESIGN OF EXPERIMENTS

In Phase-I, tests were conducted with different cutting speed, feed and depth of cut as well as with different cutting tool geometry as shown in Table 3-2 and Table 3-3; in order to select the right combination of cutting parameters that could yield the required surface quality. In Phase-II and Phase-V, cutting tests were carried out to evaluate the performance of the tool and to compare the performance without and with PFPE coated tool.

Each cutting test was repeated at least thrice and instead of repeating the tests more number of times to compare the results, the performance was analysed in different aspects such as:

- The cutting length meeting the targeted surface quality (Zygo)
- Tool wear analysis (SEM, EDS)
- Surface analysis for ploughing, material pick-up (SEM, EDS)
- Tool surface analysis (Raman, XPS)

- Machined surface analysis (Nano indentation)
- Chip analysis (SEM, TEM) and
- Microstructure analysis of machined surface (Optical microscopy)

3.7.MACHINE SET-UP

A dial gauge indicator with the smallest display of 0.1 μm was used to check and initially align the trueness of the mounted workpiece before cutting. The surface of the workpiece was set as a datum for setting the depth of cut. Single crystal diamond tool mounted on the B-table, was brought closer to the surface of the spinning workpiece. The tool was moved slowly towards the workpiece surface with a step size of 20 nm. Any chip formation was monitored in the CCD camera attached to the machine tool. Cutting force data was monitored throughout the cutting test to ensure the flatness of the workpiece.

A CNC program was prepared (Ref. Appendix-1) for face turning of the workpiece from outer to inner radius at the pre-set rpm, feed rate and depth of cut. The flow of MQL was regulated and the nozzle position was adjusted to direct the chips away from the machined surface. Chips formed with every set of cutting parameter was collected, cleaned and labelled. After every pass, the

workpiece and the cutting tool were removed from the machine and cleaned with ethanol in an ultrasonic cleaner to remove any grease from the coolant, before conducting any surface analysis. The above procedure of workpiece alignment, tool and workpiece datum setting were repeated before each experiment.

3.8.COATING TECHNIQUE

PFPE used in this study is a 0.5% solution of perfluorine polyester acid ($\text{HO-CH}_2\text{CF}_2\text{-(CF}_2\text{CF}_2\text{O)}_p\text{-(CF}_2\text{O)}_q\text{-CF}_2\text{CH}_2\text{O-OH}$, $p/q = 2/3$). The tool was coated by dipping the diamond insert into a solution containing PFPE thus forming a thin (20 – 40 Å thick) nano-scaled film of oriented fluorine - surface active molecules on the surface. This epilam coating technique has been outlined elsewhere [97] .

3.9.TRIBOMETER

Tribometer testing was carried out in a custom tribometer capable of mimicking the temperatures and loads expected in ultra precision machining. The normal load set for this testing was 500N and the temperature was varied from 20°C to 500°C. This was the highest force that was deemed safe for the

setup given the dimensions of the components involved. Based on the dimensions of the pin, the resulting stress is considerably lower than what is estimated to be generated in the cutting zone, but is within the range where the asperities will be flattened and full surface contact will be taking place. For this test, hemispherical tipped pins were made from CP-Ti and Ti-6Al-4V alloys and a disk of diamond was used with and without PFPE. Thus, four test combinations were performed. Both the pin and disk materials were the same as used in subsequent machining tests. In this test the disk (diamond insert) spins and the pin (titanium alloy) remains static. Thus, the test was essentially a twist compression test with the pin located with its centre on the axis of rotation of the disk. A Kistler reaction torque sensor allowed measurement of the resulting torque which is then expressed as a friction coefficient by factoring in the contact dimensions and the applied load.

The COF was calculated for each test and used as a performance indicator for wear. Background research has indicated that a lower coefficient of friction typically leads to lower wear rates in machining [33]. The COF was calculated as the ratio of frictional shear stress to the normal stress. Frictional shear stress in this unit is a function of the torque generated under load and the radius of the

pin print imprinted on the disk during rotation. The normal stress is a function of the applied load and the area of the pin print on the disk. 1 rpm disk rotation, which is the slowest possible rotational speed, was used to mimic seizure like conditions. Low rotational speed also has the advantage of minimizing signal noise and reduces the potential for vibration showing up in the data. Each test ran for 2 minutes, thus causing 2 complete rotations of the disk against the pin. Single replicate test points were recorded starting from 20°C and going up to about 500°C in approximately 100°C temperature intervals were performed to study the effect of temperature on friction. From thermocouple calibration the interface temperature is estimated to be within about 10% of the temperature sensor measurement.

After tribometer tests, actual cutting tests were performed using the cutting conditions outlined earlier and the surface roughness, tool life and cutting forces were compared for both CP-Ti and Ti-6-4, without and with PFPE coated tools.

3.10.CUTTING FORCE MEASUREMENT

Forces along the three orthogonal components representing the cutting force, feed force and the thrust force were measured at regular and fixed intervals during each cutting test. A Kistler 9256-C1 MiniDyn stationary multi-component dynamometer was used for measuring the cutting force. This is an extremely high sensitivity dynamometer with -13pC/N in F_y and -26 pC/N in F_x and F_z , with a measuring range of $\pm 250\text{ N}$ was exclusively designed for ultra precision machining such as diamond turning operations and could precisely measure small machining forces.

3.10.1. DATE COLLECTION AND PROCESSING

NI compact DAQ-9172 USB data acquisition system was used for collecting the force data. A LabVIEW 8.5 version was used to program the data acquisition system. The cutting force sampling rate was set at 100k samples/s and the gain used was 1 MU/V . MU is the measuring unit and in this case is N. The dynamometer was connected to a dual mode charge amplifier – Kistler 5010B which converts the input charge signals of the dynamometer into output voltage proportional to the force in Newtons. Once the data was acquired at specific

intervals, Matlab 7.1 software was used to analyse the data. All the three components of forces, F_x , F_y and F_z were analysed by computing the rms value of each component. These values were then used to compare and contrast as a part of the cutting force analysis.

3.11.SURFACE ROUGHNESS MEASUREMENT

A Zygo NewView 5000 white light interferometer equipped with MetroPro 8.1.5 software was used for measuring and analysing the roughness profile of the machined surfaces (Figure 3-5). The NewView 5000 uses non-contact scanning white light interferometry to acquire Z-resolution images and the scanning technique provides 0.1 nm vertical resolution. All the measurements were made with a x10 objective and the resulting field-of-view was 0.74 x 0.53 mm.

Surface roughness values in terms of R_a , R_z , PV and R_{rms} were recorded for each measurement taken on the workpiece surface. Surface roughness was measured in bands at fixed distance from the centre and a minimum of three measurements were made at different points before averaging the value for the particular band.

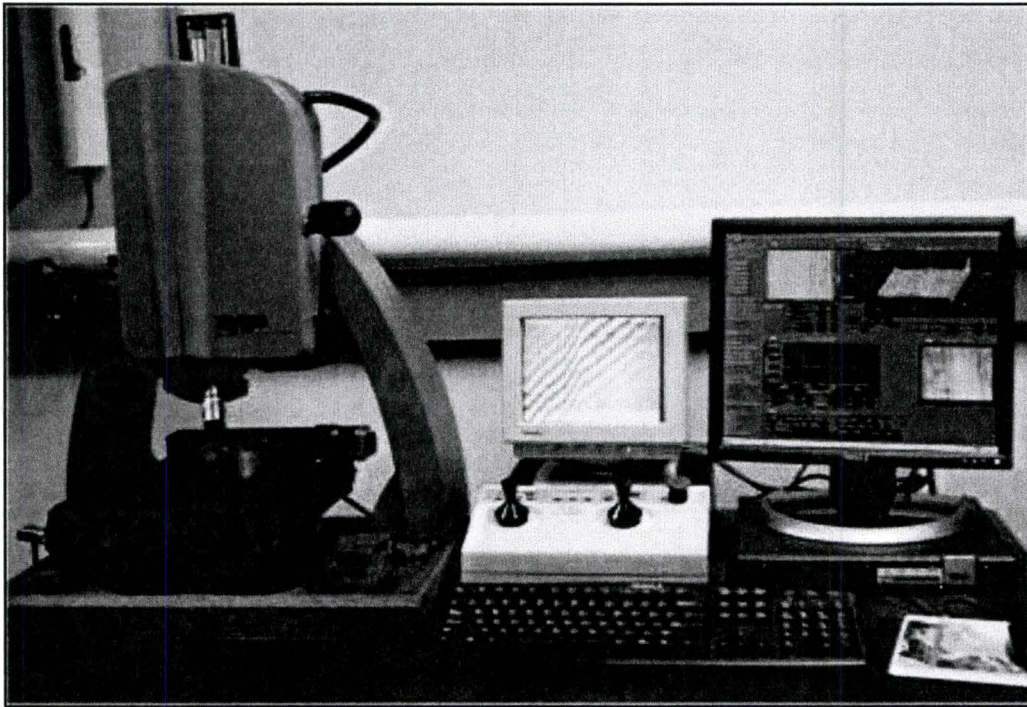


Figure 3-5: Zygo NewView 5000 White light interferometer

3.12. TOOL LIFE CRITERION

In traditional machining the end of tool life is indicated by the flank wear length of $300\mu\text{m}$. This criterion is not applicable in ultra precision machining as the cutting edge sharpness, which is typically in the range of 50 to 150 nm, is the most crucial parameter that controls the surface finish of the parts being machined and more importantly the surface quality. Since surface roughness is the most stringent parameter in machining optical surfaces, ideally the tool life should be measured in terms of wear of the cutting edge i.e. rounding-off of the

edge sharpness. Precise measurement of cutting edge radius is not trivial and could not be done reliably with the available facilities. So the tool life in this study was measured in terms of cutting distance that could be machined while meeting the surface roughness requirement of $R_{rms} \leq 10$ nm, typically set for optical applications.

3.12.1. SCANNING ELECTRON MICROSCOPY (SEM)

Cutting tools and the machined surface were examined in a high magnification Scanning Electron Microscope (SEM) Joel JSM-7000F, equipped with Energy Dispersive Spectrometer (EDS) for chemical analysis. The magnification ranges from x10 to x1, 000,000 with 0.5 to 30kV accelerating voltage and 1.2 nm (30kV) to 3 nm (1kV) resolution.

3.12.2. LASER RAMAN SPECTROSCOPY

A Laser Raman Spectrometer, Renishaw Model 2000 with two wavelengths 633nm and 514nm was used. A Raman Spectrometer is generally used for the identification of different forms of elements, for example it can

distinguish between diamond, graphite, amorphous carbon, diamond-like structures and carbon nanotubes. Laser Raman spectroscopy depends on a change in the polarization of a molecule to produce Raman scattering. When a beam of photons strikes a molecule, the photons are scattered elastically, which is referred to as Rayleigh scattering and inelastically, which is referred to as Raman scattering generating Stokes and anti-Stokes lines. Different forms of an element each have a unique signature, which can be used to identify the form of the element on a surface.

3.12.3. X-RAY PHOTOELECTRON SPECTROSCOPY

X-ray Photoelectron Spectroscopy (XPS) was also used in this study to examine the tool. XPS is a surface chemical analysis technique with the capability of determining elemental composition, oxidation state, empirical formula and impurities present in a sample. XPS takes advantage of the photoelectric effect. It measures the kinetic energy of electrons that are ejected from a sample after irradiation by x-rays. The kinetic energy of an ejected electron is related to the binding energy of that electron for a certain atom. In this way, binding energies can be used to assign peaks to atoms in a typical spectrum.

3.12.4. TEM – TRANSMISSION ELECTRON MICROSCOPY

The combined techniques of High Angle Annular Dark Field - HAADF image and Electron Energy Loss Spectroscopy Spectrum Image - EELS SI were performed on JEOL 2010 Field-emission STEM equipped with Gatan Tridem imaging filter. For the HAADF image a 1 nm scanning electron probe was chosen and the collection angle beta was set to 32 mrad. Signal collection and data processing of EELS spectrums were performed with Digital Micrograph software (Gatan, GMS 1.6.0).

3.13. NANO INDENTATION

Nanoindentation tests of the machined surfaces were carried out in a nanoindentation tester (table top unit; courtesy: CSM instruments and Micro Materials lab, UK). The tester can measure up to a maximum depth of 200 μm with a 0.04 nm depth resolution and a maximum load of 500 mN with a 0.04 mN load resolution. The nano indentation technique known as Depth-Sensing Indentation (DSI), allows the application of a specified force or displacement history, such that the force (μN) and the depth (nm) are controlled and-or measured simultaneously and continuously over a complete loading cycle. This

technique has been largely used to evaluate mechanical properties of materials at the nanoscale level, especially hardness and elastic modulus.

Chapter 4 : RESULTS AND DISCUSSIONS

4.1.PHASE-I: SELECTION OF CUTTING PARAMETERS

As explained in section 2.11, there was no suitable database available for single point diamond machining of titanium alloys. As a result cutting tests were carried out over a wide range of cutting parameters for a relatively short cutting distance of 0.2 km in CP-Ti and Ti-6Al-4V, with the objective of identifying the cutting parameters that meet the surface quality requirements of this application.

Figure 4-1 shows the surface roughness value (R_{rms}) obtained for the various combinations of cutting speed, feed and depth of cut. The surface roughness was found to be mainly affected by the adhesion of workpiece material with the diamond tool. Relationship between material microstructure i.e. grain size of the workpiece material and uncut chip thickness as discussed earlier [21] was also found to affect the chip formation and thus the surface quality.

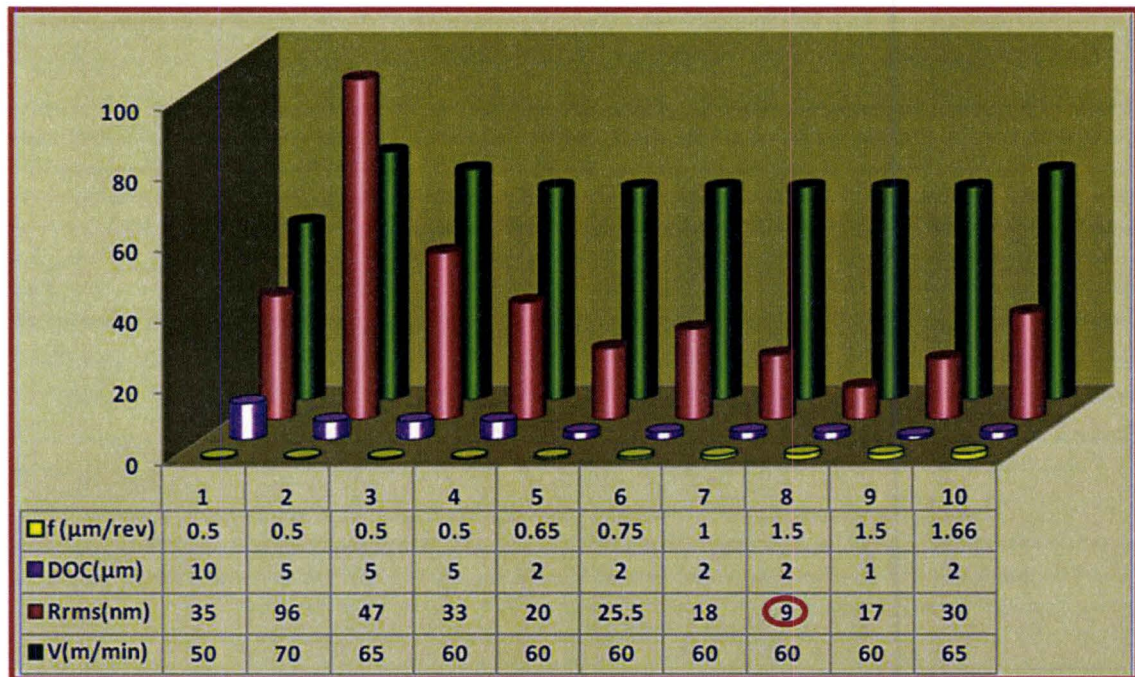


Figure 4-1: Surface roughness (R_{rms}) Vs cutting speed (V), feed (f), and depth of cut (DOC)

As explained in section 2.2, when the cutting speed was increased beyond 60 m/min accelerated wear resulted due to an increase in cutting temperature. Also, lower feed rates below $0.5\mu\text{m}/\text{rev}$ facilitate material adhesion resulting in ploughing instead of cutting and a slow speed results in low productivity. Very high depths of cut also negatively affected the surface quality as forces start to climb to a level which impacts. As shown in the plot, the lowest surface roughness value of 5 to 9 nm was obtained with the cutting speed of 60 m/min, $1.5\mu\text{m}/\text{rev}$ feed and $2\mu\text{m}$ depth of cut. With these conditions the adhesion of workpiece material on the tool was found to decrease.

Also surface machined with 0.5 $\mu\text{m}/\text{rev}$ uncut chip thickness has shown severe ploughing. Thus critical uncut chip thickness for this operation was found to be 1.0 $\mu\text{m}/\text{rev}$ where cutting dominated ploughing. But, further improvement in surface quality was achieved with uncut chip thickness of 1.5 $\mu\text{m}/\text{rev}$. Similar trends were observed with Ti-6Al-4V as well. It was also observed that increasing the clearance angle from 5° to 7.5° and cylindrical clearance produced better surface finish. But further increment would weaken the cutting edge. Thus, further experiments were carried out with this set of selected cutting parameters and tool geometry.

4.1.1.SURFACE QUALITY REQUIREMENT

The requirements for mirror surface finish are becoming more and more stringent, as expectations for quality increase and applications develop, which require much finer finishes. The parameters used to describe surface finish are typically two-dimensional (2D) with different manufacturers of surface finish measurement instruments often introducing their own parameters. Surface finish is by nature a three-dimensional (3D) representation of geometric surface irregularities. A surface can be curvy, wavy, rough, or smooth. Some general

terms associated with surface quality are roughness, waviness and form error. But only surface roughness due to cutting was considered in this study since waviness and form error are induced by machine issues such as chatter and vibration of the structure of the machine, which is out of scope of this study.

Ultra precision machining technology is commonly used for the manufacture of precision parts such as mirrors and optics where a mirror grade surface finish on the order of 10 nm R_{rms} ($\cong 7.5$ nm R_a) is required [109]. The automotive industry is requiring surfaces of certain key transmission components to be of optical quality, with targets of 10 nm R_a surface finish to be produced by direct machining without polishing. [110]. Industrial requirement set by B-Con Engineering, the industrial partner for this study for optical grade surfaces in titanium was 10 nm R_{rms} .

There are different formulas used to reduce the 2D data down to one number. In this case a root-mean-square (rms) calculation was applied to represent the roughness of the surface. It is the square root of the average of the measured height deviations squared. The data is also reported with the evaluation length or area and measured from the mean linear surface. R_{rms} is

generally more stringent than the more commonly used R_a value, which is the arithmetical mean deviation. The difference between R_a and R_{rms} measurement is shown in Appendix-2.

4.1.2.TOOL LIFE CRITERION

Conventionally, tool life is measured in terms of cutting distance machined up to a flank wear length of 300 μm . As explained in section 2.5.2 above, this conventional method of measuring tool wear is not meaningful in SPDT, as it is the cutting edge radius that dictates surface finish in this application.

4.1.2.1. Measuring the cutting edge radius

Measuring the cutting edge radius is very challenging and the author's attempts to measure the cutting edge radius are listed below:

1. A Mitutoyo Formtracer with a reported resolution of 8nm was used to trace the cutting edge radius of single crystal diamond tool. Since the stylus radius of the form tracer was more than the tool cutting edge radius it could not identify the edge radius rather it traced the edge as a sharp point (Figure 4-2).

Since this is a contact method, the stylus also left scratch marks on the diamond tool edge and damaged the edge.

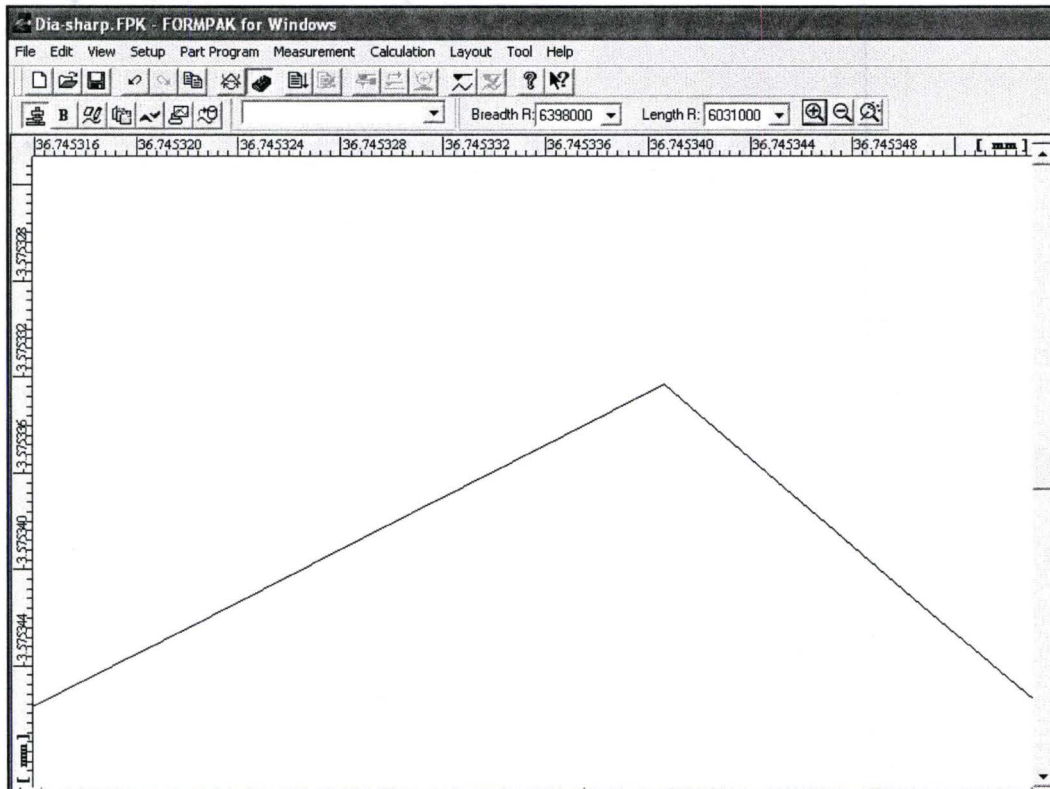


Figure 4-2: Trace of diamond cutting edge in Mitutoyo Formtracer.

2. Zygo white light interferometer, generally used for measuring the surface roughness of ultra precision components was used to estimate the cutting edge of a single crystal diamond tool. Unfortunately the in plane resolution of the data points was not sufficient to give any useful results either. Also since,

diamond is transparent and the angle of the edge is nearly 90 degrees the light reflecting back from the tool was not enough to form a clear image (Figure 4-3). Again, this method could yield only an approximation and not an accurate value of the true cutting edge radius.

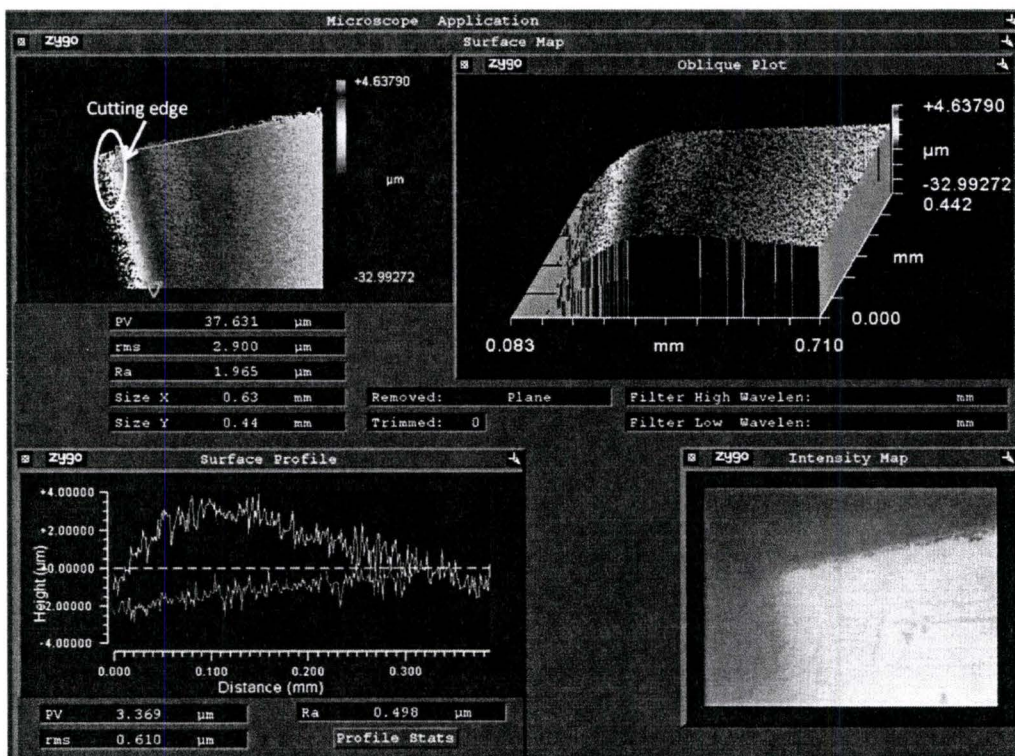


Figure 4-3: Cutting edge radius – Zygo white light interferometer image

- Another attempt was to use Silflo-replica mold material which is supplied by Taylor Hobson, to obtain a replica of the cutting edge (Figure 4-4a) and then slice it (Figure 4-4b) to measure the edge radius in the Zygo. This method did not

yield any meaningful results since the material did not form the sharp edge of the tool well and had poor reflectivity.

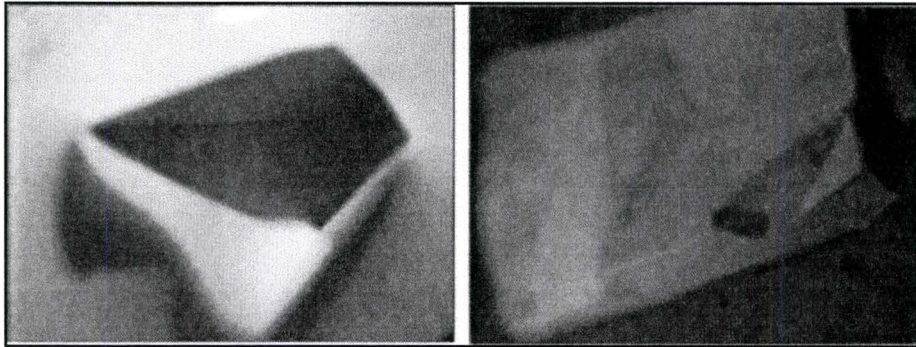


Figure 4-4: (a) Silflo replica of the diamond tool (b) sliced

4. Images obtained from JOEL 7000 scanning electron microscope – SEM (Figure 4-5) shows the nanometric edge profile of the single crystal diamond tool. Using an approximate measurement technique involving the use of curve fitting to the edge a radius of approximately 150nm for a new tool and 300nm for a worn tool was measured.

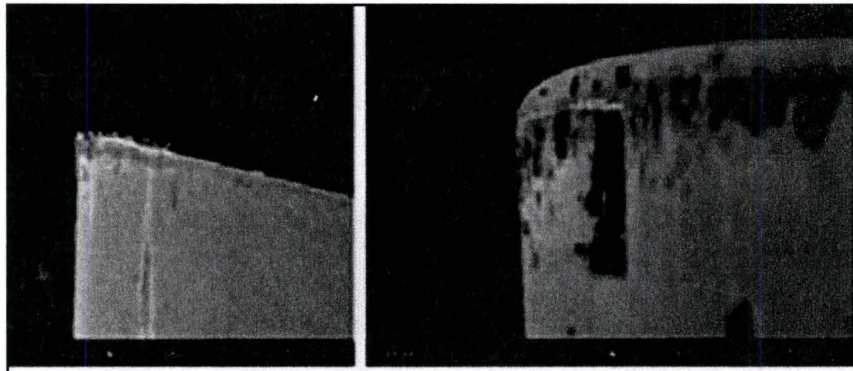


Figure 4-5: SEM images of edge profile measurement

Given the nature of the equipment and the small size of the wear spot it is difficult to repeat these measurements with the frequency needed to plot tool wear over an extended machining trial. Due to the difficulties associated with precise measuring of the cutting edge radius the distance that can be machined while meeting a surface finish value of $10\mu\text{m } R_{\text{rms}}$ is used as a standard to represent the tool life.

4.2.PHASE-II: SPDT OF TITANIUM ALLOYS

4.2.1.SURFACE ROUGHNESS

Figure 4-6 shows the surface profile as measured using the Zygo NewView 5000 – white light interferometer at an intermittent cutting distance of 4.7 km on the CP-Ti machined surface.

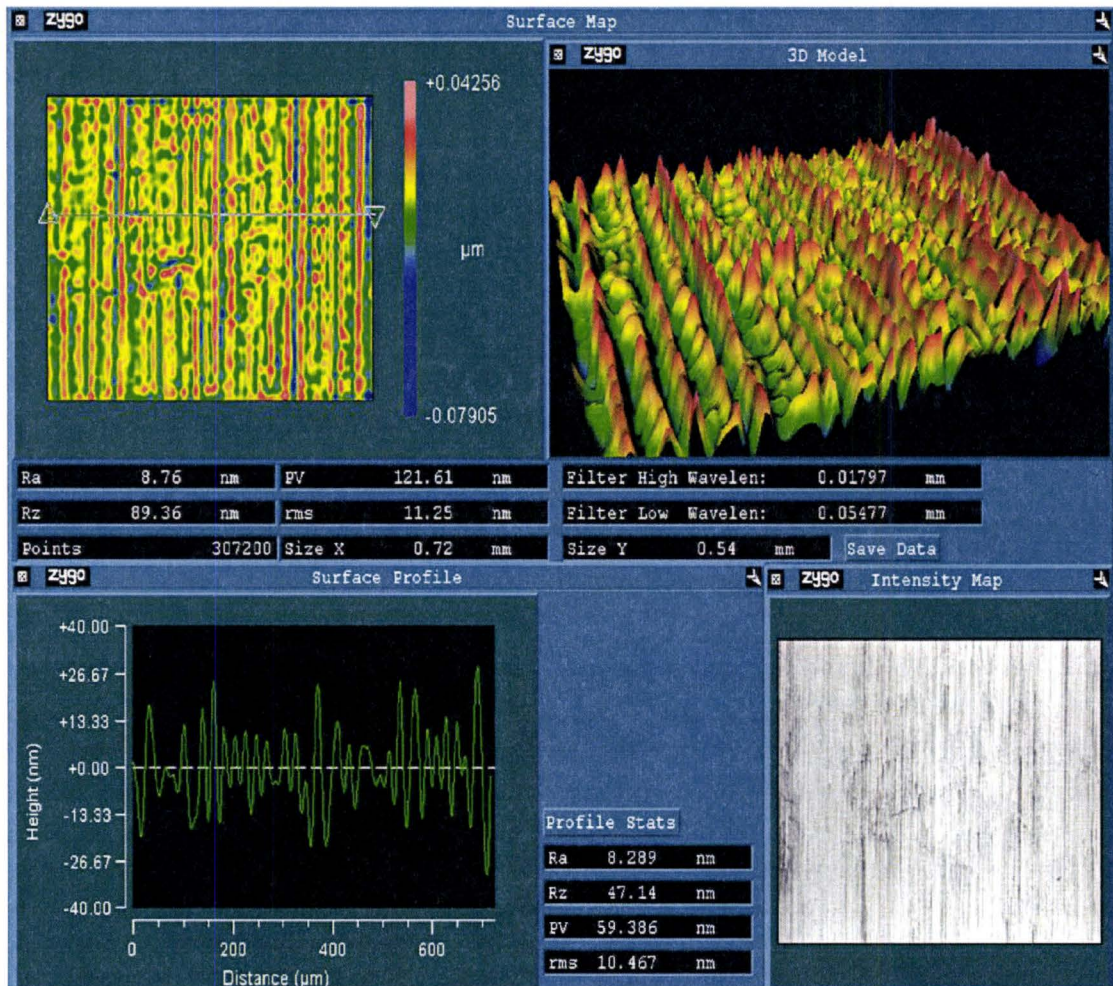


Figure 4-6: Roughness profile of CP-Ti surface machined (R_{rms} : 11.25 nm)

The R_{rms} value of this surface was measured as 11.25 nm, which is above the set industrial standard of 10 nm and so the tool would be considered worn out and no longer usable in this case. The reproducibility of the results was confirmed and it was within +/- 5%. Photographic image of the machined surface of CP-Ti is shown in Appendix-3.

Figure 4-7(a) shows the variation in surface roughness in CP-Ti with respect to the cutting distance, which also represents the tool wear. As shown in the plot (Figure 4-7a), the total distance machined that fell within the required R_{rms} value (< 10 nm) was only 1.25 km, which represents the end of effective tool life. According to Yasui et al. a minimum cutting length of 2.0 km is required to produce a typical high quality component [104], which means the tool life has to be functionally doubled before the ultra precision machining of Ti represents a reasonable process. The effective tool life of a diamond tool used to machine Ti-6Al-4V was found to be 1.7 km (Figure 4-7b). In general machinability of α - β Ti alloys such as Ti-6Al-4V are better than that of CP-Ti for the reasons discussed in section 2.1. Also, the grain size of Ti-6Al-4V is smaller compared to CP-Ti as shown in Appendix -4.

The roughness values obtained from the Zygo – white light interferometer were plotted in Figure 4-7. As could be seen, the field of view (FOV) in Zygo with the standard setting followed in this study, i.e. x10 objective and x1.0 zoom is 0.72 x 0.54 mm (Figure 4-6). With a higher magnification the FOV gets much smaller thus confining the details.

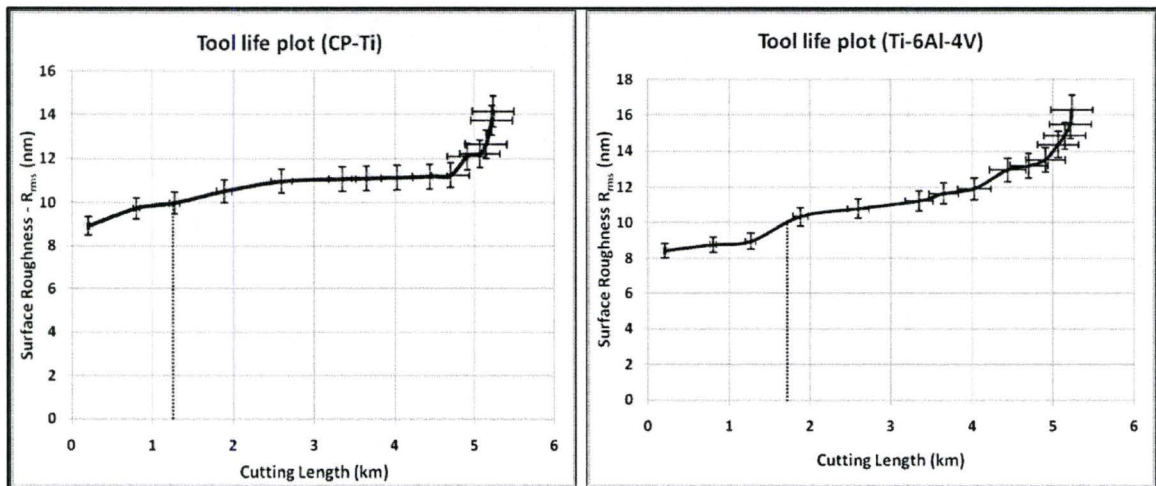


Figure 4-7: Tool life - Cutting length Vs Surface Roughness in (a) CP-Ti, (b) Ti-6Al-4V

In order to get a better insight of the roughness profile obtained, the machined surfaces were examined in a high magnification SEM. The following SEM images (Figure 4-8) compares the details obtained with a FOV similar to Zygo at x170 and an SEM image of x7000 magnification of the same surface.

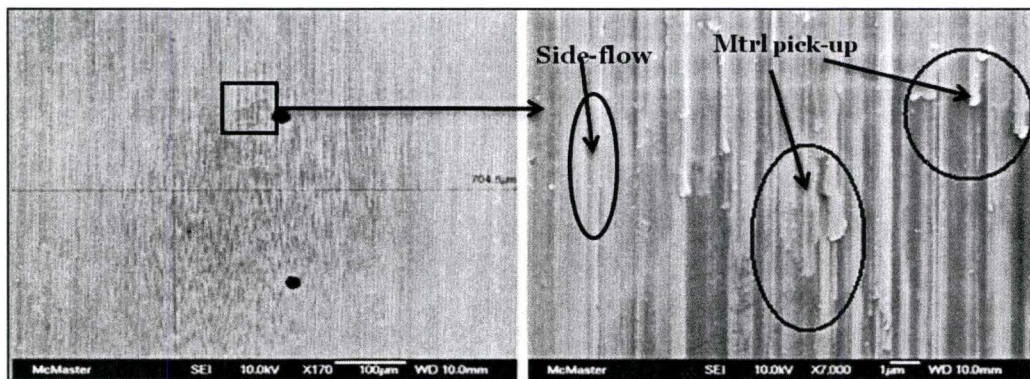


Figure 4-8: Comparison of (a) Zygo and (b) SEM – FOV showing CP-Ti machined surface

Material pick-up and side-flow in CP-Ti and Ti-6Al-4V could be seen in the SEM images shown in Figure 4-8b and Figure 4-9. These surface issues serve to increase the surface roughness value. It is also known that the wear at the cutting edge increases the amount of side-flow, which in turn would reduce the surface quality [111].

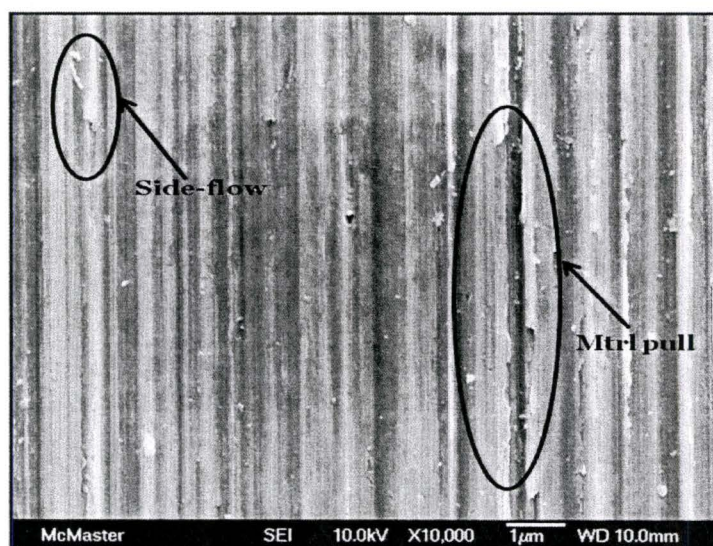


Figure 4-9: SEM image of Ti-6-4 machined surface

4.2.2. CUTTING FORCE ANALYSIS

The three components of forces namely cutting force (F_c), feed force (F_f) and thrust force (F_t) were measured at regular intervals during cutting. Root mean square (rms) value of each component measured with respect to the cutting distance was plotted for the analysis. Appendix-5 shows the force analyses of these three force components.

Generally, any variation or fluctuations in the force components are mainly attributed to the tool wear given the stability of the process and the machine being used. COF during cutting could be estimated as a ratio of the force components [33] in the following manner.

$$\text{Force ratio} = \frac{\text{Thrust force}}{\text{Cutting force}} = \left(\frac{F_t}{F_c} \right)$$

The following graph (Figure 4-11) shows the force ratio plot as a function of thrust force and cutting force when machining CP-Ti. The force ratio increases from 0.6 to 0.81 with the increase in cutting distance and a similar trend could be observed in the tool life plot as well. The COF obtained with tribometer analysis is 0.28 which is lower than that calculated by taking the ratio of the thrust and

cutting force obtained during cutting. This is due to nature of the loading, which on the tribometer is very uniform and generates pure sliding friction, while for machining the stress will vary along the chip tool contact length and the surface of contact will be fresh. The new fresh surface will be more active and increase the amount of adhesion causing the measured COF to be higher for machining.

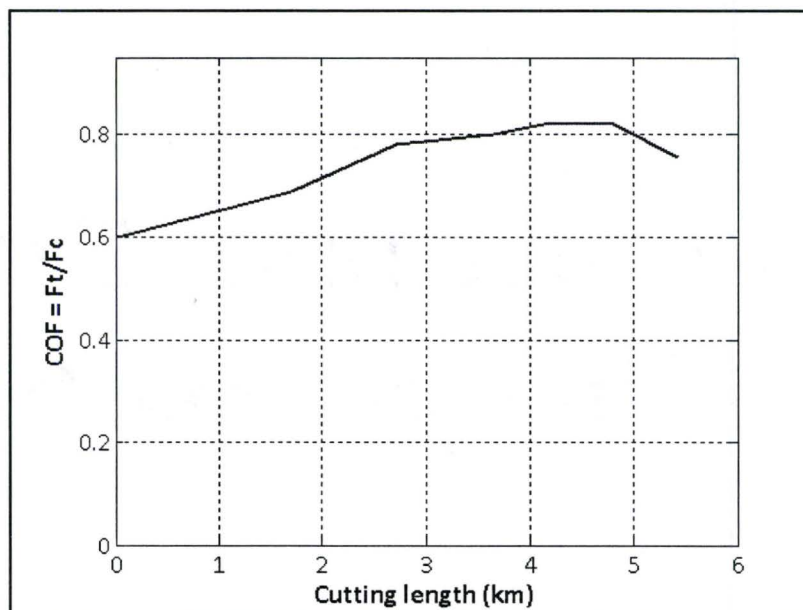


Figure 4-10: Force ratio as a function of thrust and cutting forces in CP-Ti

The cutting conditions are not exactly simulated in the tribometer. During a cutting operation, chip that flows on the rake face is new and will not come in contact with the tool again. On the contrary, in the pin-on-disc tribometer system, the pin always rubs on the same track. In addition, the contact conditions

are very much different along the secondary shear zone or along the rubbing zone with a range of high stresses and temperatures prevailing at the cutting zone where as only a narrow set of conditions exist in the tribometer test [101].

4.2.3.TOOL WEAR MECHANISMS

In order to understand the wear mechanisms taking place in the process of SPDT of titanium alloys, various characterization techniques were used to analyze the cutting tool, workpiece material and the chips. SEM image of the as received tool with a clean and sharp cutting edge is shown in Figure 4-11a.

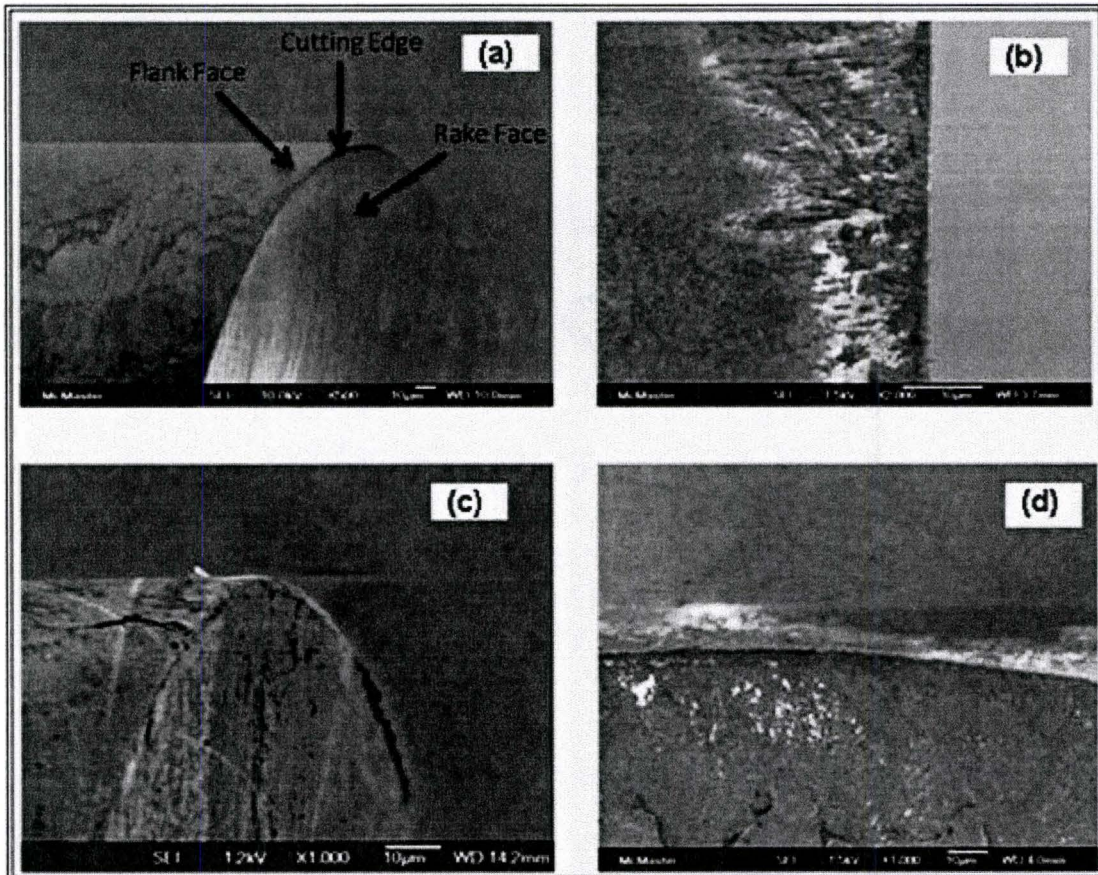


Figure 4-11: SEM images of the diamond tool (a) new tool, (b, c) adhesion of material on flank face (c, d) rake face after machining (CP-Ti)

In machining CP-Ti, as compared to the as received diamond tool, significant amounts of material adhesion could be observed on the cutting edge as well as on both the flank and rake faces of the tool (Figure 4-11b-d). Also, the amount of adhesion has increased with the increased cutting distance (b to d). The correlation between the surface roughness (Figure 4-7) and the adhesion of material with cutting distance could be observed. Thus, in order to increase the tool life i.e. the cutting distance with the targeted surface roughness, the onset of

material adhesion has to be delayed and the rate of adhesion needs to be reduced.

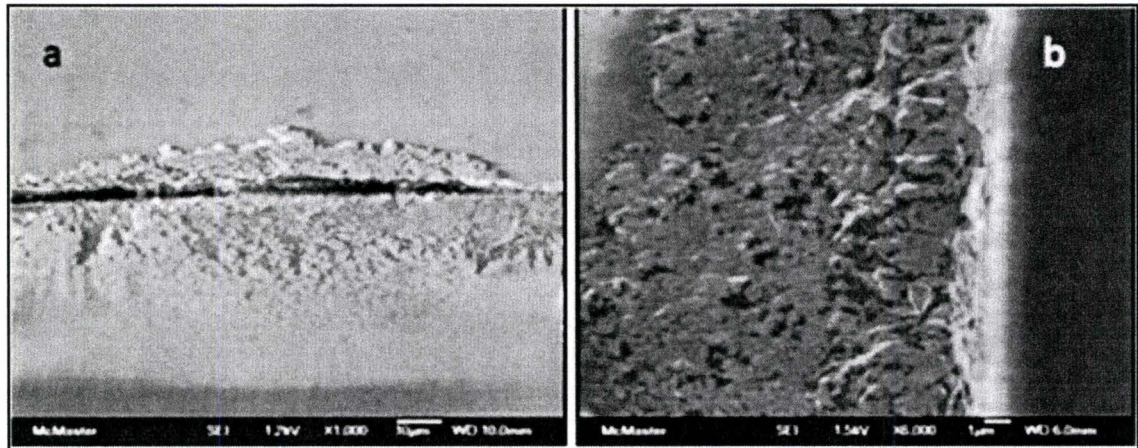


Figure 4-12: SEM images of cutting edge at (a) run-in and (b) end of cutting cycle (Ti-6Al-4V)

A similar wear pattern was observed in tools used for cutting Ti-6Al-4V. As shown in Figure 4-12b, the tool at the end of the cutting cycle which is 5.42 km showed an increased amount of material adhesion than at the initial stage (Figure 4-12a). An SEM image of a similar diamond tool used for machining aluminum for the same cutting distance is shown in Figure 4-13. Remarkable differences in the degree of workpiece material adhesion could be observed.

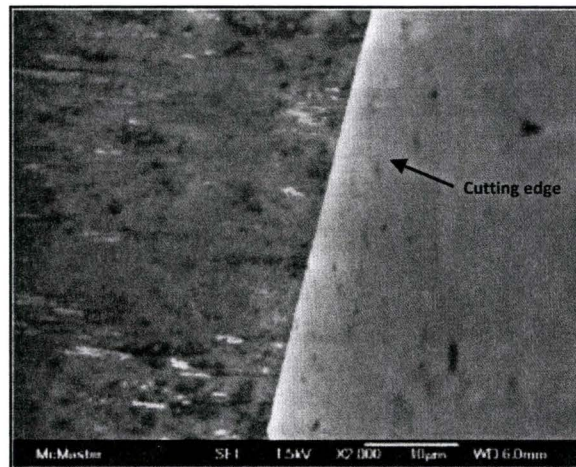


Figure 4-13: SEM image of tool used for cutting aluminum (after 5.42km)

Energy dispersive spectrum (EDS) data shown in Figure 4-14 confirmed the adhered material on the diamond tool was the workpiece material. Compared to aluminum alloys, the tool wear rate is much higher when machining the titanium alloys. This is mainly because aluminum has less solubility for carbon than titanium which readily reacts with carbon resulting in higher levels of adhesion during machining.

Additional SEM images of the machined surface that shows deterioration in surface quality with the increasing cutting distance is shown in Appendix-6. Also images of surface machined with no coolant and surface with side-flow are shown.

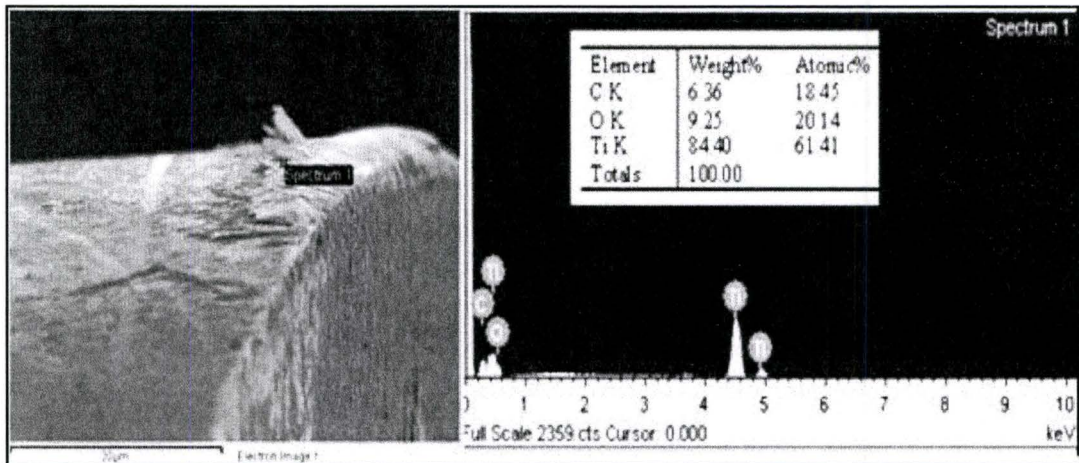


Figure 4-14: EDS spectrum of the adhered material (CP-Ti)

4.2.4. ADHESION WEAR AND CUTTING EDGE RADIUS

Titanium chips have a strong tendency to adhere to the cutting edge, particularly after the tool starts to wear [32]. At the on-set of machining, the cutting edge is extremely sharp and the tool-workpiece and the tool-chip contact region are small. In general, the sharper the edge radius the lower the resulting force components, such as shear and friction forces, will be [20].

It has also been reported that rubbing and burnishing at the cutting edge play an important role in tool wear when the radius of the cutting edge approaches the uncut chip thickness. For a given uncut chip thickness, if the edge radius is smaller, which means sharper, cutting takes place and chips are formed.

But when the edge radius gets larger or when it approaches the size of the uncut chip thickness, then the tool behaves like an indenter with large negative rake angle. Under such conditions, rubbing and ploughing of the material would dominate cutting. [112]. Rubbing and ploughing facilitates material adhesion or built-up-edge formation, which in turn further enlarges the edge radius. This cycle will accelerate over time causing the surface finish to fall out of the allowable range.

Also as explained in section 2.6.1, when the cutting edge recedes, flank wear becomes dominant. The resulting flank wear results in a loss of the clearance angle, which gives rise to increased friction. There is a strong positive correlation between friction and wear, since friction affect the adhesion rate and wear [82], with a smaller COF the adhesion will be lower and the wear rate will be reduced as explained in section 2.7.1. But when the cutting edge gets rounded-off or worn the adhesion rate increases.

Based on the above discussions, it could be observed that the wear at the cutting edge rounds-off or enlarges the edge radius to the point where material adhesion is promoted resulting in poor surface quality, which then indicates the

end of tool life. Thus, it is necessary to understand the mechanism that initiated the wear at the cutting edge.

It is well known that low thermal conductivity of titanium alloys leads to a localized region of high cutting temperature ($\geq 1000^{\circ}\text{C}$) at the tool-workpiece interface in traditional machining. Given the geometries involved the temperatures associated with ultra precision machining are expected to be much lower so as to not melt the PFPE but still high enough to trigger the reactivity of Ti that results in accelerated tool wear [7]. Also the correlation between unpaired d-electrons and COF, chemical reactivity of Ti alloys as explained in section 2.6.1 enhances the adhesion of Ti, as well and is accelerated under the temperatures and loads experienced in the contact zone.

4.2.5. CUTTING EDGE - WEAR MECHANISM

There are several discussions in the literature which conclude that during machining, the wear process in diamond tool is controlled primarily by the rate of graphitization of the diamond [47]. In machining transition metals like titanium, graphite formation at the tool-workpiece interface has been reported [113][46]. As explained in 2.6.1, several research groups have postulated that the wear

mechanism of diamond tools involves the initial transformation of tetrahedral diamond into hcp graphite, which is the thermodynamically more stable form of carbon under the usual contact conditions experienced during machining [48].

Graphitization can take place with a new tool due to the high localized cutting temperature and normal stress in the cutting zone. Under the given cutting conditions, localized normal stress as high as 33 GPa was estimated to be acting at an extremely small contact area of $3 \mu\text{m}^2$. Thus, with the high normal stress, it is not necessary for the temperature to reach 700°C for the graphitization to take place. Presence of diamond along with metastable graphite at this given stress and temperature conditions was found in the carbon phase diagram as well (Ref. Appendix-7). This argument is also supported by the phase transformation that was observed in the CP-Ti chips. As explained in section 2.1, titanium generally undergoes a phase transformation from α to β -phase at 882°C . But, XRD analysis of the CP-Ti chips (Figure 4-16) shows presence of β -phase whereas the parent material has α -phase only (Figure 4-15).

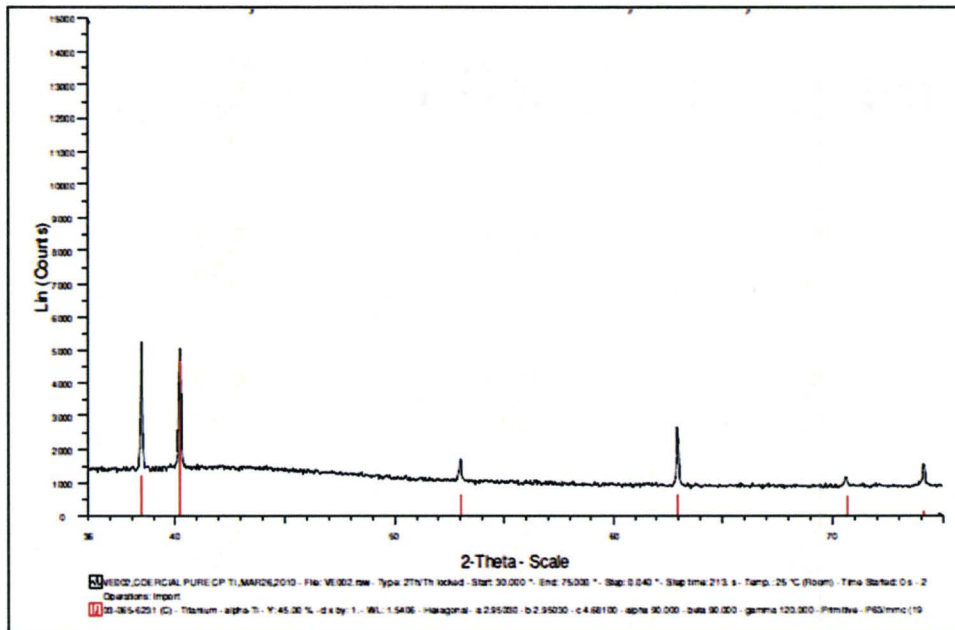


Figure 4-15: XRD image of CP-Ti workpiece

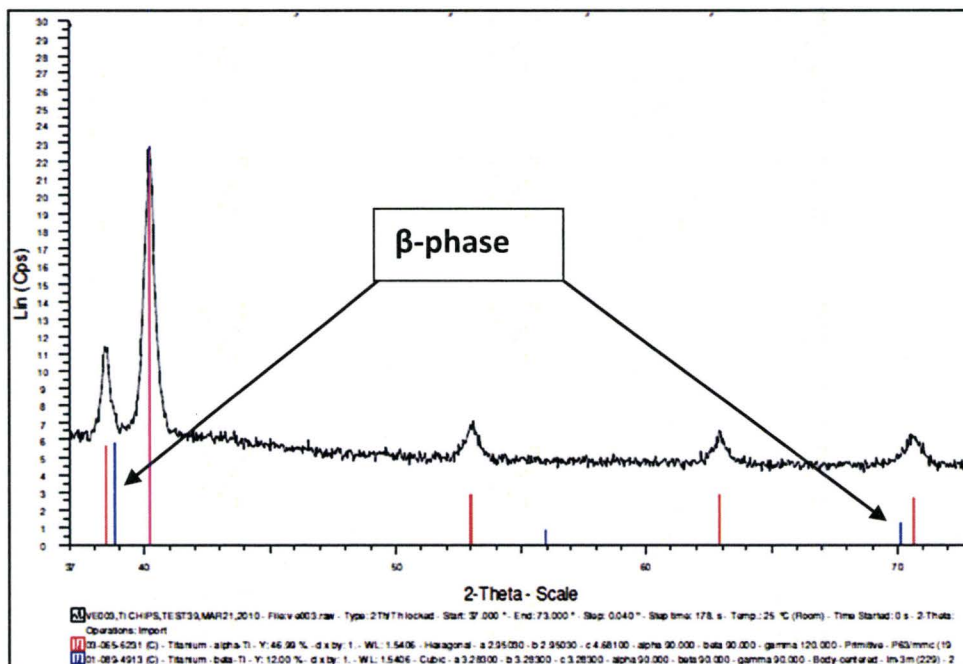


Figure 4-16: XRD image of CP-Ti chips

In order to confirm the occurrence of graphitization during the run in stage of wear the tool was analyzed for the presence of graphite. Raman spectroscopy is a fast, non-destructive method for characterizing pure diamond, crystalline graphite and amorphous carbon [114]. The spectrum, as shown in Figure 4-17, identifies a graphite peak in the diamond tool. Figure 4-7 shows the transition point where the tool wear rate has accelerated after a cutting distance of approximately 0.85 km and would relate to the point where adhesion activity increases.

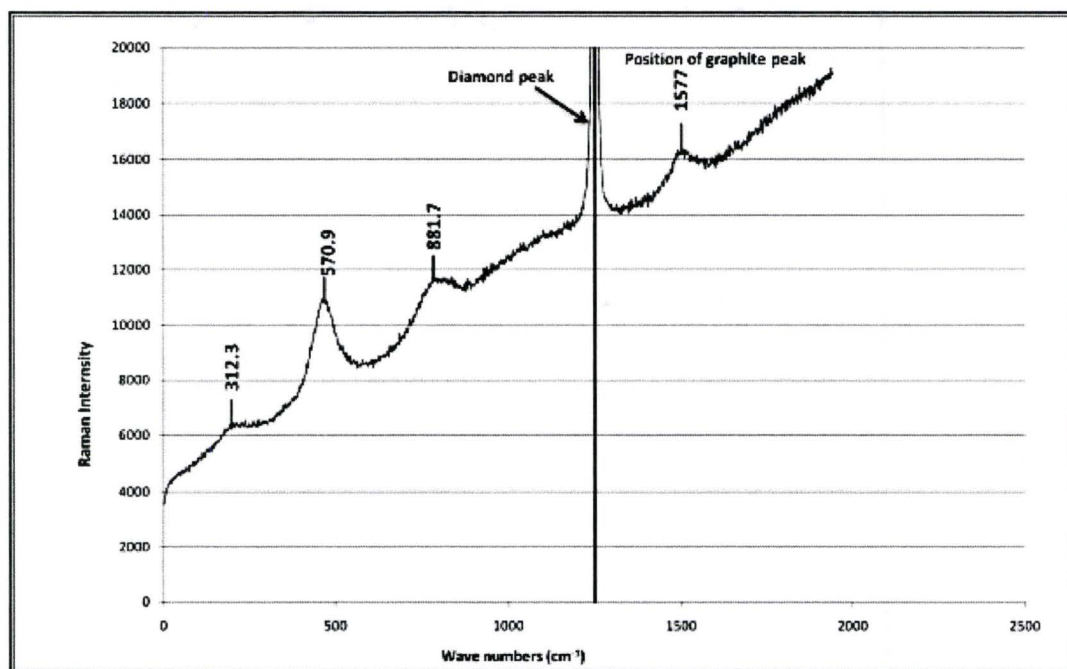


Figure 4-17: Raman spectrum of a worn diamond tool

Thus, a diamond tool used for a shorter cutting distance of 0.5 km was analysed with Raman spectroscopy. The characteristic fingerprint of diamond is a single sharp line at 1332 cm^{-1} and that of graphite is 1577 cm^{-1} . The other three peaks at approximately 312 , 570 and 880 cm^{-1} are comparable to that of TiC as reported by Klein et al. [115]. Raman spectrum of new (unused) tool, as well as the flank area of the used tool that did not come in contact with the workpiece while machining, just had a single diamond peak at 1332 cm^{-1} and no graphite peak.

In order to reconfirm the presence of graphite, XPS analysis of a similar single-crystal diamond tool used under the same cutting conditions, but analyzed at a comparatively shorter cutting distance of 0.3 km, was carried out. The analysis was done at a shorter distance to avoid the stage where carbide formation occurs. Figure 4-18 shows the XPS spectrum obtained from the tool and the presence of graphite is depicted as shown by McFeely et al., Meral et al. [116,117].

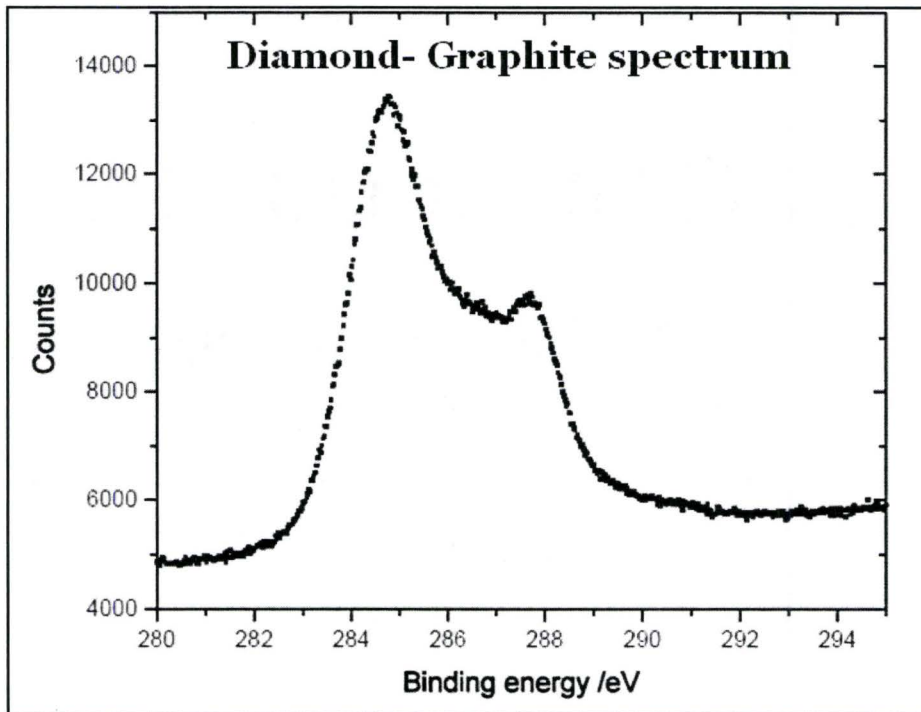


Figure 4-18: XPS spectrum of worn diamond tool with graphite

From the experimental evidence combined with the studies as reviewed in section 2.8, it was postulated that the combination of higher COF of Ti with diamond and its poor thermal conductivity increases the localized cutting temperature and normal stress acting at the tool-chip interface, thus favouring graphitization. Hence, it is graphitization that serves as the mechanism that initiates the wear at the cutting edge and enlarges the radius. This in turn accelerates material adhesion, which is further facilitated by the chemical reactivity of titanium at this elevated temperature. With material adhesion driving the surface finish degradation.

4.3.PHASE-III: WEAR MECHANISMS AND SURFACE MODIFICATIONS

It can be seen from the above section that the tool wear mechanisms is mainly driven by the higher COF at the tool-workpiece and tool-chip interface, localized high cutting temperature, high normal stress, and high chemical reactivity of the titanium alloy. Due to the high contact pressure and the small size of the contact zone the MQL coolant application is ineffective at reducing the temperature and COF. Various approaches that address these issues individually or collectively were discussed in section 2.13 and the need for a protective barrier was also postulated. In traditional machining, hard lubricious coatings are generally used as protective barriers and the disadvantages in using these coatings for SPDT were discussed in section 2.8.

4.4.CHARACTERISTIC REQUIREMENTS OF COATING MATERIAL

Thus, instead of employing a hard coating, as is traditionally considered when wear is an issue, a soft coating was considered, which would serve as a barrier to delay graphitization, reduce the COF and ultimately reduce the rate of material

adhesion. A soft coating could be used as an alternate for this application, provided the coating material meets the following requirements:

1. Ultrathin i.e. the coating thickness should be less than 1nm to avoid edge rounding
2. Provide improved lubricity and reduce the COF in the cutting zone
3. Excellent adhesiveness with the diamond surface
4. Chemically inert - no negative reaction with diamond or titanium
5. Withstand high temperature and heavy load at the cutting zone without shearing
6. The coating process should not induce any residual stress or damage the diamond tool
7. Cost effective – preferably an in-house coating technique

Metallic soft coatings such as Au and Ag have been used for coating cutting tools. But these coatings are at least 300 nm thick [118]. Longer tool life in cutting tools coated with polymers like acrylic and polypropylene have been reported in the literature as well. These polymers are coated by physical vapour

deposition – PVD technique. These polymer coatings are about 800 nm thick [119] which make them too thick and thus, not applicable for SPDT.

Extensive research on surface modification of diamond like carbon –DLC films with fluorine-containing reagent has been reported [120-122]. Surface fluorination has reduced the surface energy of DLC films, as evaluated by contact angle. Evident improvement of hydrophobic properties with the increase in contact angle (105°) was found. The fluorinated DLC films proved to have low COF (0.10) and wear compared to the non-fluorinated films. These films also have a good adhesion to the substrate.

Ether backbone and hydroxyl end groups of fluorine based lubricants such as Perfluoropolyether (PFPE) are most commonly used to fluorinate DLC surfaces. The alcohol group seems to interact with the DLC surface via hydrogen bonding. The primary effect of this is an easier organization of the solvent molecules around the reacting species and consequently slower electron transfer, which would decelerate the reaction between diamond and the unpaired d-electrons of the titanium alloys. Thus, PFPE fluorinated surface with lower surface energy,

higher wetting angle, good adhesion and lesser COF meets the requirements outlined above.

To date no other ultrathin soft coating material has been identified that meets the requirements of SPDT and developing one, for this application, would be far beyond the scope of this study.

4.4.1. CHARACTERISTICS OF PFPE COATING

1. PFPE coating thicknesses are in the range of 20-60 Å. [123].
2. PFPE being a liquid, the molecules are flexible and hence they offer lower resistance to shearing and exhibit low friction. Thermal treatment of PFPE has been shown to further reduce the coefficient of friction and increased the wear life by 30% [90]. It also has a very low surface energy and is both hydrophobic and lipophobic, which means it is not miscible with water or oil. This property makes it useful as an anti-corrosion protective coating and is able to support a lubricant film under considerable load.
3. PFPE exhibits excellent adhesiveness due to its organic-functional bonds [89].

4. PFPEs are known for their valuable operation characteristics over a wide range of temperature, as well as chemical and heat-oxidation resistance.
5. PFPE could withstand temperature up to 500°C and can operate effectively up to 450°C. PFPE fluids have very high thermal stability, high viscosity even at high molecular weights, and low vapor pressures. Metal surfaces coated with thin PFPE films offer very low surface energies with most nonpolar lubricants remaining as droplets. These droplets would be dewetted quickly from bare metal surfaces. This phenomenon is helpful in retaining the liquid lubricants on the friction surfaces during machining thus enhancing the tribological performance of liquid lubricants [124].
6. Also the coating procedure is simple with no residual stress and also the diamond tool can be safely coated without damaging the cutting edge.
7. Also, PFPE coating is very cost-effective and does not require any special set-up. PFPE coating technique is a simple in-house process with no special training requirements.

The performance of this PFPE coating on a diamond tool interacting with titanium was evaluated in a tribometer (phase IV) before validating this coating in a SPDT operation (phase V).

4.5.PHASE-IV: EVALUATION OF PFPE COATING

SEM images of CP-Ti and Ti-6Al-4V pins and the uncoated and PFPE coated diamond tools used for the tribometer tests are shown in Figure 4-19 and Figure 4-20. For both CP-Ti (Figure 4-19-a) and Ti-6Al-4V (Figure 4-20-a), severe material pull-out and wear could be seen in the pins tested on the uncoated diamond tools, where as significantly smoother surface (Figure 4-19-b), (Figure 4-20-b) was seen in the pins tested on the PFPE coated tools. COF was also lower for the PFPE coated tool.

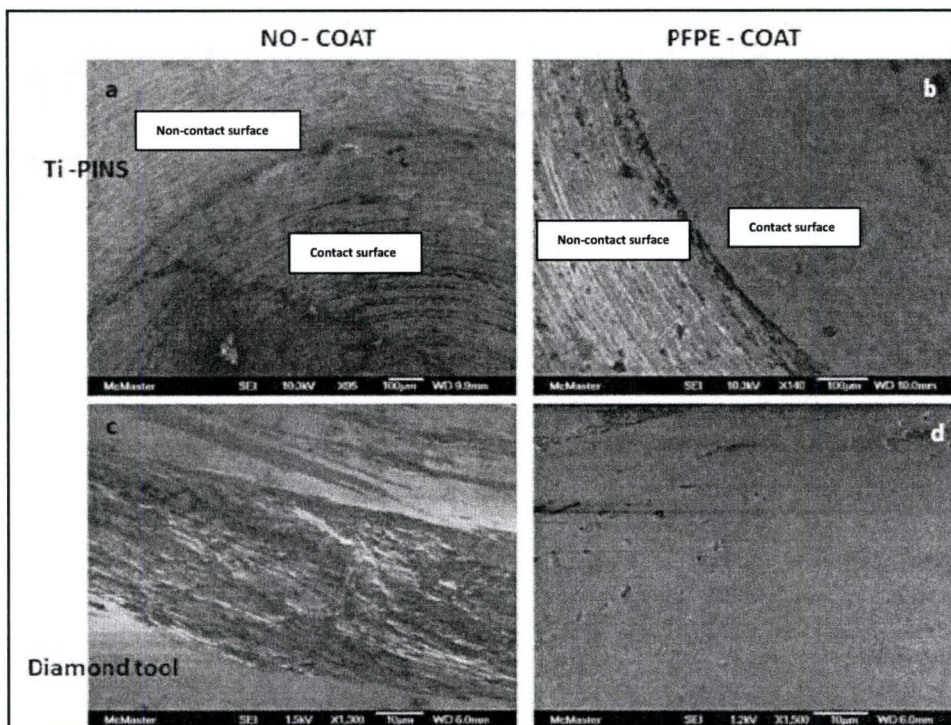


Figure 4-19: SEM images of CP-Ti pins (a & b), Diamond tools (c & d) without and with PFPE coating

Also, adhesion of the pin material for both CP-Ti and Ti-6Al-4V (Figure 4-19-c), Figure 4-20-c) could be observed in the uncoated diamond tools. The PFPE coated diamond tool (Figure 4-19-d), Figure 4-20-d) surfaces were comparatively cleaner with lesser, or in some cases, no adhesion of workpiece material evident on the surface.

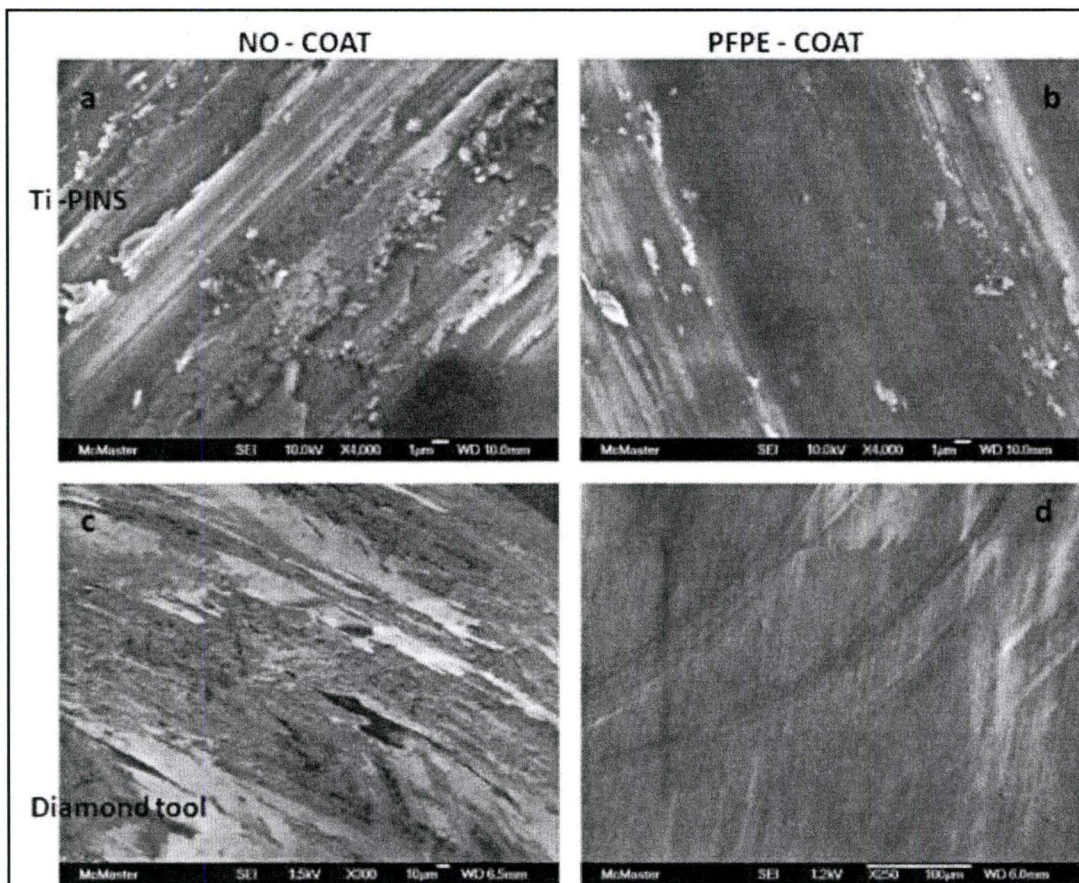


Figure 4-20: SEM images of Ti-6Al-4V pins (a & b), Diamond tools (c & d) without and with PFPE coating

Temperature Vs coefficient of friction obtained with CP-Ti and Ti-6Al-4V were plotted and shown in Figure 4-21 & Figure 4-22. It was found that the diamond tool coated with PFPE had a significantly lower COF compared to the uncoated diamond up to about 450°C for both CP-Ti and Ti-6Al-4V. CP-Ti (α alloy) has a higher COF than Ti-6Al-4V alloy, which is typical of α - β alloys. At about 600°C the friction values for diamond coated with PFPE increased dramatically and became almost equal to the friction values for the uncoated diamond.

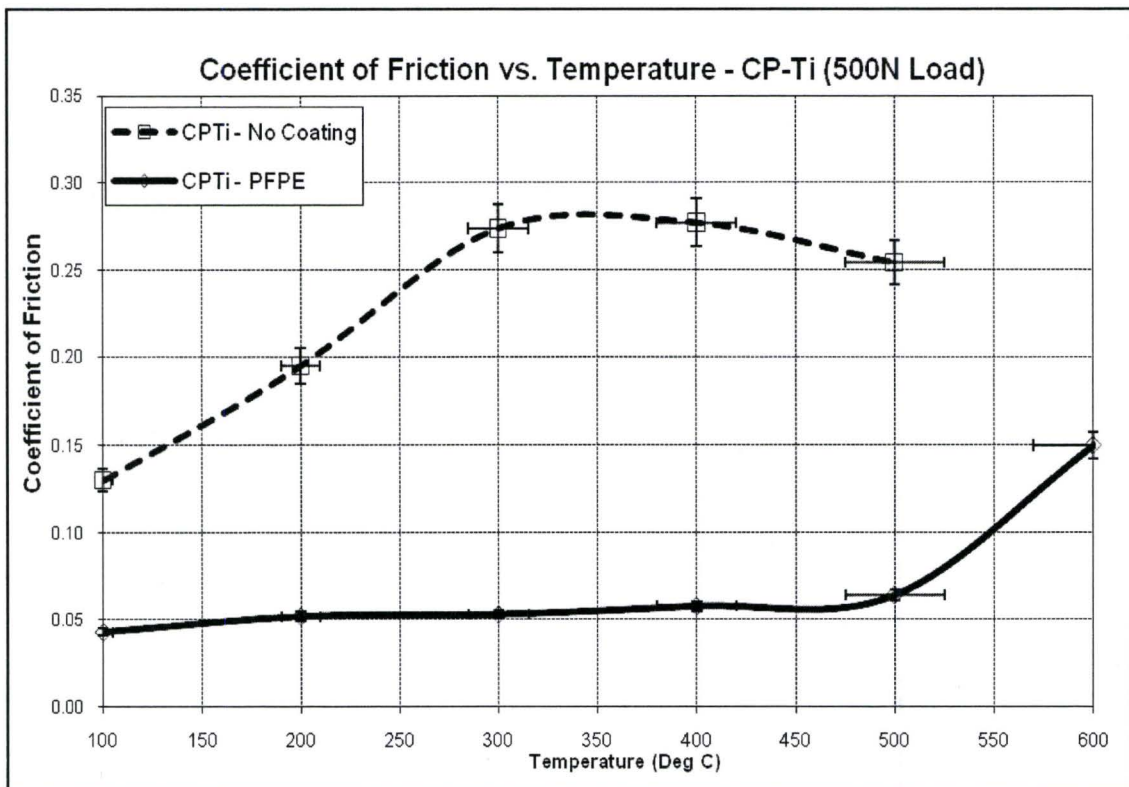


Figure 4-21: Co-efficient of Friction Vs Temperature plot of CP-Ti without and with PFPE coated tool

This occurred for all PFPE tests on both CP-Ti and Ti-6Al-4V pins, indicating that PFPE is stable up to about 450°C, at which point the coating loses its integrity and no longer acts as a protective lubricious layer.

The approach used for calculating the co-efficient of friction is:

$$\text{COF } (\mu) = \frac{\tau}{\sigma} = \frac{3T}{2F_N R}$$

Here T is the measured torque (Nm); F_N is the normal load applied (N) and R is the outer radius (m) of the circular print made by the pin on the disk. This equation was derived assuming that the frictional shear stress could be approximated by the average shear stress acting over the entire circular area. The normal load divided by the apparent contact area provides the normal stress as reported in [125]. This approach for calculating coefficient of friction was also used in similar work by other researchers [101].

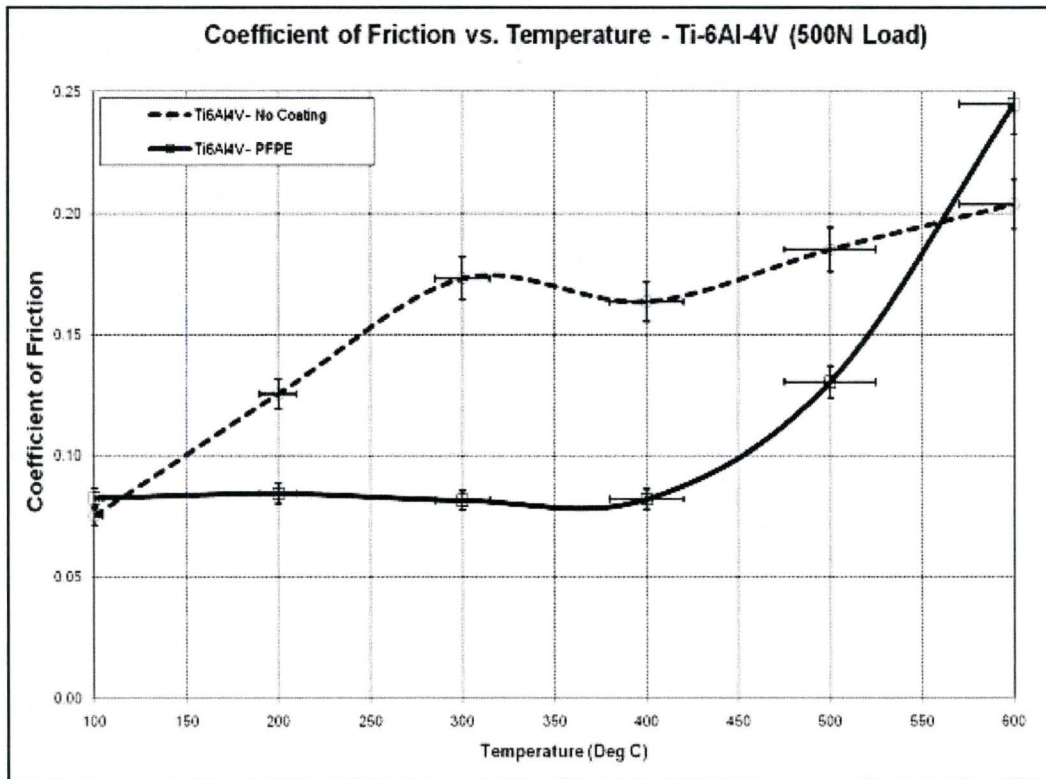


Figure 4-22: Co-efficient of Friction Vs Temperature plot of Ti-6Al-4V without and with PFPE coated tool

Thus, it is evident from the above analysis that PFPE acts as a lubricious protective barrier that reduces the COF between diamond and titanium. In order to evaluate the coating under real cutting conditions, the cutting tests were then repeated with the PFPE coated tools.

4.6.PHASE -V: MACHINING WITH PFPE COATED DIAMOND TOOL

4.6.1.SURFACE ROUGHNESS

Figure 4-23 shows the surface roughness profile of CP-Ti obtained with the PFPE coated tool. The R_{rms} value measured at a cutting distance of about 4.7 km was 7.718 nm.

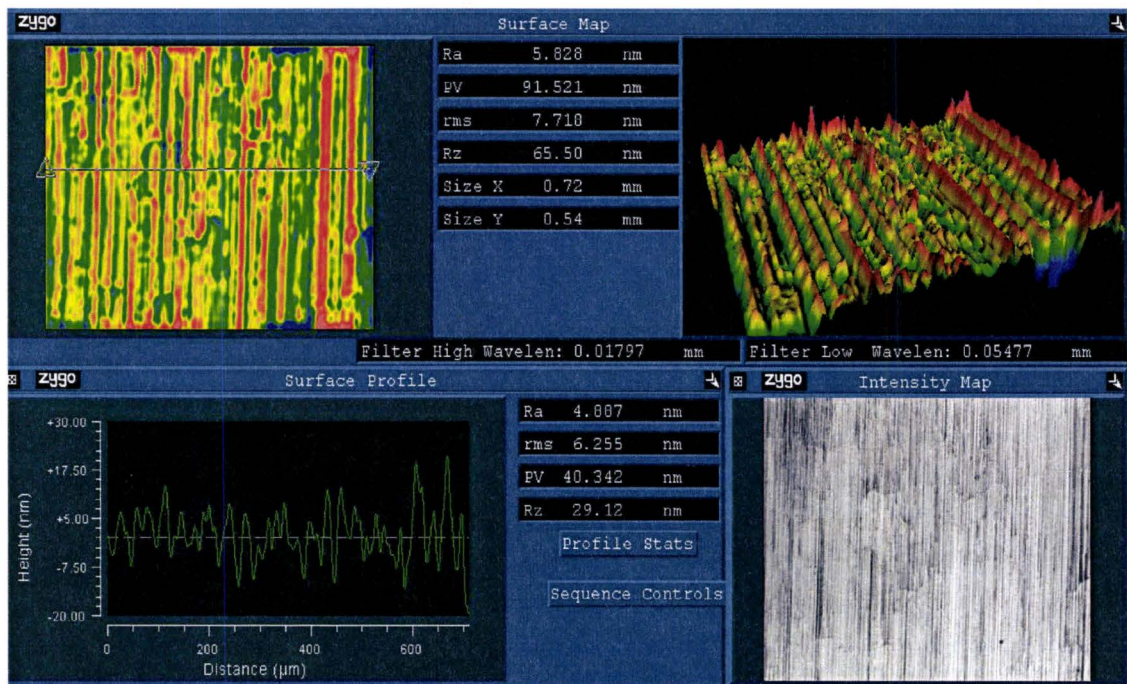


Figure 4-23: Roughness profile of CP-Ti surface machined with PFPE coated tool (R_{rms} : 7.718 nm)

Direct comparison of the surfaces machined consecutively with and without PFPE coated tools in CP-Ti and Ti-6Al-4V are shown in Figure 4-24 & Figure 4-25. The difference in surface roughness profile could be seen in the height differences in plot (c). Also, surfaces machined with PFPE coated tools are smoother (a, b) and show less surface damage (d).

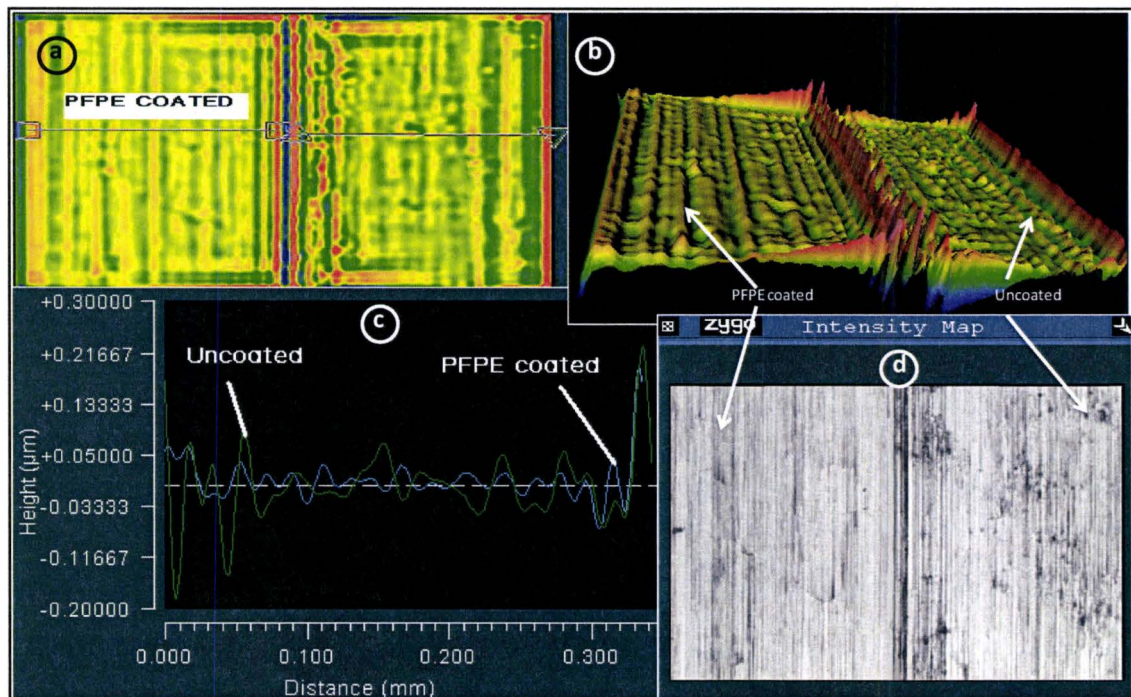


Figure 4-24: Comparison of surfaces generated in CP-Ti with PFPE coated and uncoated tools

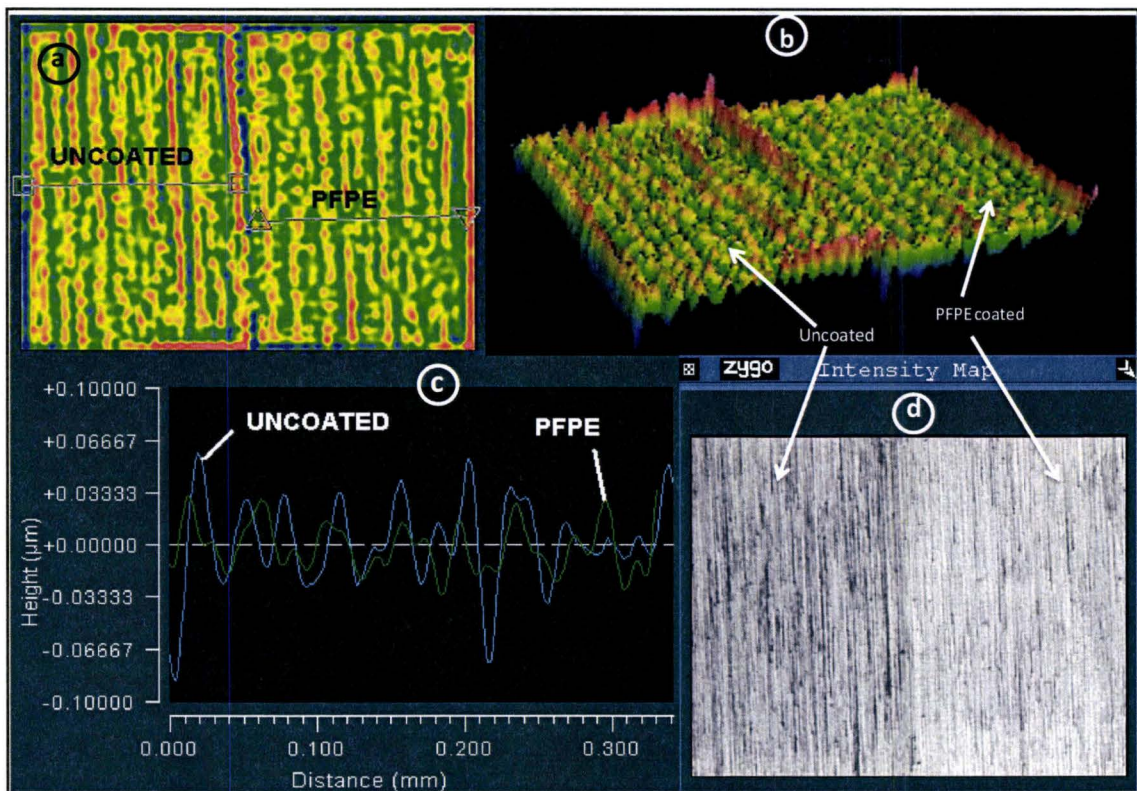


Figure 4-25: Comparison of surfaces generated in Ti-6Al-4V with PFPE coated and uncoated tools

Figure 4-26 and Figure 4-27 show the comparison of roughness values measured against the cutting distance and it is evident from the plots that not only did the PFPE coated tool produce a better surface quality it also did so for a longer cutting length. Each test was repeated at least thrice and the repeatability was found to be within $\pm 5\%$.

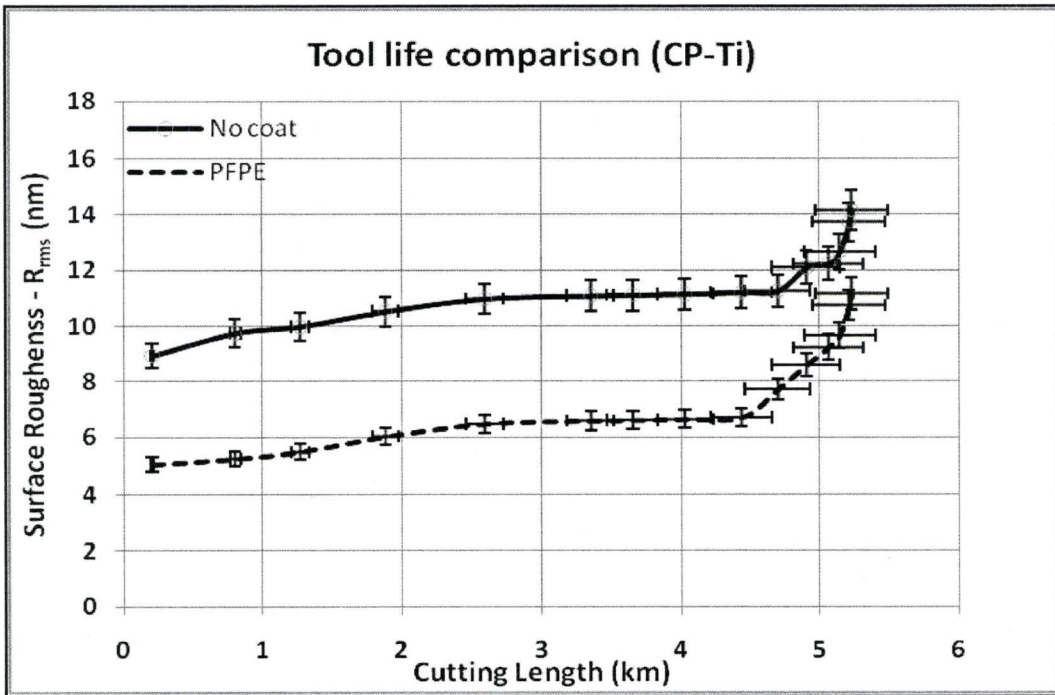


Figure 4-26: Cutting Length Vs Surface Roughness of CP-Ti without and with PFPE coating

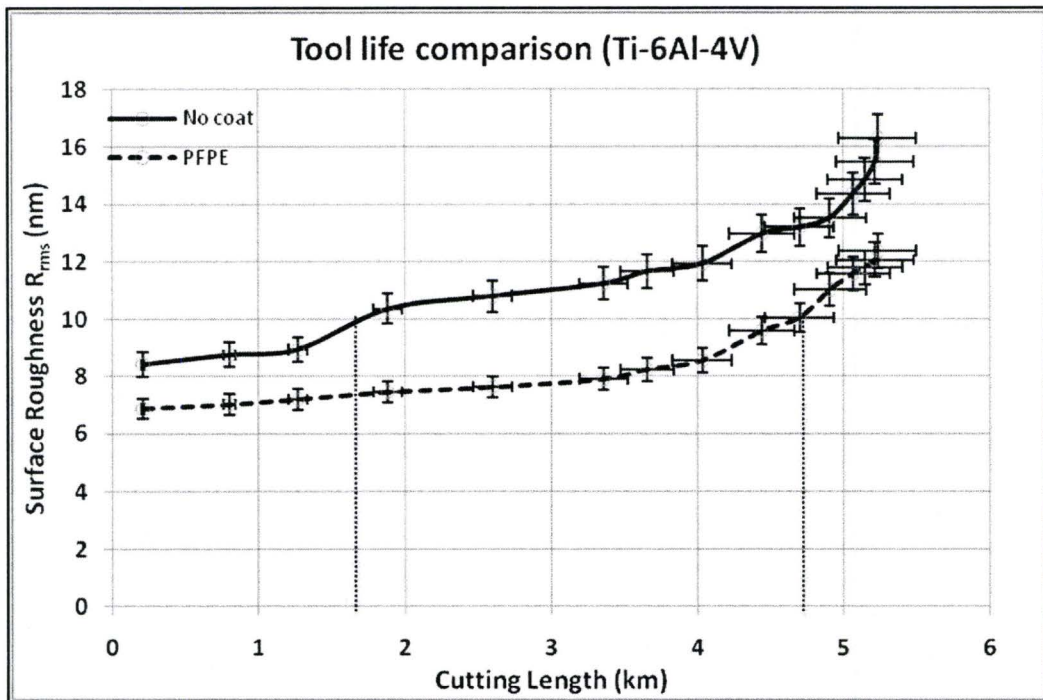


Figure 4-27: Cutting Length Vs Surface Roughness of Ti-6Al-4V without and with PFPE coating

When compared to the SEM image of the uncoated diamond tool shown in Figure 4-11a, no distinct difference in the cutting edge radius could be observed for the PFPE coated diamond tools at this magnification, as shown in Figure 4-28.

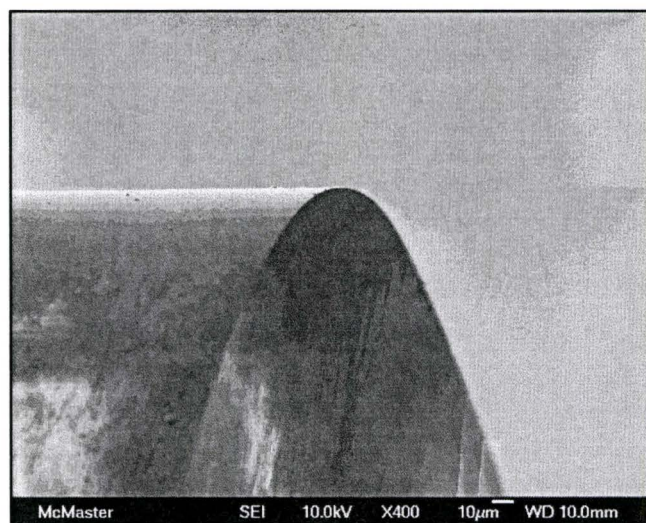


Figure 4-28: SEM image of PFPE coated diamond tool

Also, improvement in the surface quality obtained at the on-set of machining with the PFPE coated tools as shown in Figure 4-26 and Figure 4-27 ensures that the coating has not altered the cutting edge radius of the tool significantly.

But, when compared to the uncoated tool the cutting length that met the industrial requirement of surface quality in CP-Ti was 1.25 km and that of Ti-6Al-4V was 1.7 km. These values have been significantly increased through the use of PFPE coated tools to 5.1km in CP-Ti and 4.85 km in Ti-6Al-4V.

SEM images of the CP-Ti (Figure 4-29-a) and Ti-6Al-4V (Figure 4-30-a) surfaces machined with the uncoated tool shows material-pull and side-flow which affects the surface quality and increases the roughness value. Distinctive difference between the surfaces machined with PFPE coated and uncoated tools could be observed in terms of quality and surface damage both in CP-Ti as shown in Figure 4-29-b and Ti-6Al-4V as shown in Figure 4-30-b.

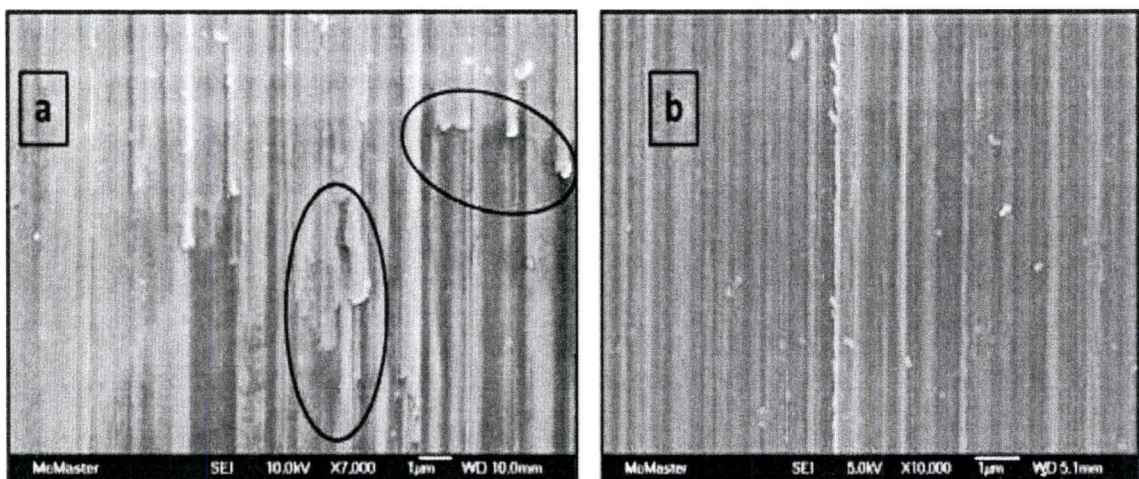


Figure 4-29: CP-Ti machined surface: (a) No coat and (b) PFPE

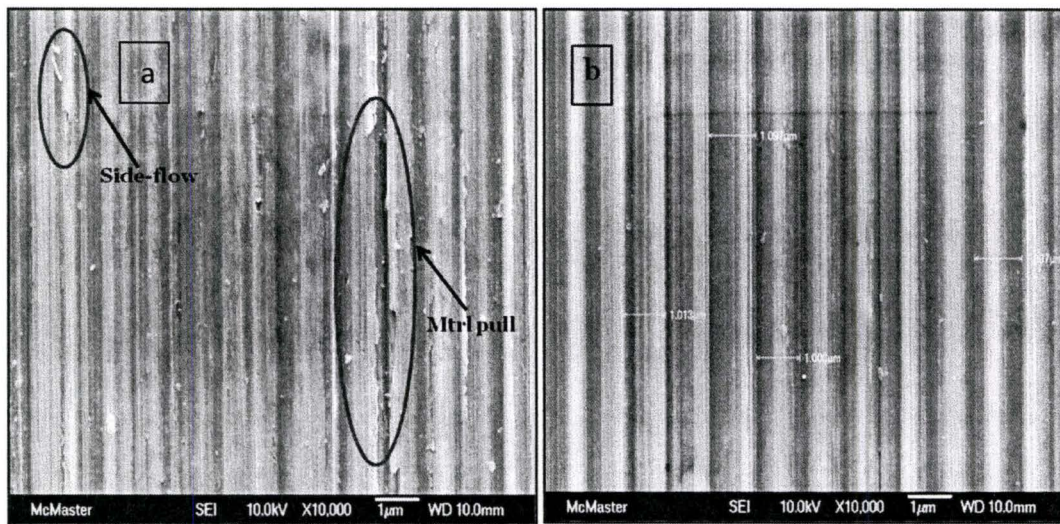


Figure 4-30: Ti-6Al-4V machined surface: (a) No coat and (b) PFPE

4.6.2. CUTTING FORCE ANALYSIS

As discussed earlier in section 4.2.2, the average COF in the cutting zone can be estimated from the ratio of the thrust force to the cutting force. The following plot compares the force ratio obtained with and without the PFPE coated tools. A significant reduction in the force ratio could be observed in SPDT of CP-Ti with the PFPE coated tool. Compared to Ti-6Al-4V alloys, the force ratio in machining CP-Ti is greater. This is due to the fact that in general Ti-6Al-4V (α - β) alloys pose better machinability than CP-Ti (α alloy). This was discussed briefly in section 2.1 of this thesis. Appendix-3 shows the analyses of the three force components measured without and with PFPE coating.

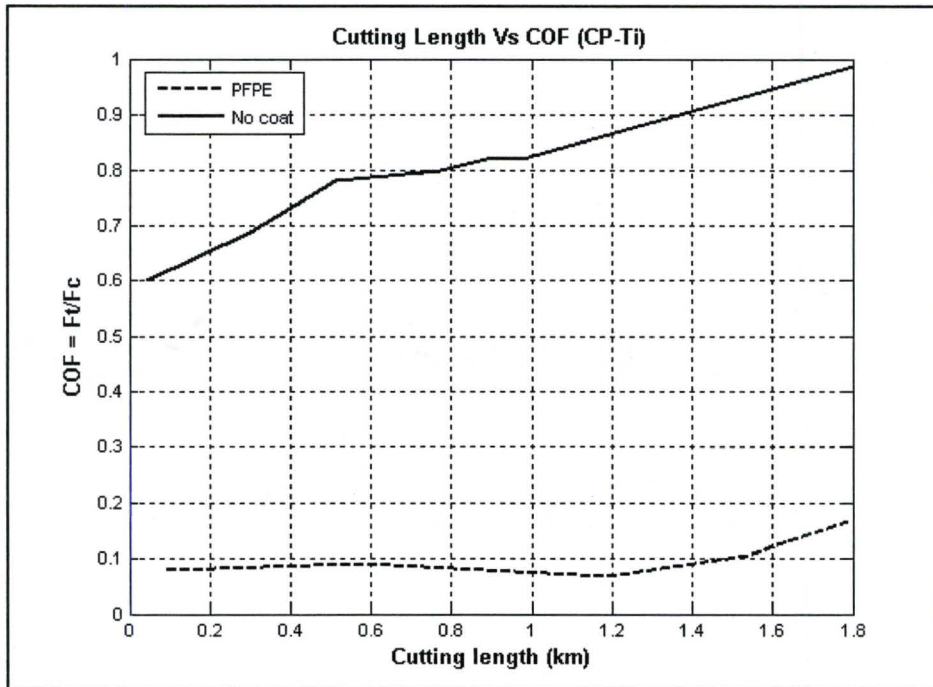


Figure 4-31: Cutting length Vs Force ratio in CP-Ti

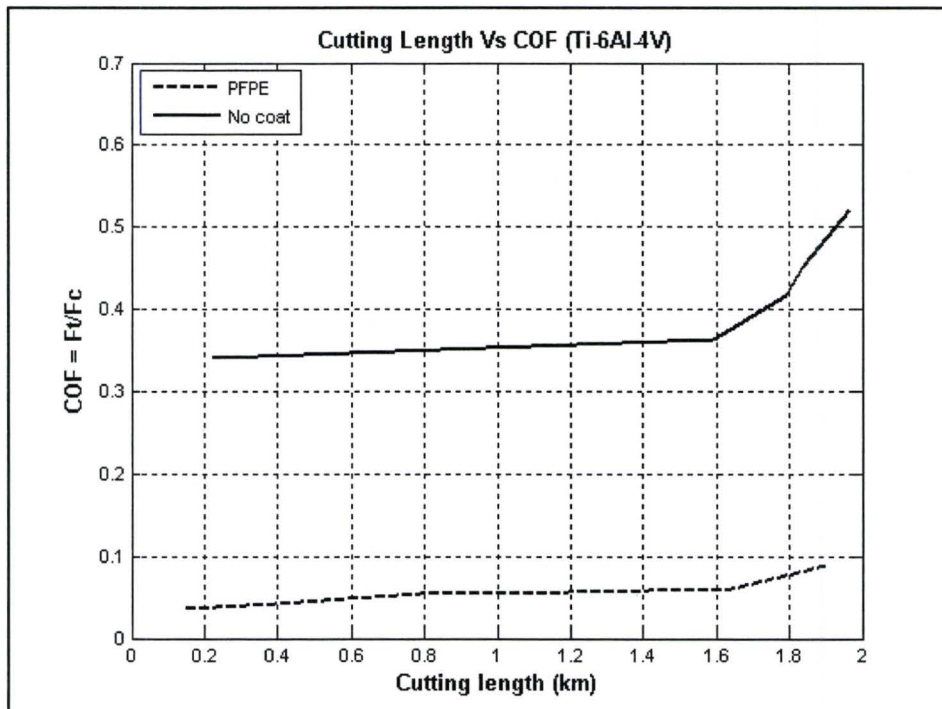


Figure 4-32: Cutting length Vs Force ratio in Ti-6-4

Reduction in the magnitude could be observed in all three force components with PFPE coating which is an indication of enhanced machinability. It could also be observed that the force ratio has a similar trend to the value obtained from the tribometer analysis. Both the tribometer study and the machining test demonstrate a reduction in COF with the use of the PFPE coating on the tool material. This difference in the values of the result implies that the surfaces generated by the machining process have chemical activities different from those of the bulk material. Also, the localized high temperature generated at the cutting region, elevates the surface energy of both the newly generated chip and the machined surface. These surfaces would be chemically more active to facilitate adhesion. Adhesion becomes extremely significant, when the undeformed chip thickness is extremely small, where the effective rake angle caused by the edge radius becomes a high negative value. This situation would also affect the chip formation and surface quality [126].

Also, machining is more aggressive than the tribometer, since when cutting, the temperature profiles, stresses and adhesion are different and most likely lead to more adhesion. Also the period of cutting is longer than the short test ran with the tribometer. Tribometer analysis is a sliding test meant to reflect

an element of cutting, that is temperature and coatings and the results are a relative comparison. The tribometer simulates the sticking region of the tool where typically the shear stress is lower than the normal compressive stress, thus COF is less for this region, whereas in metal cutting the COF is for the sticking and the sliding zone (Figure 2-22).

4.6.3.TOOL WEAR MECHANISMS

Compared to the uncoated diamond tools at the run-in stage and at the end of the effective tool life, as shown in Figure 4-33a, b; material adhesion was remarkably reduced for the PFPE coated tools under the same conditions and cutting length. As seen in Figure 4-33c, the tool cutting edge shows almost no adhesion. It could be seen that adhesion levels on the PFPE coated tools were significantly less when compared to that of the uncoated tool at a cutting distance that represents the end of uncoated tool life. Also, adhesion on the PFPE coated tool at this cutting distance is also less than that of the uncoated tool even at the run-in stage. Thus a significant reduction in adhesion is measured at the run-in stage, as well as for a longer cutting distance. This improvement is

attributed to the tool life enhancement coming from the presence of the PFPE coating.

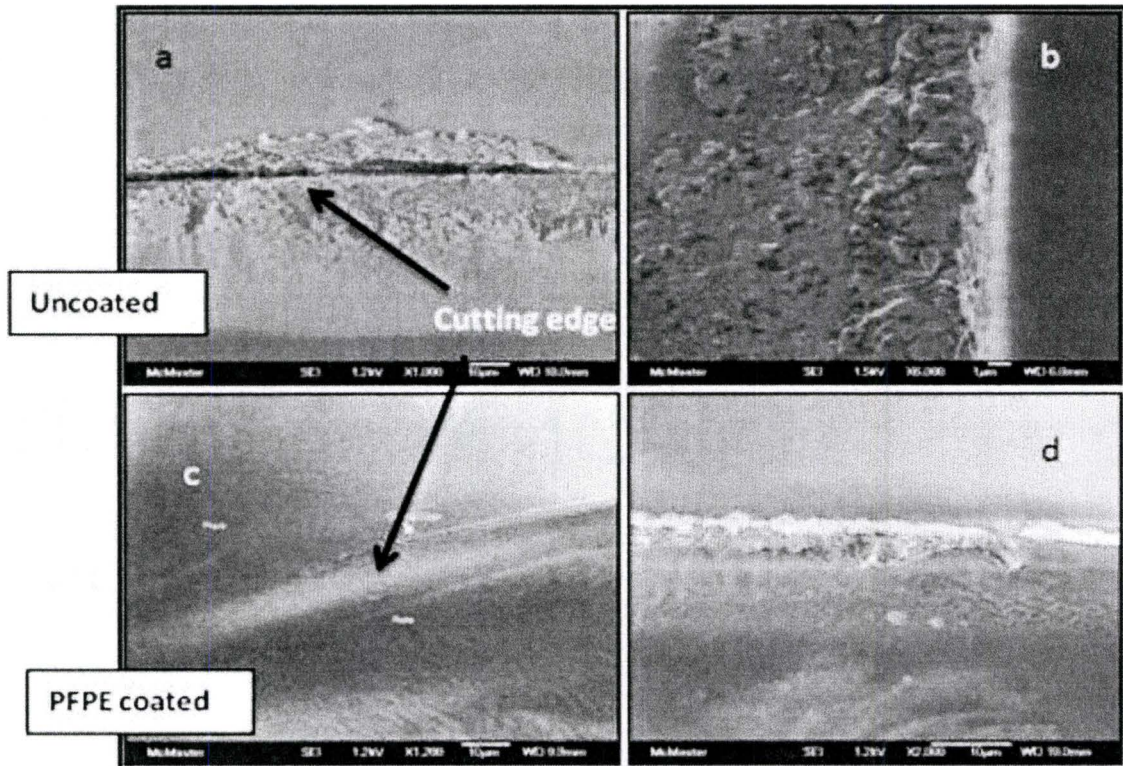


Figure 4-33: Tool cutting edge at the run-in (a,c) and intermittent cutting distance (b,d) without and with PFPE

The PFPE coated tools were further analysed with Raman spectroscopy and an XPS technique. Raman spectrum obtained from the PFPE coated tools is shown in Figure 4-34. In this case only a diamond peak could be observed indicating that graphitization of the cutting edge is not taking place.

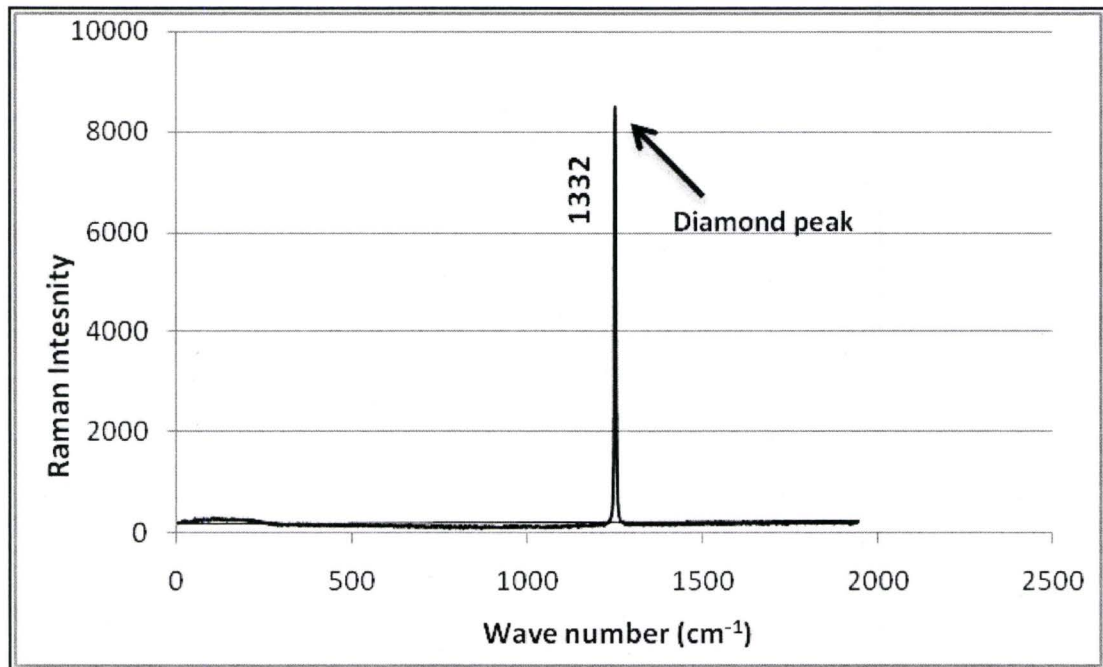


Figure 4-34: Raman spectrum of PFPE coated single-crystal diamond tool

An XPS spectrum obtained with the PFPE coated tool is shown in Figure 4-35. A similar observation as with the Raman analysis was made, as the spectrum shows a diamond peak only. Thus, it is evident from these analyses that PFPE acts as a protective barrier and hinders the graphitization process.

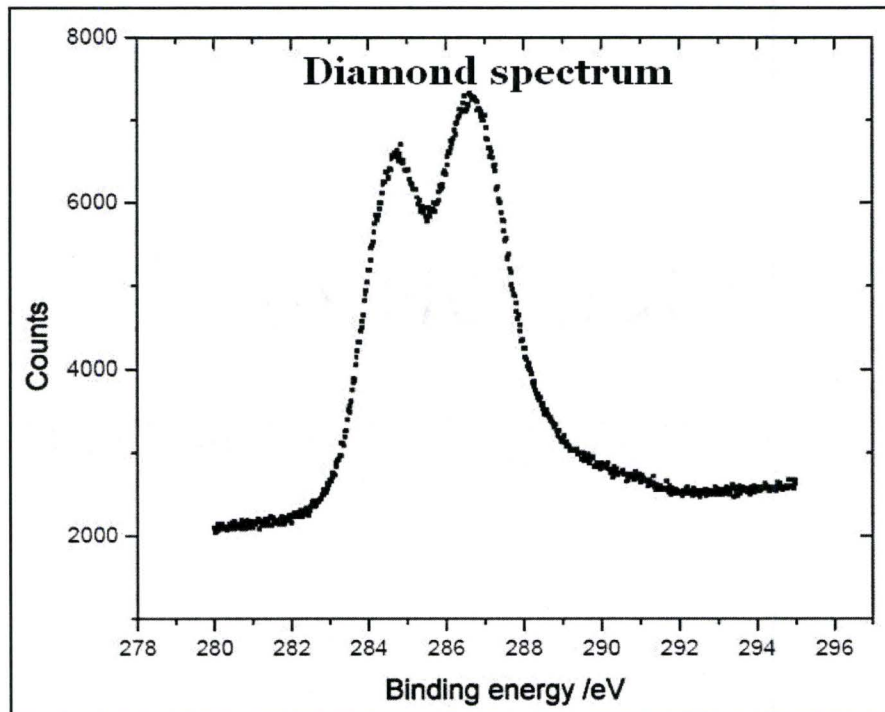


Figure 4-35: XPS spectrum of PFPE coated diamond tool

As discussed in section 2.9, PFPE has a bonded layer, a mobile layer and molecules can be trapped within the valleys or imperfections of the tool surface which can serve as a reservoir for PFPE molecules over time. The lifetime of these layers under the applied loads and temperatures is the real measure of the durability of the coating.

Bonded layer with its densely packed structure chemically adheres to the tool surface and protects the surface from solid contact. This results in lower

friction and higher durability. However, the bonded layer alone is insufficient and the mobile layer is necessary to further enhance the durability of the coating.

The mobile layer which could be referred to as the fluidic layer is flexible; offers lower resistance to shearing; enhances lubricity and reduces friction. The mobile molecules moves easily and replenishes the wear trenches compared to the bonded layer, which adheres strongly to the diamond surface. The bonded layer decreases diffusion of the mobile layer out of the contact region and, thereby prevents the loss of lubricity that would lead to rapid tool wear. It also protects the tool during the run-in condition and helps to retain the lubricant oil in the contact zone.

Since, the tools used in SPDT have some imperfections, as shown in Figure 2-6 at the cutting edge, the PFPE material can get trapped in these imperfections. As the cutting progresses, the trapped PFPE gets dragged to the surface, thus replenishing the supply in the contact zone to maintain lubricity. Similar observations have been reported by Hiroshi et al. [127] in extending the effective life of artificial joints. Together these three mechanisms work to maintain a sharp

cutting edge, reduce friction and minimize adhesion wear which in turn enhances tool life and surface quality.

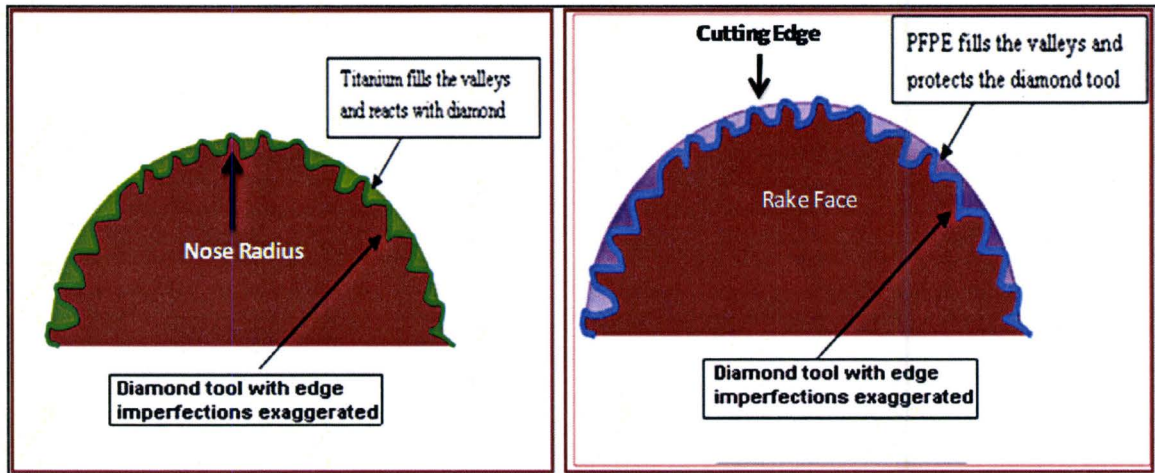


Figure 4-36: Schematic of a diamond tool with an imperfect cutting edge without and with PFPE coating (magnitude of imperfections enlarged to highlight effect)

4.6.4. CHIP ANALYSIS

Figure 4-38 shows the SEM images of the chips obtained in ultra precision machining of CP-Ti with diamond tools. Li Ning [128] has reported for traditional machining that the cutting tool performance also depends on the contact length between the chip and the tool rake face. In ultra precision machining of titanium the tool chip contact length is extremely small and the chips produced under this condition are short and curly, as shown in Figure 4-37. Severe tearing of the chip

edges is observable in the SEM images. These tears and the curling are attributed to adhesion and higher COF, as reported by Kawaseigi et al. [78]. Thus, in order to obtaining a longer functional tool life the COF must also be reduced. Thus, the protective coating being considered must also address this issue.

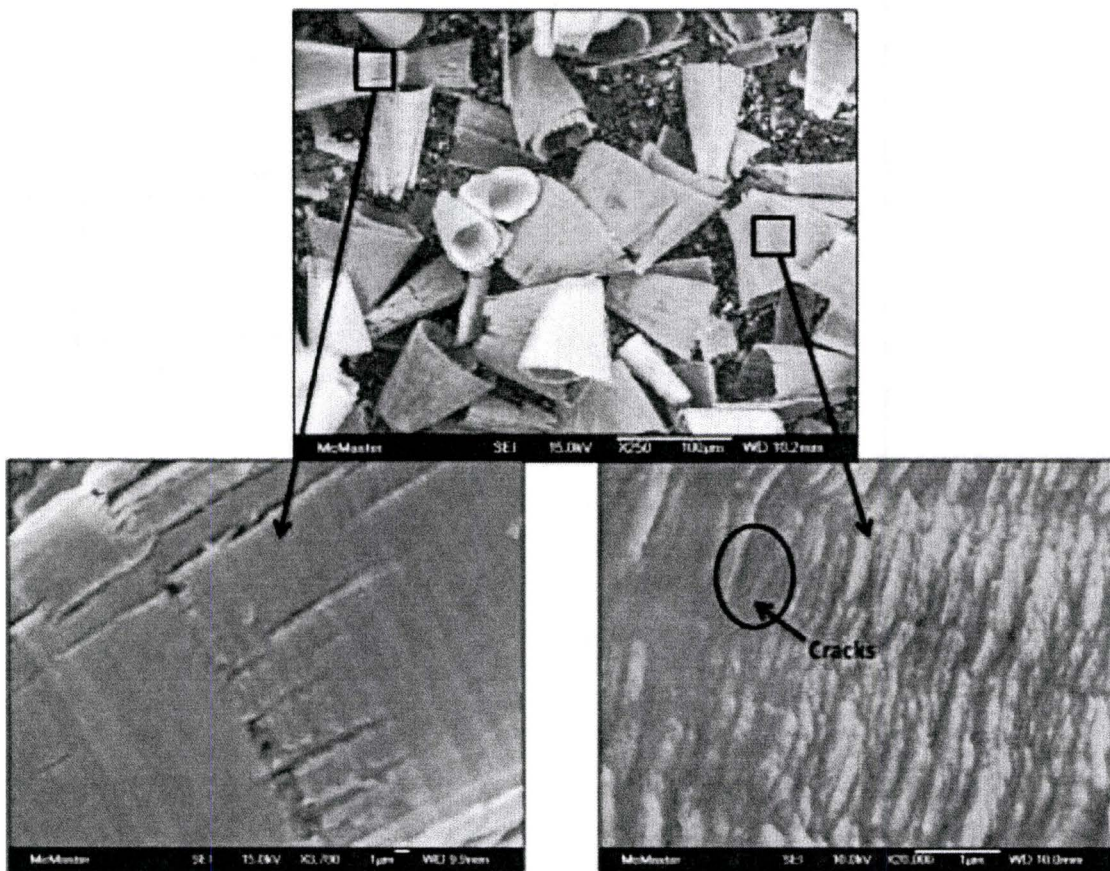


Figure 4-37: SEM images of CP-Ti chips with torn edges

Figure 4-38 shows the SEM images of chips obtained with PFPE coated diamond tools. Unlike the chips obtained with uncoated tools (Figure 4-37) no

torn edges could be seen in this case. Instead of extremely short needle like chips, flat and smooth ribbon like chips with uniform thickness and un-torn chips were formed and this could be attributed to the improved lubricity and reduced COF with the PFPE coated films.

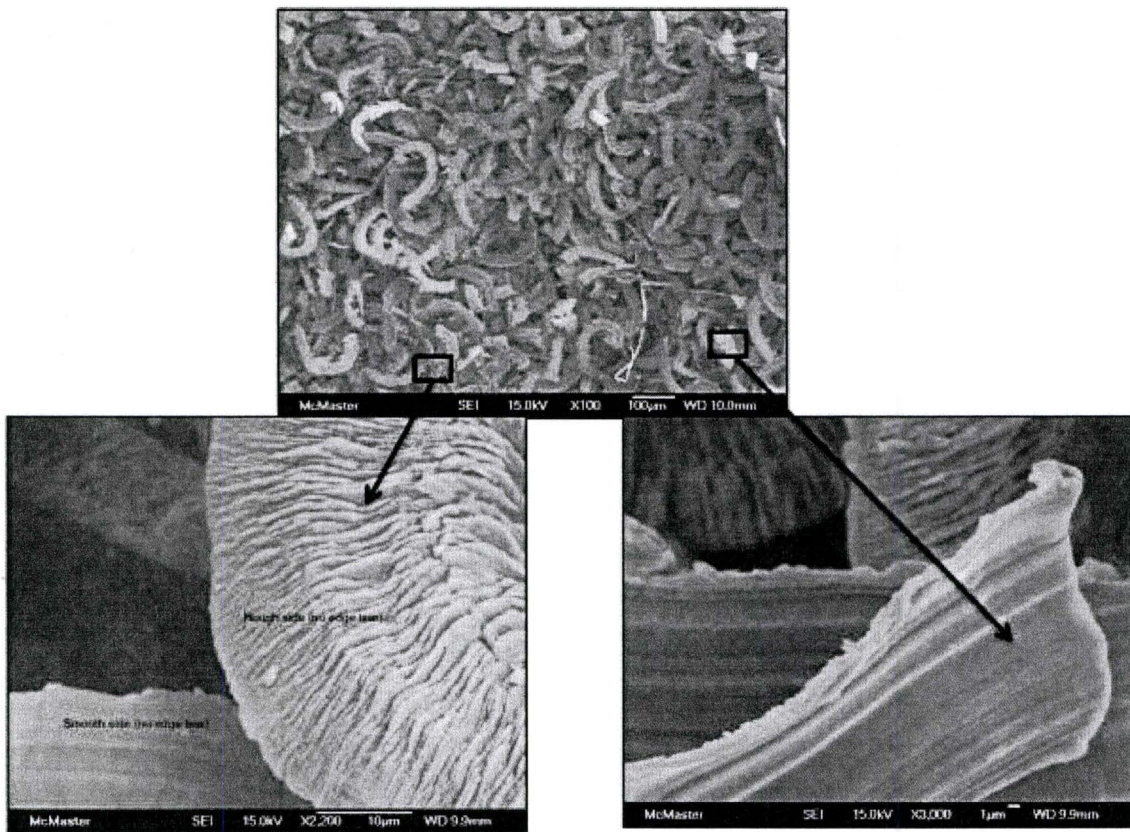


Figure 4-38: SEM images of CP-Ti chips obtained with PFPE coated tool

A change in COF between the tool and the chip could also alter the friction angle i.e. reduction in COF improves the chip flow, which in turn produces

smoother chips. This also supports the role of PFPE in improving the lubricity and reducing the COF in SPDT. Also, reduction in temperature at the chip-tool interface due to reduced COF reduces chip curling thus forming thin ribbon like chips. Thus it is evident that a reduction in the temperature was obtained with PFPE coating.

4.6.4.1. TEM analysis of chips

Traces of TiC were found from a TEM analysis of chips as shown in Figure 4-39. Electron energy loss spectrometer (EELS) was used to identify the chemical composition of the chip. As discussed in section 2.6.1, carbon atoms pulled out from the diamond lattice forms a complex, in this case TiC with the workpiece material.

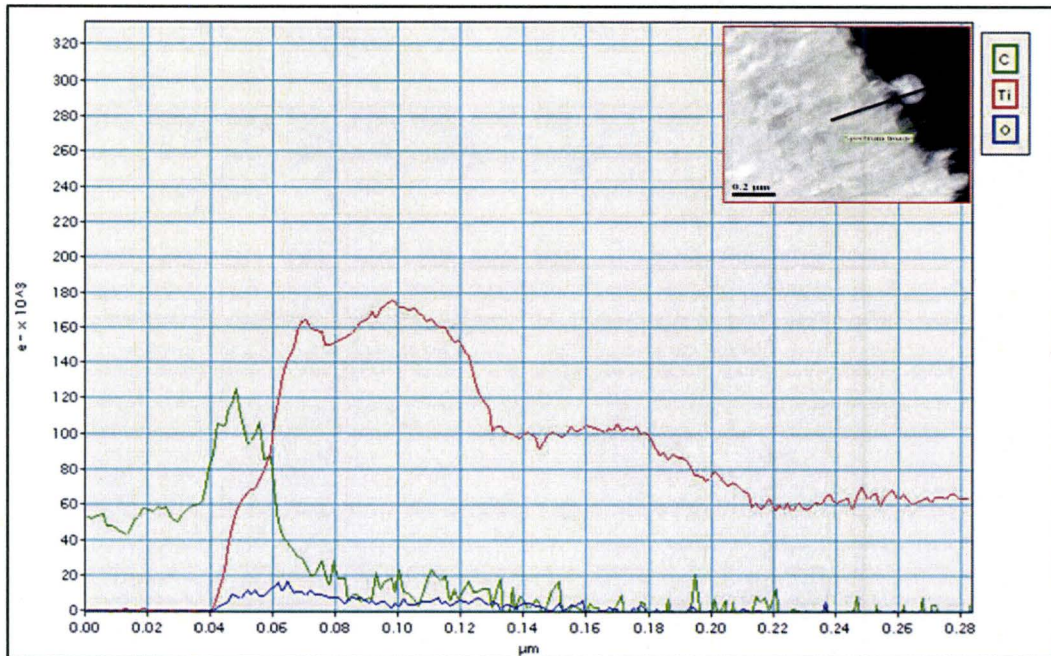


Figure 4-39: TEM – EELS of chips

4.7. MATERIAL MICROSTRUCTURE ANALYSIS

In order to obtain more insight on strain-work hardening of the work material during cutting, a cross section of the machined surface was ground, polished and etched. Retaining the edge from rounding during polishing was very challenging. Images obtained from optical microscope shows the depth of deformed layer from the machined surface.

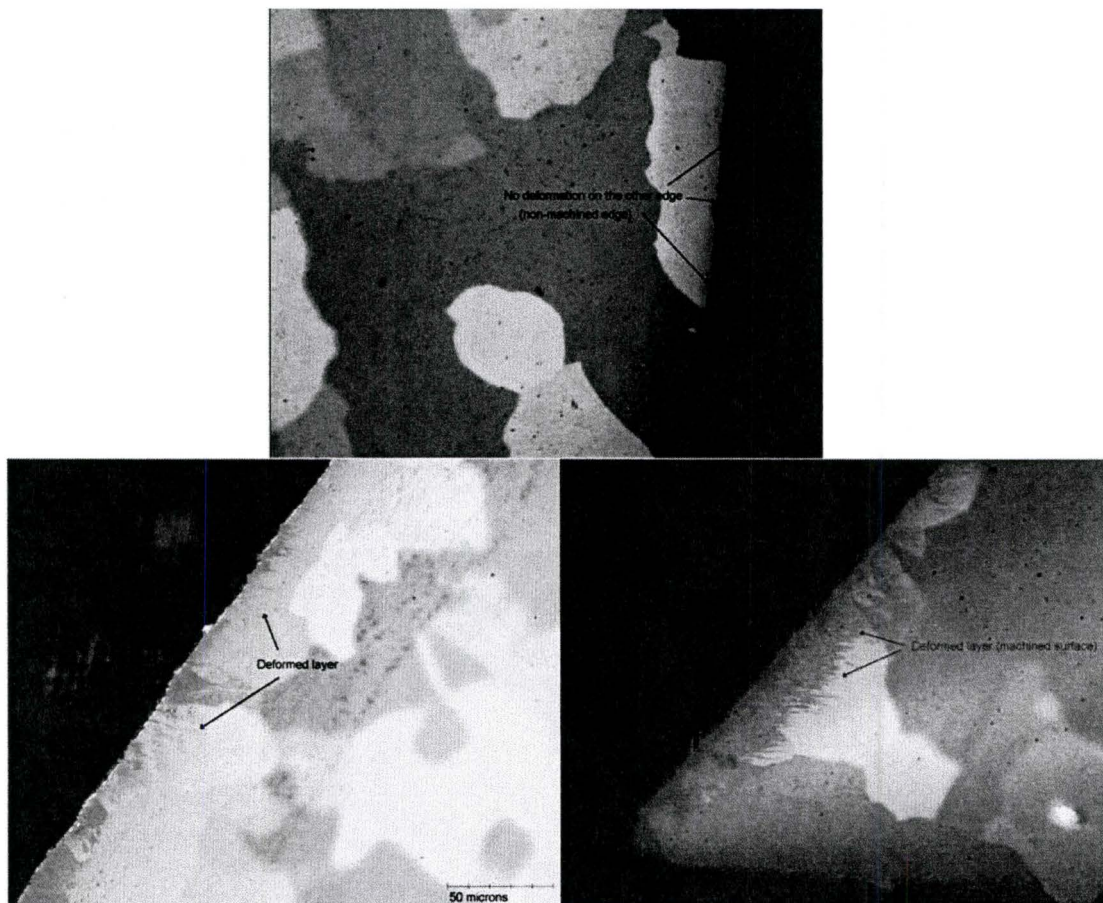


Figure 4-40: Optical image of the cross-section of the machined surface (CP-Ti)

Electron back-scatter diffraction – EBSD, analysis of the workpiece material CP-Ti and Ti-6Al-4V alloys before and after machining was also conducted to study the change in microstructure and phase transformation in the deformed layer. Unfortunately, the hardened layer was only a few nanometers thick, so not much detail could be seen under an optical microscope. But a work hardened layer could be identified by using a nano-indentation test of the machined

surface as shown in Figure 4-41. (Courtesy Dr. Bo Zhou & Dr. Nicholas Randal, CSM Instruments, Inc and Micro Materials, UK).

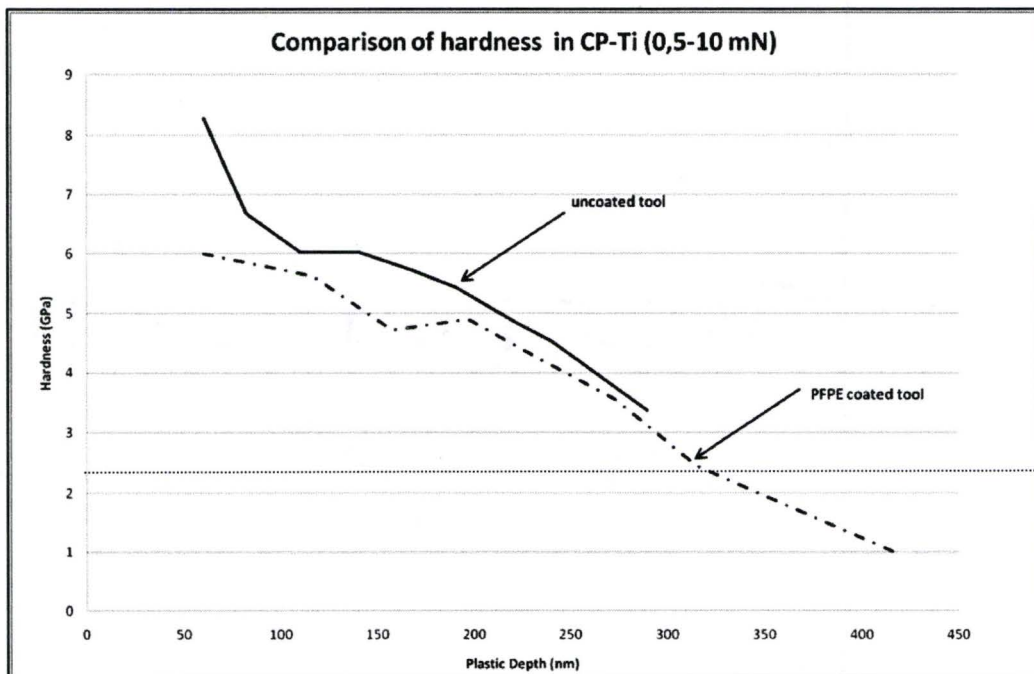


Figure 4-41: Nano Indentation on machined surface obtained without and with PFPE coated tool

It could be observed from the above figure that the depth of the work-hardened layer, as well the hardness has reduced with the PFPE coated tool, thus enhancing the integrity of the machined surface.

Chapter 5 : **CONCLUSIONS & SCIENTIFIC CONTRIBUTIONS**

5.1.CONCLUSIONS

In this attempt on extending the SPDT technique to Ti alloys, cutting parameters with which optical grade surface quality could be achieved were identified. This set of parameters could be used as a bench mark to further enhance the productivity of this process in future research.

Ti and its alloys are considered non-diamond turnable. But, the underlying tool wear mechanism that has not been studied so far was analyzed in depth in this work. In addition to the tool wear analyses, a detailed explanation for the mechanisms that drives the surface finish degradation due to the tool wear was also developed.

Graphitization of the diamond tool was identified as the mechanism that wears the cutting edge radius. The role of temperature and normal stress that prevails at the cutting zone was found to facilitate graphitization. Edge round-off due to

graphitization has lead to ploughing and side-flow and increased the COF, which in turn has accelerated the adhesion rate, hence degrading the surface quality.

Thus the need for a protective barrier to enhance the tool life and surface quality was identified. Fluorination of diamond surface with PFPE was found to interfere the graphitization process. It has also reduced the COF and thus delayed the onset of adhesion which in turn has enhanced the tool life and surface quality.

PFPE coating technique is very cost and time effective since it is a simple in-house coating process that requires no special training or set-up. Thus the PFPE coating has enhanced the tool life with improvement in cutting length and with the reduction in adhesion rate.

5.2. SCIENTIFIC CONTRIBUTIONS

1. Identified cutting parameters for SPDT of CP-Ti & Ti-6Al-4V alloys which meet industrial specification of optical grade surfaces. Tool life is still limited.
2. Identified tool wear mechanism and surface quality issues
 - a. Studied the chemical and mechanical interactions between titanium and diamond tools

- b. Identified graphitization under localized high temperature and pressure
 - c. Outlined the process by which graphitization leads to tool edge degradation and ploughing, which creates conditions that are favorable for adhesion, which impairs the surface quality, and thus limits the functional life of the tool
 - d. Phase transformation of the workpiece surface under this pressure and temperature condition is explored
3. The concept of measuring tool life in SPDT in terms of cutting length that meets the required optical grade surface roughness was proposed.
4. Identified PFPE as a lubricant and protective layer, which minimizes the wear mechanism and surface quality issues
- a) Developed an understanding of the working mechanism of PFPE coating.
 - 1. The role of PFPE as a protective barrier hindering the chemical interaction between tool and workpiece is identified
 - 2. Demonstrated the ability of PFPE to reduce friction

- a. Confirmed concept by Tribometer testing
 - b. Obtained reduction in COF between tool and workpiece during machining
 1. Cutting force ratio reduction
 2. SEM analysis of chips without and with PFPE coated tools show evidence of improved lubricity
 3. Nano-indentation show evidence of reduction in work-hardened layer
5. Tool life has doubled through the use of this cost effective coating approach
- a) This effectively opens up the use of Ti for optical grade applications
 - b) The results obtained were confirmed in an industrial application at B-Con Engineering for the machining of polymer lenses and was found to
 1. Reduce adhesion rate
 2. Enhance tool life
 3. Increase productivity

5.3. RECOMMENDATIONS AND FUTURE WORKS

- Continue to explore other options such as workpiece modification and new tool materials as they become available.
- Develop a cooling technique which can extract heat from the cutting zone without impacting the stability of the workpiece, tool or machine temperature
- Re-optimize the cutting parameters for higher productivity with PFPE coated tools
- Explore the use of PFPE for SPDT of ferrous alloys
- Use of PFPE for other applications that would require ultrathin – hydrophobic coatings.

References

- [1] Ezugwu, E.O. Key Improvements in the Machining of Difficult-to-Cut Aerospace Superalloys. *Int. J. Mach. Tools Manuf.* **2005**, *45*, 1353-1367.
- [2] LPutjering, G.; Williams, J.C.; SpringerLink. *Titanium*. **2007**.
- [3] Trent, E.M.; Wright, P.K. *Metal Cutting*, 4th ed.; Butterworth-Heinemann: Boston, **2000**; pp. 446.
- [4] Ezugwu, E.O.; Wang, Z.M. Titanium Alloys and their Machinability - a Review. *J. Mater. Process. Technol.* **1997**, *68*, 262-274.
- [5] Zoya, Z.A.; Krishnamurthy, R. Performance of CBN Tools in the Machining of Titanium Alloys. *J. Mater. Process. Technol.* **2000**, *100*, 80-86.
- [6] Bhaumik, S.K.; Divakar, C.; Singh, A.K. Machining Ti-6Al-4V Alloy with a wBN-cBN Composite Tool. *Materials and Design* **1995**, *16*, 221-226.
- [7] Ezugwu, E.O.; Bonney, J.; Yamane, Y. An Overview of the Machinability of Aeroengine Alloys. *J. Mater. Process. Technol.* **2003**, *134*, 233-253.
- [8] Hong, H.; Riga, A.T.; Cahoon, J.M.; Scott, C.G. Machinability of Steels and Titanium Alloys Under Lubrication. *Wear* **1993**, *162-64*, 34-39.
- [9] Yang, X.; Liu, C.R. Machining Titanium and its Alloys. *Mach. Sci. Technol.* **1999**, *3*, 107-139.
- [10] Komanduri, R. Some clarification on the mechanics of chip formation when machining titanium alloys. *Wear* **1982**, *76*, 15-34.
- [11] Paul, E.; Evans, C.J.; Mangamelli, A.; McGlaufflin, M.L.; Polvani, R.S. Chemical Aspects of Tool Wear in Single Point Diamond Turning. *Precis Eng* **1996**, *18*, 4-19.
- [12] McKeown, P. From Micro- to Nano-Machining - Towards the Nanometre Era. *Sens Rev* **1996**, *16*, 4-10.
- [13] Byrne, G.; Dornfeld, D.; Denkena, B. Advancing Cutting Technology. *CIRP Ann. Manuf. Technol.* **2003**, *52*, 483-507.

- [14] Ikawa, N.; Donaldson, R.R.; Komanduri, R.; Koenig, W.; Aachen, T.H.; McKeown, P.A.; Moriwaki, T.; Stowers, I.F. Ultraprecision Metal Cutting. the Past, the Present and the Future. In 41st General Assembly of CIRP; **1991** pp. 587-594.
- [15] Alan Richter. To the Point: An Overview of Applying Single-Point Diamond Tools for Direct Machining of Micro-Optics Micro manufacturing **2009**.
- [16] Komanduri, R.; Chandrasekaran, N.; Raff, L.M. Effect of Tool Geometry in Nanometric Cutting: A Molecular Dynamics Simulation Approach. *Wear* **1998**, *219*, 84-97.
- [17] Chae, J.; Park, S.S.; Freiheit, T. Investigation of Micro-Cutting Operations. *Int. J. Mach. Tools Manuf.* **2006**, *46*, 313-332.
- [18] Yuan, Z.J.; Zhou, M.; Dong, S. Effect of Diamond Tool Sharpness on Minimum Cutting Thickness and Cutting Surface Integrity in Ultraprecision Machining. *J. Mater. Process. Technol.* **1996**, *62*, 327-330.
- [19] Ikawa, N.; Shimada, S.; Tanaka, H. Minimum Thickness of Cut in Micromachining. *Nanotechnology* **1992**, *3*, 6-9.
- [20] Kim, J.; Kim, D.S. Theoretical Analysis of Micro-Cutting Characteristics in Ultra-Precision Machining. *J. Mater. Process. Technol.* **1995**, *49*, 387-398.
- [21] Simoneau, A.; Ng, E.; Elbestawi, M.A. Chip Formation during Microscale Cutting of a Medium Carbon Steel. *Int. J. Mach. Tools Manuf.* **2006**, *46*, 467-481.
- [22] Asai, S.; Taguchi, Y.; Horio, K.; Kasai, T.; Kobayashi, A. Measuring the very Small Cutting-Edge Radius for a Diamond Tool using a New Kind of SEM having Two Detectors. *CIRP Ann. Manuf. Technol.* **1990**, *39*, 85-88.
- [23] Fang, F.Z.; Chen, L.J. Ultra-Precision Cutting for ZKN7 Glass. *CIRP Ann. Manuf. Technol.* **2000**, *49*, 17-20.
- [24] Lucca, D.A.; Seo, Y.W.; Komanduri, R. Effect of Tool Edge Geometry on Energy Dissipation in Ultraprecision Machining. *CIRP Ann. Manuf. Technol.* **1993**, *42*, 83-86.

- [25] Li, X.P.; Rahman, M.; Liu, K.; Neo, K.S.; Chan, C.C. Nano-Precision Measurement of Diamond Tool Edge Radius for Wafer Fabrication. **2003**; pp. 358-362.
- [26] Gao, W.; Asai, T.; Arai, Y. Precision and Fast Measurement of 3D Cutting Edge Profiles of Single Point Diamond Micro-Tools. *CIRP Ann. Manuf. Technol.* **2009**, *58*, 451-454.
- [27] Kopalinsky, E.M.; Oxley, P.L.B. Size-effects in metal removal processes. In *Mechanical Properties at High Rates of Strain*, **1984**, Proceedings of the Third Conference.; pp. 389-396.
- [28] Yan, J.; Syoji, K.; Tamaki, J. Some Observations on the Wear of Diamond Tools in Ultra-Precision Cutting of Single-Crystal Silicon. *Wear* **2003**, *255*, 1380-1387.
- [29] Evans, C. Cryogenic Diamond Turning of Stainless Steel. In 41st General Assembly of CIRP, August 18, 1991 - August 24, **1991**; pp. 571-575.
- [30] Kendall, K. Adhesion: Molecules and Mechanics. *Science* **1994**, *263*, 1720-1725.
- [31] Carrilero, M.S.; Bienvenido, R.; Sanchez, J.M.; Alvarez, M.; Gonzalez, A.; Marcos, M. A SEM and EDS Insight into the BUL and BUE Differences in the Turning Processes of AA2024 Al-Cu Alloy. *Int. J. Mach. Tools Manuf.* **2002**, *42*, 215-220.
- [32] Zlatin et al. Procedures and Precautions in Machining Titanium Alloys. *Titanium Sci. & Tech* **1973**, *1*, 489-504.
- [33] Shaw, M.C. *Metal Cutting Principles.*; Oxford University Press, c 1996: Oxford : Clarendon Press; New York, **1996**; pp. 594.
- [34] N. Ikawa and S. Shimada. Diamond Tools for Ultra-Precision Cutting. *Trans. JSME* **1985**, *50*, 1321-1326.
- [35] Casstevens, J.M. Diamond turning of steel in carbon-saturated atmospheres. *Precis Eng* **1983**, *5*, 9-15.

- [36] Moriwaki, T.; Shamoto, E.; Inoue, K. Ultra-Precision Diamond Turning of Stainless Steel by Applying Ultrasonic Vibration. *Journal of the Japan Society of Precision Engineering* **1991**, *57*, 1983-8.
- [37] Pramanik, A.; Neo, K.S.; Rahman, M.; Li, X.P.; Sawa, M.; Maeda, Y. Cutting Performance of Diamond Tools during Ultra-Precision Turning of Electroless-Nickel Plated Die Materials. In 6th Asia Pacific Conference on Materials Processing (6th APCMP) 2003, 22-25 Sept. **2003**; pp. 308-13.
- [38] Sanger, G.M. Perspective on precision machining, polishing and optical requirements. In *Contemporary Methods of Optical Fabrication*. **2007** pp. 90-104.
- [39] Fischer, R.E. *Encyclopedia of Materials Science and Engineering; Diamond Turning; Diamond Turning.*; Pergamon Press; MIT Press: Oxford; Cambridge, Mass., **1986**.
- [40] Bundy, F.P.; Bassett, W.A.; Weathers, M.S.; Hemley, R.J.; Mao, H.K.; Goncharov, A.F. Pressure-Temperature Phase and Transformation Diagram for Carbon; Updated through 1994. *Carbon* **1996**, *34*, 141-153.
- [41] Kern, G.; Hafner, J. Ab Initio Molecular-Dynamics Studies of the Graphitization of Flat and Stepped Diamond (111) Surfaces. *Physical Review B (Condensed Matter)* **1998**, *58*, 13167-75.
- [42] Qian, J.; Pantea, C.; Voronin, G.; Zerda, T.W. Partial Graphitization of Diamond Crystals Under High-Pressure and High-Temperature Conditions. *J. Appl. Phys.* **2001**, *90*, 1632-7.
- [43] Davies, G.; Evans, T. Graphitization of Diamond at Zero Pressure and at a High Pressure. *Proceedings of the Royal Society of London, Series A (Mathematical and Physical Sciences)* **1972**, *328*, 413-27.
- [44] De Vita, A.; Galli, G.; Canning, A.; Car, R. A Microscopic Model for Surface-Induced Diamond-to-Graphite Transitions. *Nature* **1996**, *379*, 523-6.
- [45] H. Tanaka, S. Shimada, N. Ikawa, M. Higuchi and K. Obata. Difference in Wear Patterns of Diamond Cutting Tool Depending on Work Materials. *Proc ICPE* **2001**, 179-183.

- [46] Kohlscheen, J.; Stock, H.-.; Mayr, P. Tailoring of Diamond Machinable Coating Materials. *Precis Eng* **2002**, *26*, 175-182.
- [47] Thornton, A.G.; Wilks, J. Tool wear and solid state reactions during machining. *Wear* **1979**, *53*, 165-187.
- [48] Narulkar, R.; Bukkapatnam, S.; Raff, L.M.; Komanduri, R. Graphitization as a Precursor to Wear of Diamond in Machining Pure Iron: A Molecular Dynamics Investigation. *Computational Materials Science* **2009**, *45*, 358-66.
- [49] Oya, A.; Marsh, H. Phenomena of catalytic graphitization. *J. Mater. Sci.* **1982**, *17*, 309-322.
- [50] Liu, H.; Wang, L.; Wang, A.; Lou, T.; Ding, B.; Hu, Z. Preparation of Nanometer Size TiC Particulate Reinforcements in Ti Matrix Composites Under High Pressure. *Nanostructured Materials* **1997**, *9*, 177-180.
- [51] Jiwang YAN, Katsuo SYOJI and Tsunemoto KURIYAGAWA. Chip Morphology of Ultra-Precision Diamond Turning of Single Crystal Silicon. *Journal of the Japan Society for Precision Engineering* **1999**, *65*, 1008-1012.
- [52] Wada, R.; Kodama, H.; Nakamura, K.; Mizutani, Y.; Shimura, Y.; Takenaka, N. Wear characteristics of single crystal diamond tool. *CIRP Ann. Manuf. Technol.* **1980**, *29*, 47-52.
- [53] Wong, C.J. Fracture and wear of diamond cutting tools. *J Eng Mater Technol Trans ASME* **1981**, *103*, 341-345.
- [54] Ikawa, N.; Shimada, S.; Tsuwa, H. Microfracture of Diamond as Fine Tool Material. *CIRP Ann. Manuf. Technol.* **1982**, *31*, 71-74.
- [55] Shimada, S.; Tanaka, H.; Higuchi, M.; Yamaguchi, T.; Honda, S.; Obata, K. Thermo-Chemical Wear Mechanism of Diamond Tool in Machining of Ferrous Metals. *CIRP Ann. Manuf. Technol.* **2004**, *53*, 57-60.
- [56] Brinksmeier, E.; Glabe, R.; Osmer, J. Ultra-Precision Diamond Cutting of Steel Molds. *CIRP Ann. Manuf. Technol.* **2006**, *55*, 551-554.

- [57] Hitchiner, M.P.; Wilks, J. Factors affecting chemical wear during machining. *Wear* **1984**, *93*, 63-80.
- [58] Gubbels, G.P.H.; Van, D.B.; Hoep, A.L.; Delbressine, F.L.M.; Van Halewijn, H. Diamond Tool Wear when Cutting Amorphous Polymers. *CIRP Ann. Manuf. Technol.* **2004**, *53*, 447-450.
- [59] Uddin, M.S.; Seah, K.H.W.; Li, X.P.; Rahman, M.; Liy, K. Effect of Crystallographic Orientation on Wear of Diamond Tools for Nano-Scale Ductile Cutting of Silicon. *Wear* **2004**, *257*, 751-759.
- [60] Malz, R.; Brinksmeier, E.; Preu, W.; Kohlscheen, J.; Stock, H.-.; Mayr, P. Investigation of the Diamond Machinability of Newly Developed Hard Coatings. *Precis Eng* **2000**, *24*, 146-152.
- [61] Zhou, M.; Ngoi, B.K.A. Effect of Tool Wear and Tool Setting on Profile Accuracy of Diamond-Turned Nonferrous Components. *Mater. Manuf. Process.* **2001**, *16*, 79-89.
- [62] Weule, H.; Huntrup, V.; Tritschle, H. Micro-Cutting of Steel to Meet New Requirements in Miniaturization. *CIRP Ann. Manuf. Technol.* **2001**, *50*, 61-64.
- [63] Brehl, D.E.; Dow, T.A. Review of Vibration-Assisted Machining. *Precis Eng* **2008**, *32*, 153-72.
- [64] Chao, C.L.; Chou, W.C.; Chao, C.W.; Chen, C.C. Material Removal Mechanisms Involved in Rotary Ultrasonic Machining of Brittle Materials. *Key Eng Mat* **2007**, *329*, 391-396.
- [65] Moriwaki, T.; Shamoto, E. Ultraprecision Diamond Turning of Stainless Steel by Applying Ultrasonic Vibration. In 41st General Assembly of CIRP, August 18, 1991 - August 24, **1991**; pp. 559-562.
- [66] Shamoto, E.; Suzuki, N.; Hino, R.; Tsuchiya, E.; Hori, Y.; Inagaki, H.; Yoshino, K. A New Method to Machine Sculptured Surfaces by Applying Ultrasonic Elliptical Vibration Cutting. In 2005 International Symposium on Micro-NanoMechatronics and Human Science, Eighth Symposium on Micro- and Nano-Mechatronics for Information-Based Society - the 21st Century COE Program, November 7, **2005** - November 9, 2005; pp. 84-89.

- [67] Wu, Y.; Sun, A.; Zhu, X.; Zhao, B. Brittle-Ductile Transition of Micro-Nano Composite Ceramics using Ultrasonic Vibration Grinding. *Sichuan Daxue Xuebao (Gongcheng Kexue Ban)/Journal of Sichuan University (Engineering Science Edition)* **2007**, *39*, 113-117.
- [68] Zhong, Z.W.; Lin, G. Diamond Turning of a Metal Matrix Composite with Ultrasonic Vibrations. *Mater. Manuf. Process.* **2005**, *20*, 727-735.
- [69] Zhou, M.; Liu, X.D.; Huang, S.N. Ultraprecision Ductile-Regime Cutting of Brittle Materials. In ; **2007** pp. 395-399.
- [70] Wang, Z.Y.; Rajurkar, K.P. Cryogenic Machining of Hard-to-Cut Materials. *Wear* **2000**, *239*, 168-175.
- [71] Hong, S.Y.; Markus, I.; Jeong, W. New Cooling Approach and Tool Life Improvement in Cryogenic Machining of Titanium Alloy Ti-6Al-4V. *Int. J. Mach. Tools Manuf.* **2001**, *41*, 2245-2260.
- [72] Tartaj, J.; Moure, C.; Duran, P. Cooling Approaches and Cutting Temperatures in Cryogenic Machining of Ti-6Al-4V. *Int. J. Mach. Tools Manuf.* **2001**, *41*, 1417-1437.
- [73] Paul, S.; Dhar, N.R.; Chattopadhyay, A.B. Beneficial Effects of Cryogenic Cooling Over Dry and Wet Machining on Tool Wear and Surface Finish in Turning AISI 1060 Steel. *J. Mater. Process. Technol.* **2001**, *116*, 44-48.
- [74] Hong, S.Y.; Ding, Y.; Jeong, W. Friction and Cutting Forces in Cryogenic Machining of Ti-6Al-4V. *Int. J. Mach. Tools Manuf.* **2001**, *41*, 2271-2285.
- [75] Venugopal, K.A.; Tawade, R.; Prashanth, P.G.; Paul, S.; Chattopadhyay, A.B. Turning of Titanium Alloy with TiB₂-Coated Carbides Under Cryogenic Cooling. *Proceedings of the Institution of Mechanical Engineers, Part B (Journal of Engineering Manufacture)* **2003**, *217*, 1697-707.
- [76] Neo, K.S.; Rahman, M.; Li, X.P.; Khoo, H.H.; Sawa, M.; Maeda, Y. Performance Evaluation of Pure CBN Tools for Machining of Steel. In *6th Asia Pacific Conference on Materials Processing (6th APCMP) 2003*, 22-25 Sept. **2003**; pp. 326-31.

- [77] Zareena, A.R.; Rahman, M.; Wong, Y.S. Binderless CBN Tools, a Breakthrough for Machining Titanium Alloys. Transactions of the ASME. Journal of Manufacturing Science and Engineering **2005**, *127*, 277-9.
- [78] Kawasegi, N.; Sugimori, H.; Morimoto, H.; Morita, N.; Hori, I. Development of Cutting Tools with Microscale and Nanoscale Textures to Improve Frictional Behavior. *Precis Eng* **2009**, *33*, 248-254.
- [79] Sugihara, T.; Enomoto, T. Development of a Cutting Tool with a nano/micro-Textured Surface-Improvement of Anti-Adhesive Effect by Considering the Texture Patterns. *Precis Eng* **2009**, *33*, 425-429.
- [80] S. Sakamoto, H. Yasui and A. Shinozaki. Development of Precision Coated-Cemented-Carbide Tools for Ultra-Precision Cutting of Titanium and Titanium Alloys. Proceeding of ASPE annual meeting **2004**, *34*, 634-637.
- [81] Koshy, P. Manufacturing Processes - MP-1, Teaching Material. **2005**.
- [82] Rabinowicz, E. *Friction and Wear of Materials*. --.; Wiley: New York, **1965**; pp. 244.
- [83] Miyoshi, K.; Buckley, D.H. Adhesion and friction of single-crystal diamond in contact with transition metals. *Applications of surface science* **1980**, *6*, 161-172.
- [84] Miyoshi, K.; Buckley, D.H. Adhesion and friction of single-crystal diamond in contact with transition metals. *Applications of surface science* **1980**, *6*, 161-172.
- [85] Wang, M.; Miyake, S.; Matsunuma, S. Nanowear Studies of PFPE Lubricant on Magnetic Perpendicular Recording DLC-Film-Coated Disk by Lateral Oscillation Test. *Wear* **2005**, *259*, 1332-1342.
- [86] Sinha, S.K.; Satyanarayana, N.; Boon, H.O. Tribology of a Novel UHMWPE/PFPE Dual-Film Coated Onto Si Surface. *Sensors and Actuators A (Physical)* **2006**, *128*, 98-108.
- [87] Tani, H.; Matsumoto, H. Spreading Mechanism of PFPE Lubricant on the Magnetic Disks. Transactions of the ASME. Journal of Tribology **2001**, *123*, 533-40.

- [88] Yamamoto, H.; Ohkubo, Y.; Ogawa, K.; Utsumi, K. Application of a Chemically Adsorbed Fluorocarbon Film to Improve Demolding. *Precis Eng* **2009**, *33*, 229-34.
- [89] Liu, H.; Bhushan, B. Nanotribological Characterization of Molecularly Thick Lubricant Films for Applications to MEMS/NEMS by AFM. In *Fourth International Conference on Scanning Probe Microscopy, Sensors and Nanostructures*, **2003**, *10*; pp. 321-40.
- [90] Satyanarayana, N.; Sinha, S.K. Tribology of PFPE Overcoated Self-Assembled Monolayers Deposited on Si Surface. *Journal of Physics D (Applied Physics)* **2005**, *38*, 3512-22.
- [91] Tagawa, N.; Tateyama, T.; Mori, A.; Kobayashi, N.; Fujii, Y.; Ikegami, M. Spreading of Novel Cyclotriphosphazine-Terminated PFPE Films on Carbon Surfaces. *Journal of Tribology* **2004**, *126*, 751-754.
- [92] [Http://www.Solvaysolexis.com/static//wma/pdf/5/4/3/4/fom_thin.Pdf](http://www.Solvaysolexis.com/static//wma/pdf/5/4/3/4/fom_thin.Pdf).
- [93] Kato, T.; Kawaguchi, M.; Sajjad, M.M.; Choi, J. Friction and Durability Characteristics of Ultrathin Perfluoropolyether Lubricant Film Composed of Bonded and Mobile Molecular Layers on Diamond-Like Carbon Surfaces. *Wear* **2004**, *257*, 909-15.
- [94] Bhushan, B. Magnetic Media Tribology. State of the Art and Future Challenges. *Wear* **1990**, *136*, 169-197.
- [95] Delucchi, M.; Turri, S.; Barbucci, A.; Novelli, S.; Cerisola, G. Investigation on Physico-Chemical and Electrochemical Properties of Fluoropolyether Coatings. *Progress in Organic Coatings* **2002**, *44*, 227-232.
- [96] Yamamoto, H.; Ohkubo, Y.; Ogawa, K.; Utsumi, K. Application of a Chemically Adsorbed Fluorocarbon Film to Improve Demolding. *Precis Eng* **2009**, *33*, 229-34.
- [97] Dosbaeva, J.; Fox-Rabinovich, G.; Dasch, J.; Veldhuis, S. Enhancement of Wet- and MQL-Based Machining of Automotive Alloys using Cutting Tools with DLC/polymer Surface Treatments. **2008** pp. 346-351.

- [98] Fox-Rabinovich, G.; Kovalev, A.I.; Wainstein, D.L.; Shuster, L.S.; Dosbaeva, G.K. Improvement of 'Duplex' PVD Coatings for HSS Cutting Tools by PFPE (Perfluoropolyether 'Z-DOL'). *Surf Coat Technol* **2002**, *160*, 99-107.
- [99] Veldhuis, S.C.; Dosbaeva, G.K.; Benga, G. Application of Ultra-Thin Fluorine-Content Lubricating Films to Reduce tool/workpiece Adhesive Interaction during Thread-Cutting Operations. *Int. J. Mach. Tools Manuf.* **2007**, *47*, 521-528.
- [100] Lovell, M.R.; Cohen, P.; Menezes, P.L.; Shankar, R. Tribological Characterization of Machining at very Small Contact Areas. *Journal of Tribology* **2009**, *131*, 042201 (7 pp.).
- [101] Zemzemi, F.; Bensalem, W.; Rech, J.; Dogui, A.; Kapsa, P. New Tribometer Designed for the Characterisation of the Friction Properties at the tool/chip/workpiece Interfaces in Machining. *Tribo Test* **2008**, *14*, 11-25.
- [102] Stachowiak, G.W.; Batchelor, A.W. *Engineering Tribology*, 3rd ed.; Elsevier Butterworth-Heinemann: Amsterdam ; Boston, **2005**; pp. 801.
- [103] Shigehiko Sakamoto, Akira Shinozaki, Heiji Yasui. Possibility of Ultra-Precision Cutting of Titanium Alloy with Diamond Tool. *ASPE* **2005**, *2*, 1-4.
- [104] Yasui, H.; Sakamoto, S.; Kawada, M. Ultra-Precision Cutting of Titanium Alloys by using Coated Carbide Bite. *Journal of the Japan Society of Precision Engineering* **2002**, *68*, 928-32.
- [105] Zhang, Y.; Zhou, Z.; Xiu, W.; Xia, Z. Influence of Cutting Parameters on Diamond turning Titanium Alloy. In 3rd International Symposium on Advanced Optical Manufacturing and Testing Technologies, AOMATT **2007**: State Key Laboratory of Optical Technology for Microfabrication; Sichuan Optical Society (SOS).
- [106] Colafemina, J.P.; Jasinevicius, R.G.; Duduch, J.G. Surface Integrity of Ultra-Precision Diamond Turned Ti (Commercially Pure) and Ti Alloy (Ti-6Al-4V). *Proceedings of the Institution of Mechanical Engineers, Part B (Journal of Engineering Manufacture)* **2007**, *221*, 999-1006.

- [107] Narutaki, N.; Murakoshi, A.; Motonishi, S. STUDY ON MACHINING OF TITANIUM ALLOYS. In *CIRP Annals* **1983**: Manufacturing Technology, 33rd General Assembly of CIRP.; pp. 65-69.
- [108] Sun, J.; Wong, Y.S.; Rahman, M.; Wang, Z.G.; Neo, K.S.; Tan, C.H.; Onozuka, H. Effects of Coolant Supply Methods and Cutting Conditions on Tool Life in End Milling Titanium Alloy. *Mach. Sci. Technol.* **2006**, *10*, 355-70.
- [109] Sreejith, P.S.; Ngoi, B.K.A. Material Removal Mechanisms in Precision Machining of New Materials. *International Journal of Machine Tools and Manufacture* **2001**, *41*, 1831-1843.
- [110] Corbett, J.; McKeown, R.A.; Peggs, G.N.; Whatmore, R. Nanotechnology: International Developments and Emerging Products. *CIRP Ann. Manuf. Technol.* **2000**, *49*, 523-545.
- [111] Jasinevicius, R.G.; De Campos, G.P.; Montanari, L.; Tsukamoto, R.; Garcia, J.P.; Camargo, R.; Duduch, J.G.; Porto, A.J.V. Influence of the Mechanical and Metallurgical State of an Al-mg Alloy on the Surface Integrity in Ultraprecision Machining. *Journal of the Brazilian Society of Mechanical Sciences and Engineering* **2003**, *25*, 222-228.
- [112] Moriwaki, T. Machinability of Copper in Ultra-Precision Micro Diamond Cutting. *CIRP Ann. Manuf. Technol.* **1989**, *38*, 115-118.
- [113] Narayan, R.J. Adhesion Properties of Functionally Gradient Diamond Composite Films on Medical and Tool Alloys. *J. Adhes. Sci. Technol.* **2004**, *18*, 1339-65.
- [114] Filik, J. Raman Spectroscopy: A Simple, Non-Destructive Way to Characterise Diamond and Diamond-Like Materials. *Spectroscopy Europe* **2005**, *17*, 10-17.
- [115] Klein, M.V.; Holy, J.A.; Williams, W.S. Raman Scattering Induced by Carbon Vacancies in TiCx. *Physical Review B (Solid State)* **1978**, *17*, 1546-56.
- [116] McFeely, F.R.; Kowalczyk, S.P.; Ley, L.; Cavell, R.G.; Pollak, R.A.; Shirley, D.A. X-Ray Photoemission Studies of Diamond, Graphite, and Glassy Carbon Valence Bands. *Physical Review B (Solid State)* **1974**, *9*, 5268-78.

- [117] Merel, P.; Tabbal, M.; Chaker, M.; Moisa, S.; Margot, J. Direct Evaluation of the sp³ Content in Diamond-Like-Carbon Films by XPS. *Appl. Surf. Sci.* **1998**, *136*, 105-110.
- [118] Xu, Z.; Rowcliffe, D. Deriving Mechanical Properties of Soft Coatings using Nanoindentation: An Application of Mechanism-Based Strain Gradient Plasticity. *Surface and Coatings Technology* **2002**, *157*, 231-237.
- [119] Coldwell, H.L.; Dewes, R.C.; Aspinwall, D.K.; Renevier, N.M.; Teer, D.G. The use of soft/lubricating Coatings when Dry Drilling BS L168 Aluminium Alloy. *Surface and Coatings Technology* **2004**, *177-178*, 716-726.
- [120] Shimizu, S. *Diamond and Related Materials Research.*; Nova Science Publishers: New York, **2008**; pp. 449.
- [121] Navarrini, W.; Bianchi, C.L.; Magagnin, L.; Nobili, L.; Carignano, G.; Mentrangolo, P.; Resnati, G.; Sansotera, M. Low Surface Energy Coatings Covalently Bonded on Diamond-Like Carbon Films. *Diamond & Related Materials* **2010**, *19*, 336-341.
- [122] Moolsradoo, N.; Watanabe, S. Modification of Tribological Performance of DLC Films by Means of some Elements Addition. *Diamond & Related Materials* **2010**, *19*, 525-529.
- [123] Lei, R.Z.; Gellman, A.J.; Jones, P. Thermal Stability of Fomblin Z and Fomblin Zdol Thin Films on Amorphous Hydrogenated Carbon. *Tribology Letters* **2001**, *11*, 1-5.
- [124] Gu, G.; Shen, X.; Feng-ling Qing. Preparation and Tribological Performance of Perfluoropolyether Derived Coatings. *Appl. Surf. Sci.* **2007**, *253*, 6980-6.
- [125] Pytel, A.; Kiusalaas, J. *Engineering Mechanics : Statics.*; HarperCollins College Publishers: New York, **1994**; pp. 521.
- [126] Yan, J.; Sasaki, T.; Tamaki, J.; Kubo, A.; Sugino, T. Chip Formation Behaviour in Ultra-Precision Cutting of Electroless Nickel Plated Mold Substrates. *Key Eng Mat* **2004**, *257-258*, 3-8.

[127] Sawano, H.; Warisawa, S.; Ishihara, S. Study on Long Life of Artificial Joints by Investigating Optimal Sliding Surface Geometry for Improvement in Wear Resistance. *Precis Eng* **2009**, *33*, 492-498.

[128] Ning, L. Nano-Multilayered Self-Adaptive Hard PVD Coatings for Dry High Performance Machining, Ph.D. Thesis **2007**.

[129] Zazula JM. On graphite transformations at high temperature and pressure induced by absorption of the LHC beam. LHC Project Report 78/97, CERN, Geneva; **1997**.

APPENDIX -1

CNC program used for facing:

G71 ; Metric

G90 ; Absolute

G40 ; Tool compensation off

G00 C0.0 ; C-axis set perpendicular

G01 X2.0 Z60.0 ; Start position outside the w/p

M04 S185 ; Set spindle rotation – CCW, adjust rpm

G01 X1.0 Z42.2 F50.0 ; Start position at outer radius of workpiece, and
closer to surface

M07 ; Coolant ON

G01 Z15.0 F0.28 ; End position (F xx mm/ min NOT f xx microns/rev)

G04 F1 ; Dwell time 1 sec

G01 X1.0 F10.0 ; Retract tool and move out

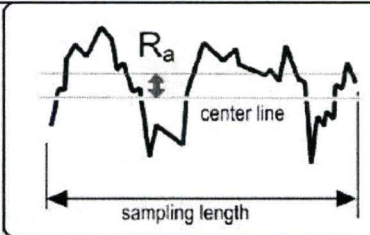
G01 X2.0 Z60.0 ; Return to start position

M09 ; Coolant OFF

M05 ; Spindle stop

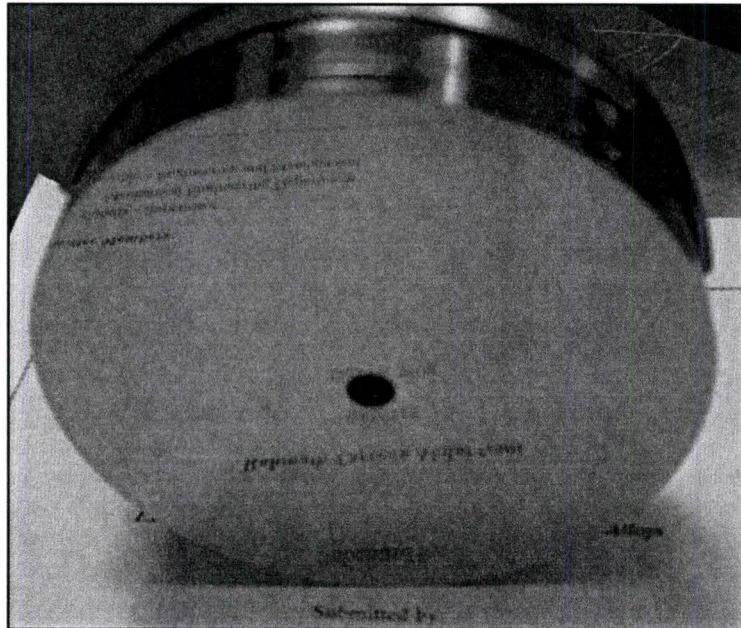
M30 ; Program End

APPENDIX -2

<p>R_a</p>	<p>Arithmetical mean deviation. The average roughness or deviation of all points from a plane fit to the test part surface. Available for profile and areal data.</p> $R_a = \frac{1}{L} \int_0^L z(x) dx$	
<p>R_q (rms)</p>	<p>Root-mean-square (rms) roughness. The average of the measured height deviations taken within the evaluation length or area and measured from the mean linear surface. Available for profile and areal data. R_q is the rms parameter corresponding to R_a.</p> $R_q = \sqrt{\frac{1}{L} \int_0^L z^2(x) dx}$	

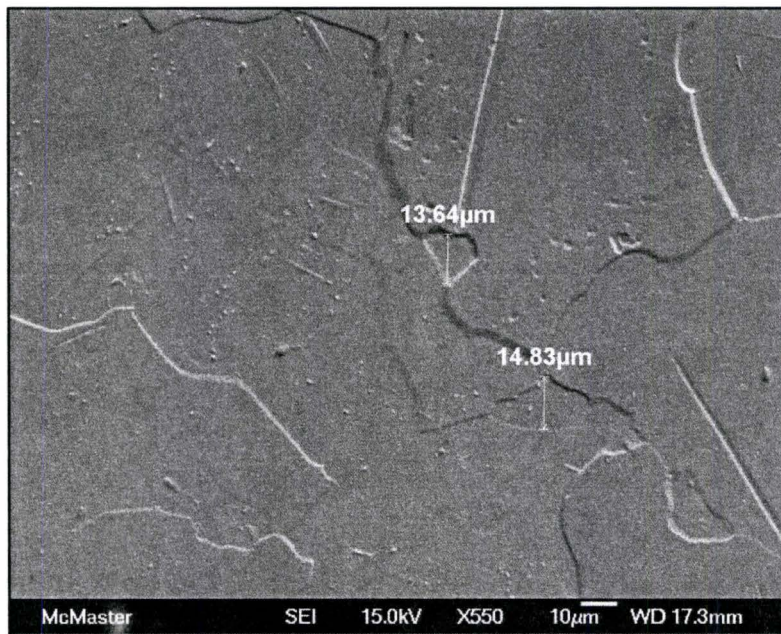
APPENDIX -3

Photographic image of the machined surface (CP-Ti)



APPENDIX -4

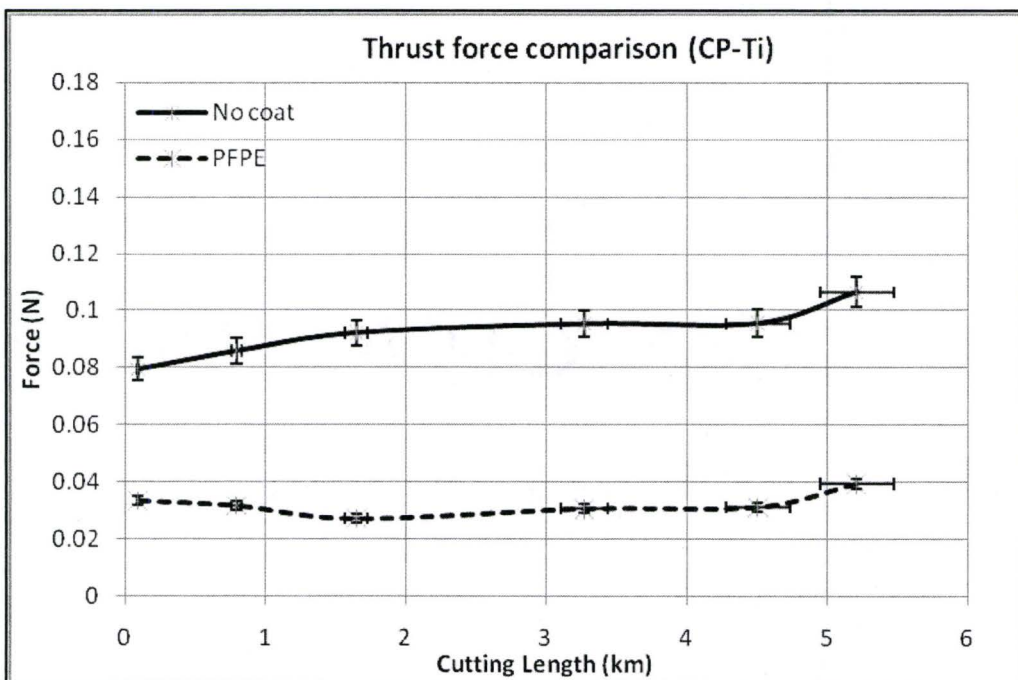
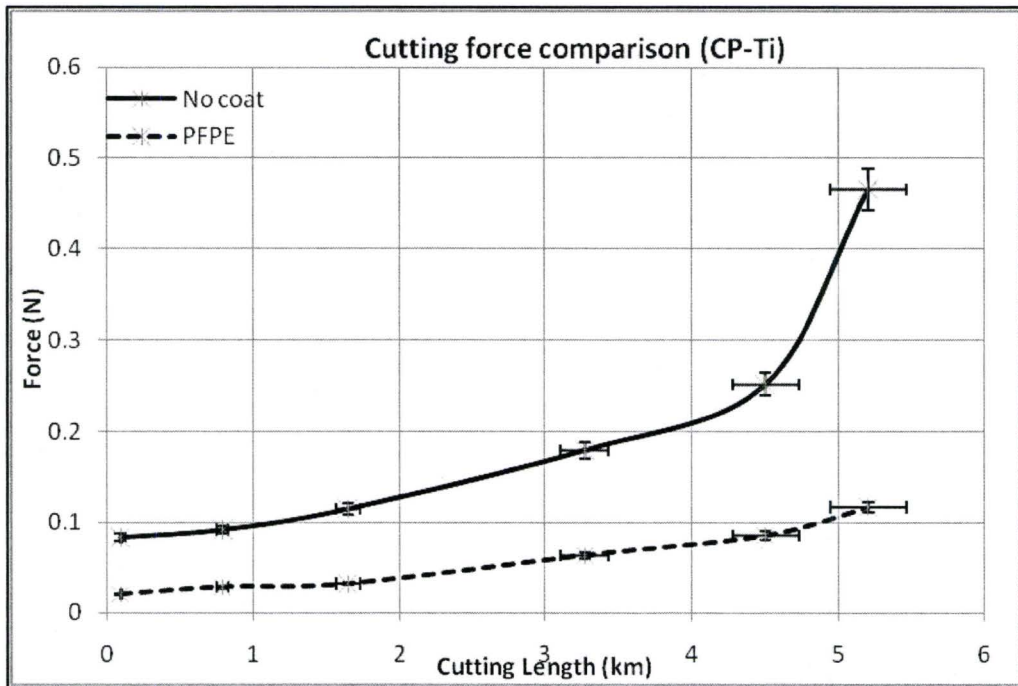
Microstructure of CP-Ti

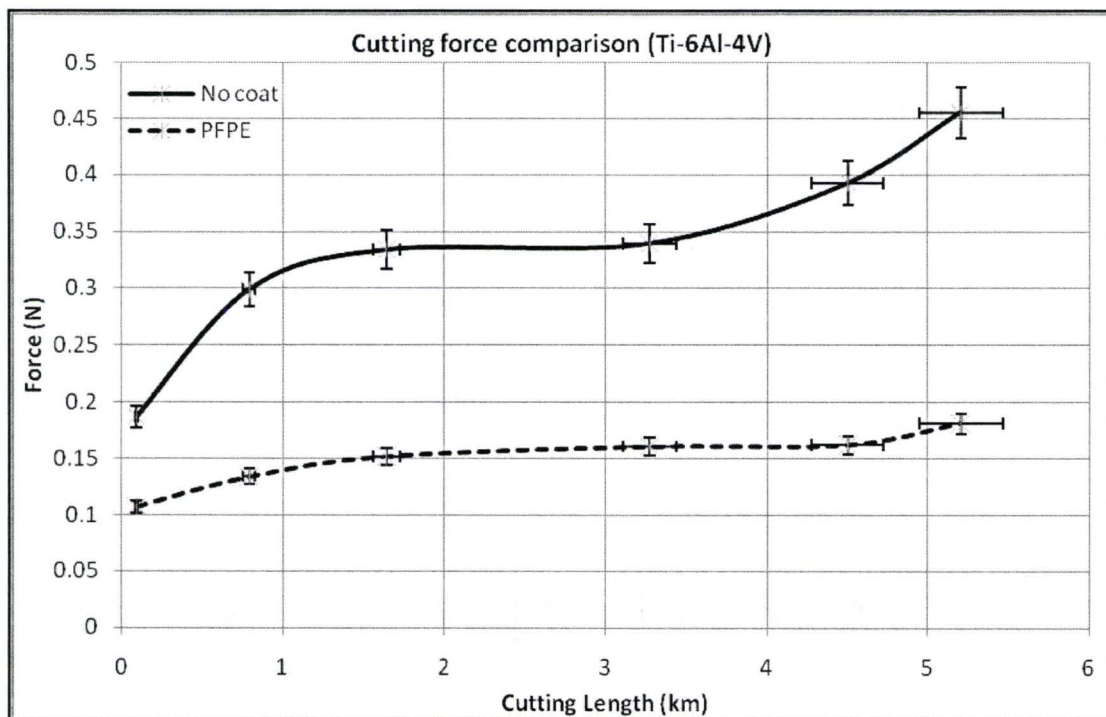
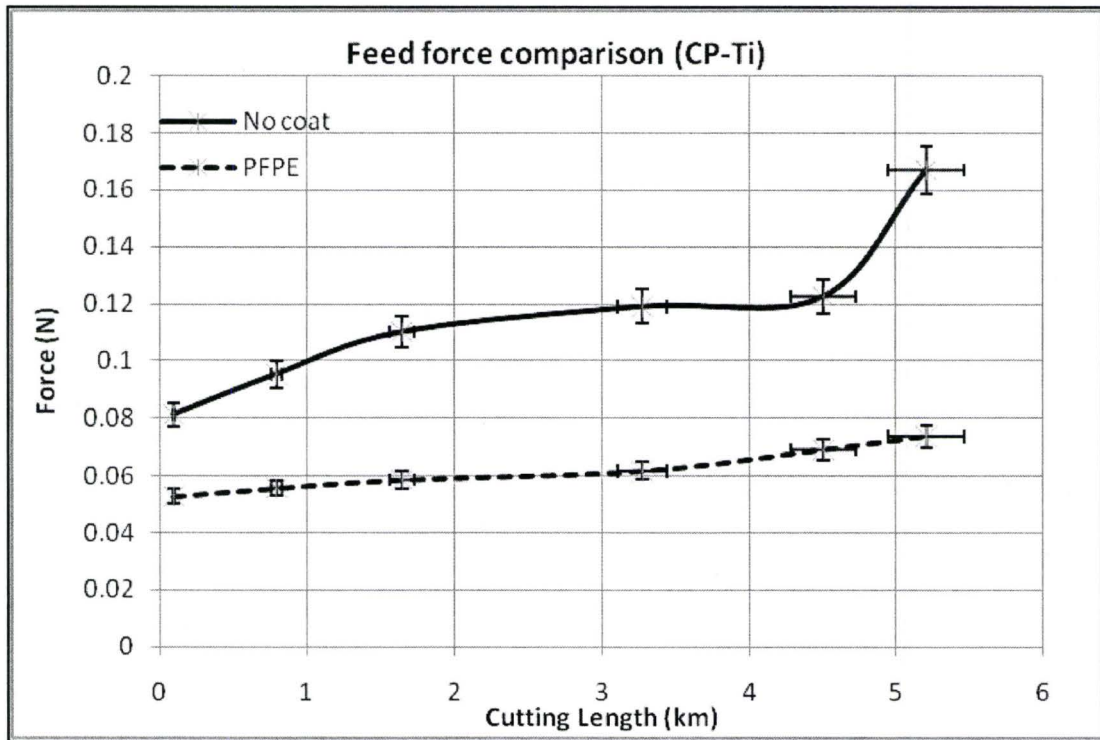


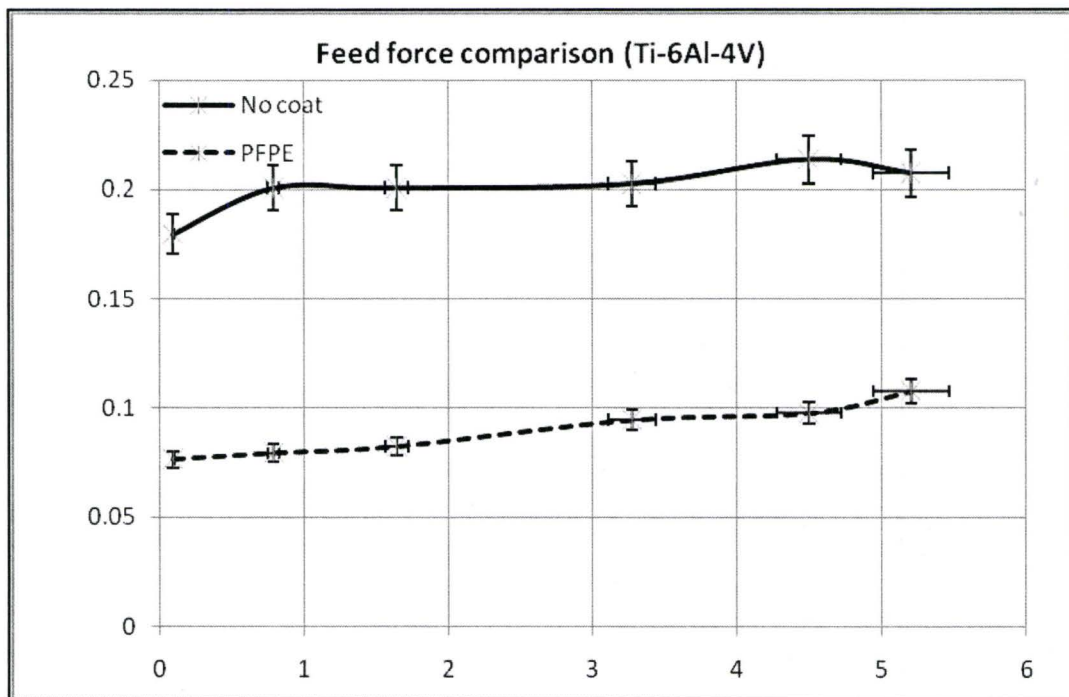
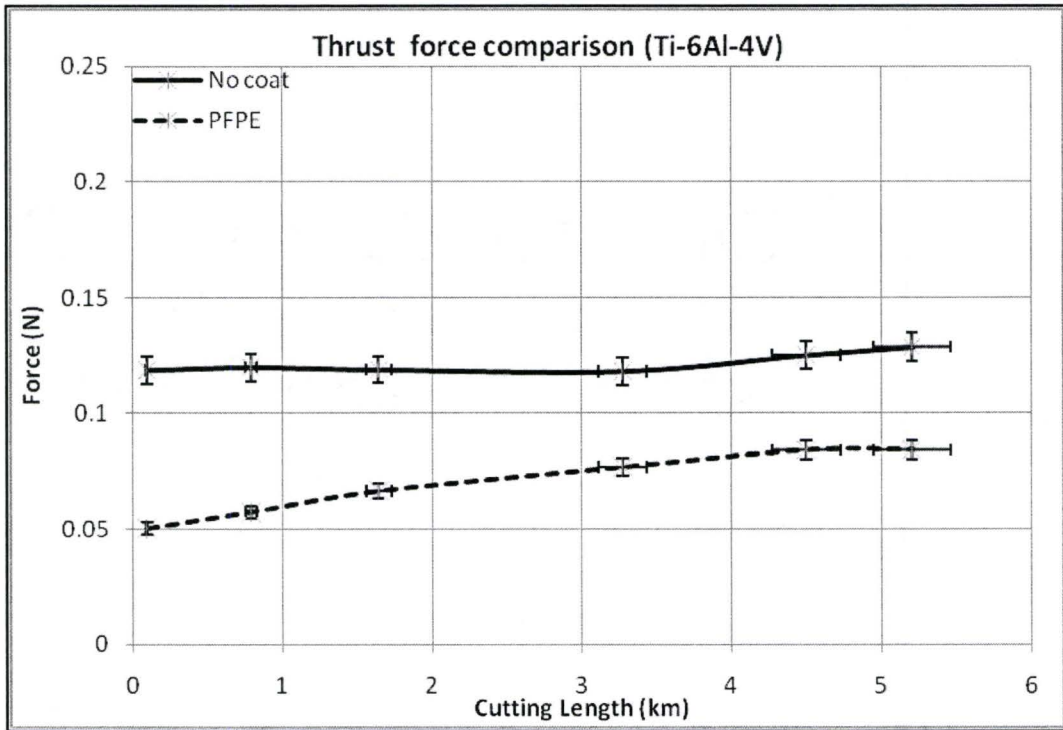
Microstructure of Ti-6Al-4V



APPENDIX -5







APPENDIX -6

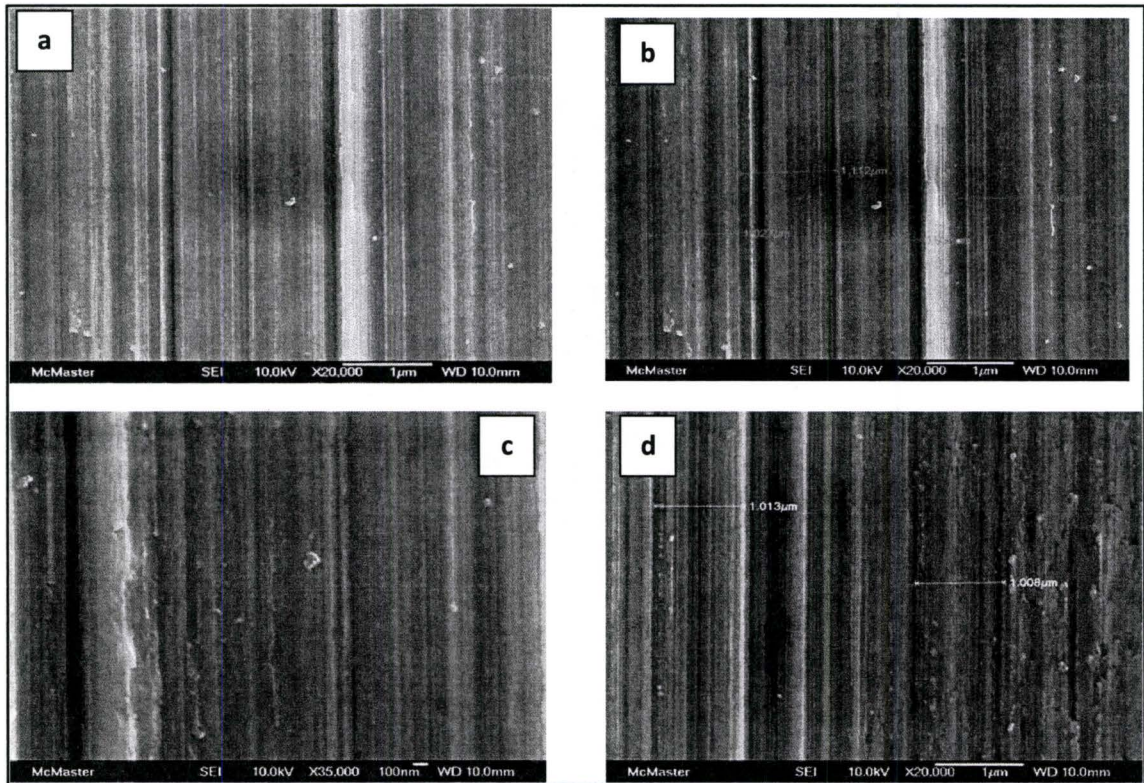
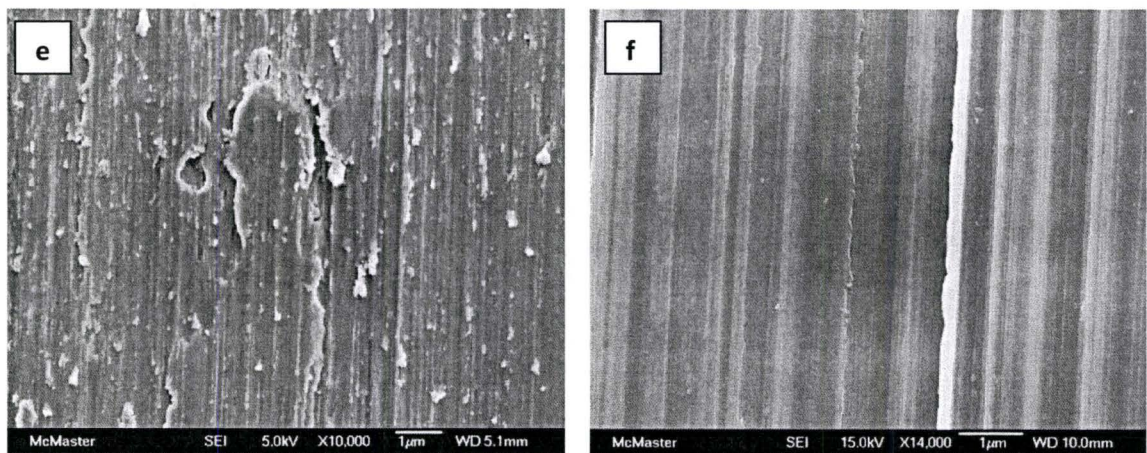


Fig. a - d: Surface quality deterioration with increasing cutting distance



(e) Surface machined without coolant

(f) Surface showing ploughing (side-flow)

APPENDIX -7

Carbon phase – diagram [129]

